Cardiovascular Function in Ectotherm Sauropsids

Dissertation der Fakultät für Biologie
der Ludwig-Maximilians-Universität München

Ulrike Campen

München, September 2017

Diese Dissertation wurde angefertigt

unter der Leitung von Prof. Dr. J. Matthias Starck/ Prof. Dr. Gerhard Haszprunar

im Bereich von Biologie: Systematische Zoologie/ Zoologie

an der Ludwig-Maximilians-Universität München

Erstgutachter/in:	Prof. Dr. Gerhard Haszprunar
Zweitgutachter/in:	Prof. Dr. Dirk Metzler
Tag der Abgabe:	21. September 2017
Tag der mündlichen Prüfung:	28. Mai 2018

ERKLÄRUNG

Ich versichere hiermit an Eides statt, dass meine Dissertation selbständig und ohne unerlaubte Hilfsmittel angefertigt worden ist.

Die vorliegende Dissertation wurde weder ganz, noch teilweise bei einer anderen Prüfungskommission vorgelegt.

Ich habe noch zu keinem früheren Zeitpunkt versucht, eine Dissertation einzureichen oder an einer Doktorprüfung teilzunehmen.

München, den 09. Juni 2018

Ulrike Campen

Conducted within the framework of the Graduate School ‘Life Science Munich’.

Supported by a Graduiertenstipendium nach dem Bayerischen Eliteförderungsgesetz (BayEFG) des Bayerischen Staatsministeriums für Wissenschaft, Forschung und Kunst.

Previous publications of parts of this thesis

Parts of this thesis have already been published in

Campen R. and Starck J.M. 2012. Cardiovascular circuits and digestive function of intermittent-feeding sauropsids. Pp. 133-154. Chapter 09 in: Comparative Physiology of Fasting, Starvation, and Food Limitation. M. McCue (ed.) Springer Verlag, Heidelberg New York.

Springer gave their permission to use parts of the publications for the thesis per email:

With reference to your request to reprint material in which Springer Science and Business Media control the copyright, our permission is granted free of charge and at the following conditions:

- Springer material represents original material which does not carry references to other sources (if material in question refers with a credit to another source, authorization from that source is required as well);
- requires full credit [Springer and the original publisher/journal title, volume, year of publication, page, chapter/article title, name(s) of author(s), figure number(s), original copyright notice] to the publication in which the material was originally published, by adding; with kind permission from Springer Science+Business Media B.V.;
- may not be altered in any manner. Abbreviations, additions, deletions and/or any other alterations shall be made only with prior written authorization of the author and/or Springer Science + Business Media.
- may not be republished in Electronic Open Access.

This permission

a. is non-exclusive.

Contribution remarks

The research questions and all methods were put forward by myself.

Methods were chosen by myself. Concerning application of the methods I was supported by the following cooperation partners:

For the morphological part of the thesis:

- Dr. Marcus Settles from the Institute of Radiology of the Klinikum rechts der Isar of the TU Munich, who conducted the magnetic resonance imaging scans.
- Dr. Bernhard Ruthensteiner of the Zoological State Collection Munich, who conducted the X-ray micro-computed tomography.
- AG Starck, Department Biology II of LMU München supplied a workstation and laboratory access during large parts of this thesis.
- Valuable advice concerning the area of histology and bio-imaging came from Prof. Dr. Gerhard Haszprunar, PD Dr. Martin Hess, and Prof. Dr. J. Matthias Starck.

For the computational simulation part of the thesis:

- Dr. Meike Wittmann and Prof. Dr. Dirk Metzler from the Statistical Genetics Group at the LMU Biocenter translated my ideas into a mathematical algorithm, programmed the code in the language *R*, and made valuable suggestions for the physiological adjustment of the program code.
- Dr. Philipp Rautenberg from the German Neuroinformatics Node G-Node translated the algorithm into the language *Python* and set up the database.
- Dr. Meike Wittmann, Prof. Dr. Matthias Starck, Prof. Dr. Dirk Metzler, and Dr. Philipp Rautenberg are coauthors of a publication on the simulation model which has not been published yet. Their contributions to the manuscript have gone into this thesis.

- The German Neuroinformatics Node G-Node allowed me to use their infrastructure for calculation and data storage.

The interpretation of the results was carried out by myself. During experimental performance and preparation of the manuscripts, discussion with and support by Prof. Dr. Dirk Metzler, Prof. Dr. Gerhard Haszprunar, Dr. Meike Wittmann, Dr. Philipp Rautenberg, Prof. Dr. Matthias Starck, PD Dr. Martin Heß, Dr. Nadine Gerth, and Dipl. Biol. Kathrin Jakob helped me a lot to state my ideas more precisely.

Abstract

Although the anatomy of the heart and its outflow tract differs between crocodiles and all other extant ectotherm sauropsids (i.e. Chelonia, Rhynchocephalia, and Squamata), they share one unique feature: All ectotherm sauropsids are able to bypass the pulmonary circulation and to redirect blood volumes returning from the systemic circulation directly back into the systemic circulation. Lepidosauria and Testudines use the interconnected three chambers of their ventricle for pulmonary bypass, and they are also able to bypass the systemic circulation. All ectotherm sauropsids possess two aortae. In crocodiles, they emerge from different ventricles, which is the mechanism that enables a pulmonary bypass. Their aortae are interconnected by two structures: The *Foramen Panizzae* and the aortic anastomosis. They enable exchange of blood volumes between the two aortae carrying blood from the two ventricles. This thesis evaluates the functional significance of bypass and blood flow through the *Foramen Panizzae* and the anastomosis from two sides: First, it examines the morphology of bypass related structures in crocodiles and snakes using a variety of histological and bioimaging methods. These methods are also compared regarding their strengths and weaknesses for the examination of the structures of interest in. Second, a computational multi-compartment model was developed to simulate blood volume distribution in dependence from pulmonary bypass and the blood flow through the *Foramen Panizzae* and the aortic anastomosis in the crocodilian body. Additionally, I examined the impact of these parameters on physiological measurements that are often used in physiological experiments on the cardiovascular function in ectotherm sauropsids. Apart from supporting knowledge on some already examined anatomical details, the present contribution adds information on so far unexamined species and structures, amongst them a description of the cardiac cartilage clasp in *Crocodylus niloticus* while the function of bypass in snakes remains unclear. The data from histology and bioimaging contributed to the paramaters chosen for the simulation model. The results of the simulation indicate that – apart from its known impact on

supplying the lungs and digestive tract – pulmonary bypass reduces blood supply of the anterior and posterior body regions of crocodiles. Blood flow through *Foramen Panizzae* and aortic anastomosis is from the right into the left aorta without pulmonary bypass and inverts at its onset. As a consequence of vascular arrangement, decreasing blood flow into the pulmonary circulation during pulmonary bypass decreases left-ventricular return and consequently total cardiac stroke volume, with zero left-ventricular return at complete bypass. I conclude that pulmonary bypass must be incomplete or of limited duration. The simulation model shows that blood flows balance within a few heart beats after a change in pulmonary bypass, or *Foramen Panizzae*/ aortic anastomosis flow. The results support the idea that pulmonary bypass may improve digestive function by supporting gastric acid secretion and buffering the postprandial alkaline tide rather than being an adaptation to extended diving periods in crocodiles. The disadvantageous effects of pulmonary bypass on oxygen supply to the digestive tract may be eliminated by the so far undiscussed course of branches of the right aorta which additionally supply the digestive tract with oxygen-rich blood. Pulmonary bypass might also contribute to thermoregulation.

Content

1 Comprehensive introduction

Ectotherm sauropsids possess a heart and cardiac outflow tract anatomy that is unique among amniotes. Basic cardiac anatomy differs severely between crocodiles and the rest of ectotherm sauropsids (Chelonia, Rhynchocephalia, and Squamata). One anatomical difference between the groups lies in the separation of the ventricular chambers (Fig. 1): While Chelonia, Rhynchocephalia, and Squamata possess a ventricle that is subdivided into three interconnected chambers (the *cavum arteriosum, cavum venosum*, and *cavum pulmonale* (Brücke, 1852)), crocodiles possess only two ventricular chambers that are completely separated by a ventricular septum. An overview of vertebrate phylogeny and the evolution of cardiac chambers can be found in Jensen et al. (2014) and "reptilian" cardiac evolution and ontogeny was studied by Jensen et al. (2013) and Poelmann et al. (2014, 2017). Another difference is the arrangement of the large cardiac outflow vessels: All groups possess one pair of aortae (the ancestral number of systemic outflow vessels in Amniota) and a pulmonary trunk that branches into two pulmonary arteries shortly after emergence. In Chelonia, Rhynchocephalia, and Squamata, the pulmonary trunk emerges from the cavum pulmonale, and the aortae both emerge from another one of the three ventricular chambers. In crocodiles, the pulmonary trunk emerges from the right ventricle (as in mammals and birds), but the origin of the two aortae is special: The right aorta originates from the left ventricle and the left aortae originates from the right ventricle together with the pulmonary trunk (Webb, 1979; White, 1956).

As a consequence of their cardiac anatomies, all ectotherm sauropsids are able to bypass the pulmonary circulation and redirect systemic blood directly back into the systemic circulation. Chelonia, Rhynchocephalia, and Squamata are in addition able to bypass the systemic circulation and redirect blood from the pulmonary circulation directly back into the pulmonary circulation.

Traditionally, bypassing the pulmonary circulation has been called a "right-to-left shunt" or R-L shunt, while bypassing the systemic circulation has been called a

"left-to-right shunt" or L-R shunt (e.g. Baker and White, 1970; Berger and Heisler, 1977; Johansen and Hol, 1960). This nomenclature originates from the tradition of calling the systemic circulation the 'left circulation', because the left ventricle pumps blood into the systemic circulation in (non-fetal) humans. Vice versa, the pulmonary circulation can be called the 'right circulation'. Blood volume redistribution caused by systemic or pulmonary bypass result in changes in the oxygen and carbon-dioxide content of the blood supplied to various body regions. In crocodiles, two connections between the aortae may additionally affect blood distribution and oxygen/ carbon dioxide distribution in the crocodilian body: The *Foramen Panizzae* and the aortic anastomosis, two connections between the aortae that emerge from different ventricles and carry blood with different oxygen/ carbon dioxide content. The cardiovascular anatomy of Chelonia, Rhynchocephalia, Squamata and Crocodylia is subject of Chapter 1.1 of this thesis.

A variety of functional hypothesis about pulmonary and systemic bypass have been supposed. It has been hypothesized that the redirection of blood volumes and its impact on blood oxygen and carbon-dioxide content serve physiological functions like diving, digestion, exercise, thermoregulation or growth, but none of these hypotheses has been really proven. The existing hypotheses are reviewed in Chapter 1.2 of this thesis.

To understand the functional significance of bypass in ectotherm sauropsids, this thesis evaluates systemic and pulmonary bypass from two sides: One part comprises a comparative description of bypass-relevant cardiovascular structures of Chelonia, Rhynchocephalia, Squamata and Crocodylia with a focus on snakes and crocodiles (Chapters 2.1, 3.1, and 4.2) to evaluate the anatomical setting of pulmonary and systemic bypass. In a second part, a computational simulation is used to examine blood volume distribution in crocodiles depending on the degree of pulmonary bypass, and blood flow through the *Foramen Panizzae* and the aortic anastomosis quantitatively (Chapters 2.2, 3.2 and 4.3) to allow a re-evaluation of the existing functional hypothesis and infer possible limitations that morphology might set to

pulmonary bypass, and blood flow through the *Foramen Panizzae* and the aortic anastomosis.

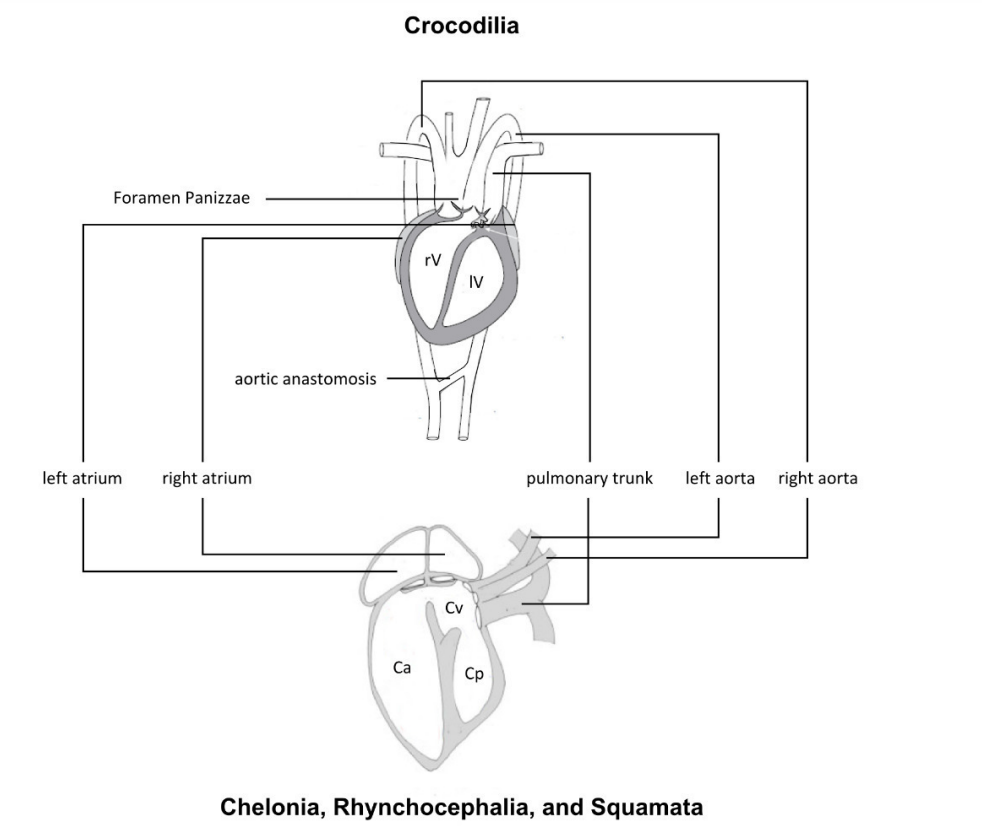

Fig. 1: Schematic illustration of the anatomy of the heart and its outflow tract of Crocodylia compared with the general organization of the heart of Chelonia, Rhynchocephalia, and Squamata (ventral view).
Abbreviations: rV/lV: right/left ventricle; Ca: *cavum arteriosum*; Cv: *cavum venosum*; Cp: *cavum pulmonale*. Combined and adapted from Axelsson et al. (1996) and Starck (2009).

1.1 Morphology of the heart and cardiac outflow tract of ectotherm sauropsids

1.1.1 Chelonia, Rhynchocephalia, and Squamata

In Chelonia, Rhynchocephalia, and Squamata the hearts consist of a left and right atrium and a single ventricle that is functionally subdivided into three chambers: the *cavum arteriosum* (left), the *cavum venosum* (medial), and the *cavum pulmonale* (right). The *cavum arteriosum* and the *cavum venosum* have also been summarized as the *cavum dorsale*, while the *cavum pulmonale* was referred to as the *cavum ventrale* (Mathur, 1944). The ventricle is crossed by trabeculae which show different density in different parts of the ventricle and are suspected to assist in guiding blood streams (e.g. Jensen et al., 2010a). Between the *cavum arteriosum* and the other two ventricular chambers, a nearly complete separation exists: the interventricular septum. The only connection between the *cavum arteriosum* and the *cavum venosum* is the interventricular channel. It is positioned at the cranial part of the ventricle, close to the connections between the atria and the ventricle. Therefore, it might be overlapped by the atrioventricular valves during ventricular diastole, separating blood streams from the two atria (Fig. 2 A). The *cavum arteriosum* receives inflow from the left atrium. The *cavum venosum* and the *cavum pulmonale* are directly connected, but the wide connection between them can be closed (completely or incompletely) by the muscular ridge (Mahendra and Viviridis, 1942; German 'Muskelleiste', sometimes also referred to as 'horizontal septum'). The muscular ridge is projecting from the ventral ventricular wall and the opposing ‘bulbuslamelle’ , a protuberance of the vascular wall (called ‘Fleischpolster’ by Brücke (1852)). In contrast, the *cavum arteriosum* and the *cavum pulmonale* lack a direct connection (Farrell and Gamperl, 1998; Jensen et al., 2010b; Mathur, 1944; Starck, 2009; Webb, 1979; Webb et al., 1971; Webb et al., 1974).

Induced by a pacemaker in the sinus venosus to the atria and the ventricles (Valentinuzzi et al., 1969), blood from the left atrium enters the *cavum arteriosum*

during ventricular diastole, and blood from the right atrium flows through the *cavum venosum* into the *cavum pulmonale* (Fig. 2 A). As mentioned above, blood streams from the two atria are divided by the long atrioventricular valves that can overlap and thereby close the interventricular canal when they are open, as it is the case in pythons (Jensen et al., 2014b; Starck, 2009). The atrioventricular valves close during ventricular systole, consequently the interventricular canal opens and blood from the *cavum arteriosum* can pass the *cavum venosum* to reach the aortae (Fig. 2 B/ 2 C). The *cavum venosum* and the *cavum pulmonale* are (completely or incompletely) separated by the muscular ridge during ventricular systole, which moves towards the opposing ‚Bulbuslamelle' (Brücke, 1852; Hopkinson et al., 1837; Jensen et al., 2010a; Starck, 2009). Thus, flow from the *cavum venosum* is generally directed into the aortae and blood from the *cavum pulmonale* into the *truncus pulmonalis*, but it is possible that either the *cavum venosum* or the *cavum pulmonale* or both contain admixtures of blood bypassing the one or other circulation (Jensen et al., 2010a, 2010b; Starck, 2009; Webb et al., 1971; White, 1968, 1959; see Fig. 2 C). According to Jensen et al. (2010a), Wang and Altimiras (2003), and Wang et al. (2002) the muscular ridge of pythons is able to close so tightly that the 'systemic side' (*cavum arteriosum* and *cavum venosum*) and the 'pulmonary side' (*cavum pulmonale*) can build up different pressures in the systemic (high pressure) and pulmonary (low pressure) circulation. The *cavum arteriosum* is equipped with a thicker muscular wall (myocardium) than the *cavum pulmonale*, enabling the generation of higher forces (Zaar et al., 2007). From what is known today, pressure in the pulmonary and systemic circulation is similar in most Chelonia, Rhynchocephalia, and Squamata, therefore blood is distributed according to the vascular resistance of the circulations and pulmonary bypass seems to be the predominant state in the majority of 'reptiles', as the *cavum arteriosum* and *cavum venosum* together are larger than the *cavum pulmonale* (Jensen et al., 2014b). However, the comparion of the sizes of the cava does not allow for a conclusion about the dynamics within the ventricle that may cause different bypass patterns including cross-over shunts. A discussion recently arised if different vascular distensibilities in

the two circuits might predominantly impact shunting patterns in amphibians and 'reptiles' with unseparated ventricles, based on a study by Hillman et al. (2014). A follow-up metaanalysis by Filogonio et al. (2017), however, showed that these different vascular distensibilities cannot be the only factor determining shunt patterns, but additional factors as vasoconstriction and vasodilation must play a role.

If the muscular ridge separates the *cavum venosum* and the *cavum pulmonale* pressure-tightly from each other during ventricular systole, as it is necessary for building up different pressures in the circulations, three factors could decide about the degree of pulmonary or systemic bypass, as suggested by Starck (2009): The timing of the opening and closing of the atrioventricular valves, the closure of the muscular ridge, and the capacity of the cava might determine the volume of blood that is directed into the pulmonary and systemic circulation. If the muscular ridge closes early during the ventricular systole, not all blood returning from the systemic circulation might have left the *cavum venosum*; thus, it bypasses the pulmonary circulation and is redirected into the aortae. If the muscular ridge closes later, blood returning from the pulmonary circulation can have entered the *cavum pulmonale*; thus, it bypasses the systemic circulation and is redirected into the pulmonary arteries. A situation where no blood volumes bypass one or the other circulation could be produced if the muscular ridge closes at an intermediate point of time (Campen and Starck, 2012; Starck, 2009). If the muscular ridge does not close pressure-tight or if it is even too short to separate the *cavum venosum* and the *cavum pulmonale* from each other at all, mixing of the not physically separated blood streams most likely occurs in these cava and blood distribution would occur depending either (1) on the afterload of the two circuits during systole (Filogonio et al., 2016; Joyce et al., 2016) (2) the sizes of the cava if there are no differences in the afterload. According to Jensen et al. (2014b), bypass is not regulated by outflow resistances but it is the relative volume of the *cavum venosum* that determines shunt levels. However, independent of the size of the cava, interventricular mixing of blood streams caused be turbulences can occur. This mixing can cause a situation where pulmonary and systemic bypass occurs at the same time.

The distribution of mixed volumes into the circulations is often referred to as a washout shunt (e.g. Hicks et al., 1996; Jensen et al., 2010a). Surgical dissection of the muscular ridge leads to homogenized blood in the outflow vessels (Steggerda and Essex, 1957). According to Jensen et al. (2010a), the remarkably small *cavum venosum* of pythons does not enable large volumes to be shunted into one or the other direction. However, the volumes of the cava and the length of the muscular ridge are very heterogeneous in different taxa (e.g. Jensen et al., 2014; Starck, 2009), therefore shunts of larger extent might occur in other species.

The large arteries are commonly surrounded by a cartilaginous ring in sauropsids (Farmer, 2011). Cardiac cartilages, or a 'Cartilago cordis', can be found in many vertebrates. Young (1994) examined 42 species of snakes and found a cardiac cartilage in eleven of them with a large variation in shape, size, and location. He could not find a correlation of the presence of cardiac cartilage with body size, taxonomic relationships, or habitat preference. In contrast to this, the cardiac cartilage found in crocodiles might play a role for blood volume distribution in the crocodilian body. It is described in Chapter 1.1.2 of this thesis.

The anatomy of the heart of Chelonia, Rhynchocephalia, and Squamata is correlated with the pattern of the major arteries emerging from the left and right ventricle and supplying the different body regions (Campen and Starck, 2012; Farmer, 2011; Hafferl, 1933; Hochstetter, 1898). The reduction of several pairs to a single pair of aortae as found in ectotherm sauropsids is a synapomorphic character of amniotes, being further modified in birds and mammals that have independently reduced one of the two aortae (Gegenbauer, 1901). Farmer (2011) and Campen and Starck (2012) recently reviewed the arterial vascular patterns of tetrapods. In Chelonia, Rhynchocephalia, and Squamata, the left and the right aortae emerge from the *cavum venosum*. The carotid and subclavian arteries and several smaller arteries emerge from the right aortic arch, ramify into the head region, the thoracic musculature and the thymus. Major vessels do not branch off the left aortic arch before the latter fuses with the left aorta further caudal to form the dorsal aorta.

Blood vessels supplying the gastrointestinal tract may either branch off the left aorta or, further caudally, branch off the dorsal aorta that is formed by the merging of the left and right aortae. The pattern of blood supply of the stomach and the small intestine differs in major clades of sauropsids (Campen and Starck, 2012; Farmer, 2011; Hafferl, 1933; Hochstetter, 1898), compare Fig. 3. In most Testudines (Fig. 3, *Clemmys* spec.), monitor lizards (e.g. Fig. 3, *Varanus niloticus*), and some agamids, blood supply of the stomach and to the anterior part of the small intestine branches off from the left aorta (*Aa. coeliaca mesenterica*). In other sauropsids, amongst them *Python regius* (Starck and Wimmer, 2005), *Boa constrictor* and *Lacerta viridis* (Hafferl, 1933), a series of visceral arteries emerges from the dorsal aorta (Fig. 3).

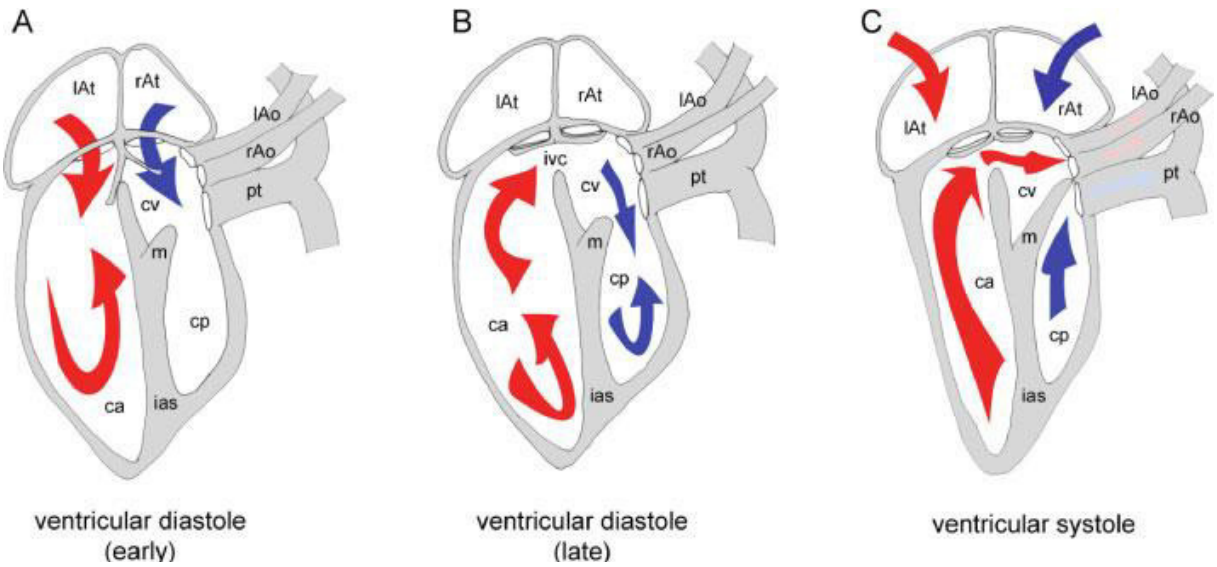

Fig. 2: Schematic drawing of the functioning of the heart of *Python regius*.
Abbreviations: ca: *cavum arteriosum*; cv: *cavum venosum*; cp: *cavum pulmonale*; lAt/rAt: left/right atrium; ivc: interventricular canal; ias: interventricular septum; m: muscular ridge; lAo/rAo: left/right aorta; pt: pulmonary trunk. Blood flow pattern is indicated by red and blue arrows, while red color indicates oxygen-rich and blue color oxygen-poor blood. Notice that this schematic drawing assumes neither systemic nor pulmonary bypass. From Starck (2009).

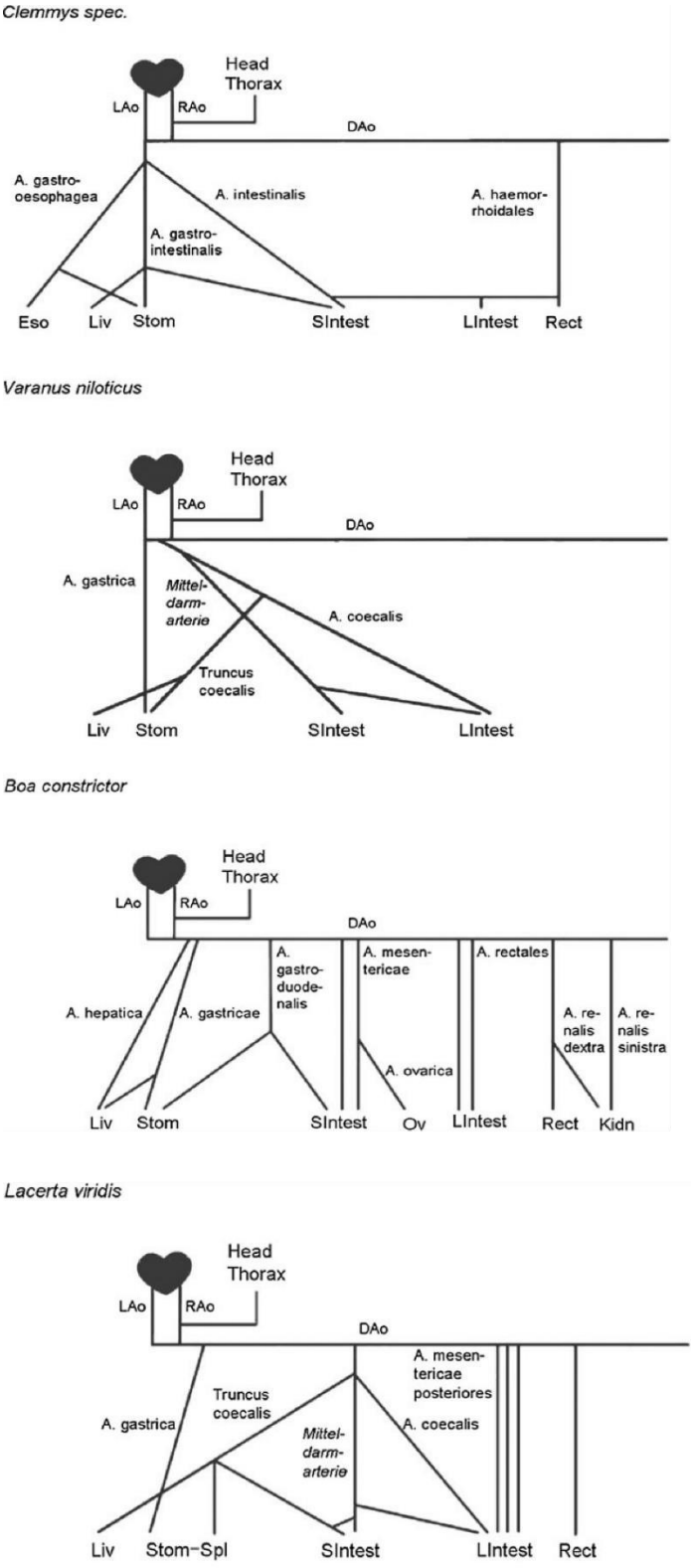

Fig. 3: Ramification patterns of the left and right aorta in different squamates and turtles.
Graphs combine information from Farmer (2011), Hafferl (1933), Hochstetter (1898), and Starck and Wimmer (2005). Abbreviations: Lao/Rao/DAo: left/right/dorsal aorta; Eso: esophagus; Liv: liver; Stom: stomach; SIntest: small intestine; Ov: ovaries; LIntest: large intestine; Rect: rectum; Kidn: kidneys. This figure is part of Campen and Starck (2012; Fig. 9.2); with kind permission from Springer Science+Business Media B.V..

1.1.2 Crocodiles

Crocodiles combine the ancestral two aortae of sauropsids with the derived ventricular condition with two completely separated ventricles. While both aortae emerge from the *cavum venosum* in all other taxa of ectotherm sauropsids, the origin of the two aortae in crocodiles is unique: While the right aorta emerges from the left ventricle receiving oxygen-rich, carbon-dioxide-poor blood returning from the lungs, the left aorta emerges from the right ventricle together with the pulmonary trunk, receiving deoxygenated blood returning from the systemic circulation (e.g. Webb, 1979; White, 1956). Therefore, crocodiles can redirect right-ventricular blood into the body, bypassing the pulmonary circulation. Another unique feature of the crocodilian circulatory system is the presence of two connections between these two aortae that allow for blood exchange between the aortae: The *Foramen Panizzae* and the aortic anastomosis. The latter possibility may affect blood distribution in the crocodilian body in addition to pulmonary bypass. The extent of blood flow through the left aorta, the *Foramen Panizzae*, and the aortic anastomosis determines blood supply of various areas of the crocodilian body.

The degree of pulmonary bypass in crocodiles is determined by two structures: the bicuspid valves at the basis of the left aorta and the cog-teeth-like valves arranged circularly at the basis of the pulmonary trunk. The cog-teeth-like valves consist of cartilaginous tissue nodes (Syme et al., 2002). On the level of the nodes, the pulmonary artery is surrounded by the cranial part of the myocardium. If the cog-teeth-like valves at the basis of the pulmonary trunk are open and the bicuspid valves at the basis of the left aorta are closed, a pulmonary bypass does not happen, but blood is directed into the pulmonary arteries. The left-aortic bicuspid valves stay closed during low pressure within the right ventricle, then blood does not flow into the left aorta (Fig. 4 A). It is generally assumed that under standard conditions (e.g. normal breathing) the left aorta does not receive blood from the right ventricle but receives oxygen-rich, carbon-dioxide-poor blood from the right aorta through the *Foramen Panizzae*. To induce

pulmonary bypass, the cog-teeth-like valves close and blood is ejected into left aorta instead of the lungs (Fig. 4 B). The cog-teeth-like valves are presumably closed as a consequence of contraction of the cranial myocardium that hence presses the tissue nodes against each other. Consequently, the increasing blood pressure in the right ventricle overcomes the compliance to the bicuspid valve and blood is ejected into the left aorta (Axelsson et al., 1997; Franklin and Axelsson, 2000; Syme et al., 2002).

The *Foramen Panizzae* (Panizza, 1833) is a window-like opening at the basis of the aortae which are separated from each other by second heart field derived tissue everywhere else (Poelmann et al., 2017). The detailed morphology of the *Foramen Panizzae* was not illustrated in the original description by Panizza (1833) and remains poorly studied up to now. Greenfield and Morrow (1961) presented a semi-schematic drawing showing that the bicuspid valves of left and right aorta reach far into the aortae, overlapping the *Foramen Panizzae* (see Fig. 5). During systole, the bicuspid valves are pressed against the aortic wall by blood streaming from the ventricle and might hence obstruct blood flow through the *Foramen Panizzae*. During diastole, however, the blood flow through the *Foramen Panizzae* is not obstructed by the (closed) aortic valves. Axelsson et al. (1996) observed the in-situ perfused beating heart of *Crocodylus rhombifer.* They describe that the *Foramen Panizzae* is obstructed by the medial cusp of the right aortic valve during systole and that the left aortic valves are shorter and less obstructive to blood flow. In contrast, Webb (1979) described that both the left and right aortic valves prevent blood flow through the *Foramen Panizzae* during systole. Axelsson et al. (1996) measured that the diameter of the *Foramen Panizzae* is 35–40% of the right aorta's diameter (approx. 12-16% of the cross-section area, respectively) and concluded that these circumstances enable significant blood exchange between the aortae during diastole.

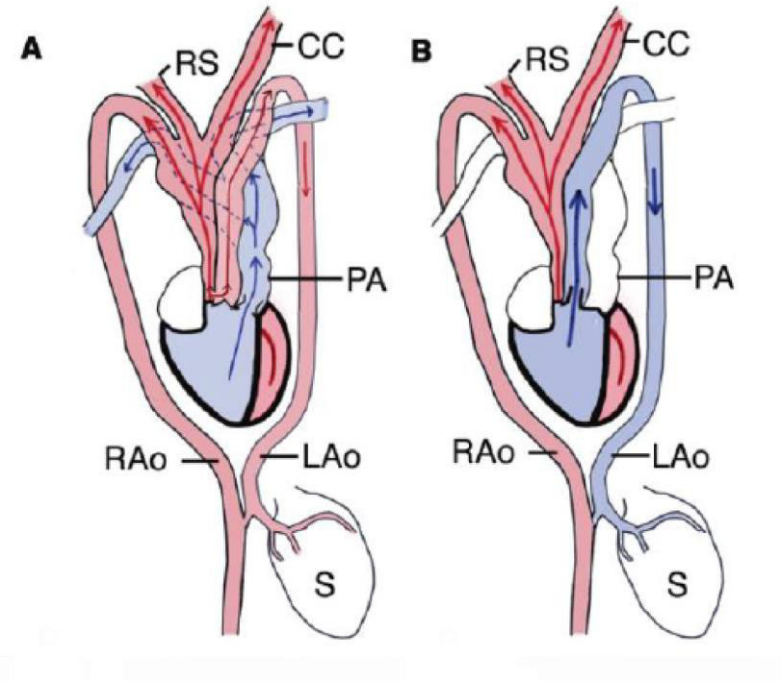

Fig. 4: Blood flow through the crocodilian heart without (A) and with complete (B) pulmonary bypass.
Abbreviations: RS: right subclavian artery; CC: common carotid artery; PA: pulmonary artery; RAo/LAo: right/left aorta; S: stomach. Farmer et al. (2008).

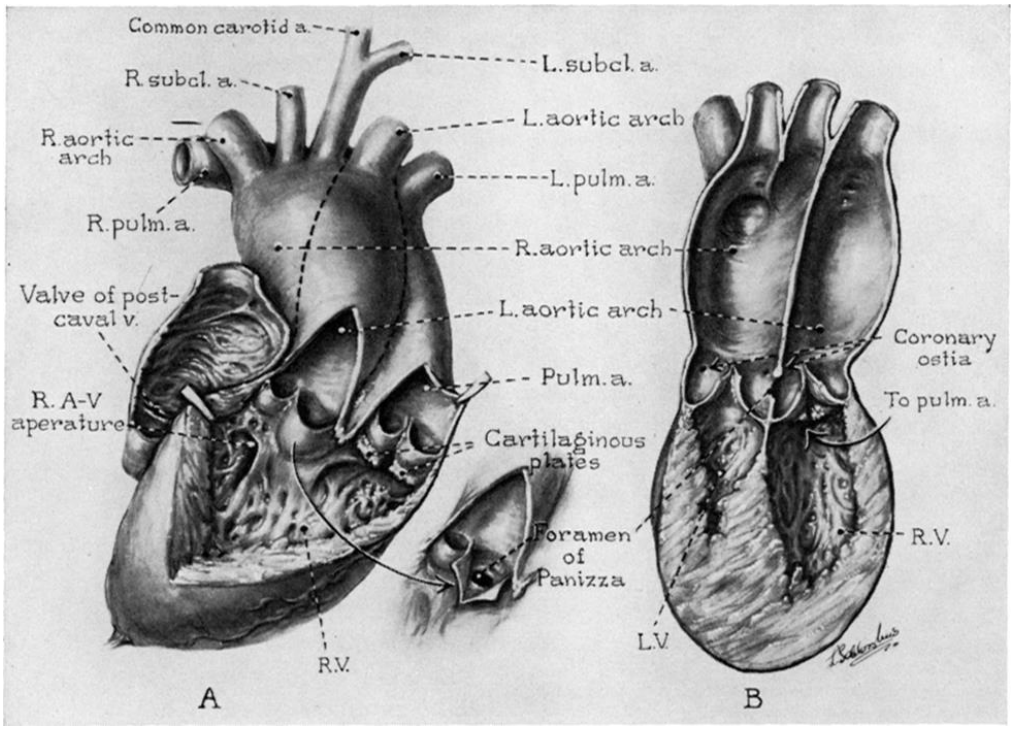

Fig. 5: The interior of the alligator heart in the anterior (A) and lateral (B) view.
Of particular interest are the cartilaginous plates in the right ventricular outflow tract and the interaortic *Foramen of Panizza* behind the anterior leaflet of the right aortic valve. Greenfield and Morrow (1961; Fig. 2).

The aortic anastomosis of crocodiles is a vascular connection between the right and left aorta. It is positioned distally to the branch-off of vessels supplying the head and thorax, but before the right aorta ramifies to supply the posterior body regions and the left aortic vessels spread over the digestive tract. Active regulation of the diameter of the aortic anastomosis is plausible, as Karila et al. (1995) described that it has a well-developed adventitia and media with a dense innervation. Also Axelsson et al. (1997) reported remarkable vasal activity. Based on immunohistochemical tests, Axelsson and Franklin (2001), Axelsson et al. (2001), and Karila et al. (1995) found that the *Foramen Panizzae* and the aortic anastomosis are sensitive to adrenaline. These authors proposed an active role of the *Foramen Panizzae* and the aortic anastomosis in exchanging blood volumes between the right and the left aorta.

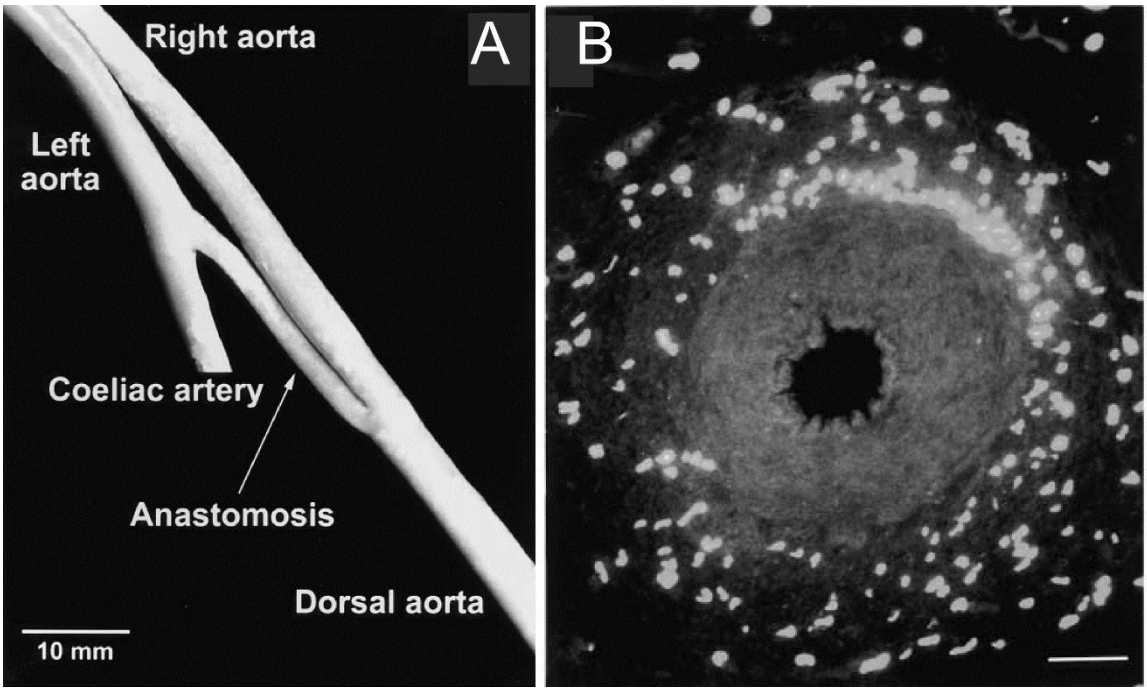

Fig. 6: The aortic anastomosis in a dilated state.
A: A vascular corrosion cast (methyl methacrylate-Mercox CL-2B) of the anastomosis and associated arteries showing the relative sizes of these vessels. B: Immunohistochemical treated sections of the anastomosis showing immunoreactivity to substance P. Axelsson and Franklin (1997, Fig. 2).

The multipart cardiac cartilage of crocodiles has a much more complex structure than the cartilaginous rings of some snakes being situated around their large arteries. Rathke (1866) provided the presumably first description of the cartilaginous bodies in the crocodilian heart:

> "Dicht vor der angeführten Spalte [*Foramen Panizzae*, annotation of UC] befindet sich zur Spannung des vorderen Randes derselben ein Knorpelstreifen, der als ein Fortsatz von einer nur sehr massig grossen Knorpelplatte zu betrachten ist; die in Hinsicht der Form einige Aehnlichkeit mit der grösseren Hälfte einer durch einen Querschnitt ungleich getheilten Ellipse hat, in die Scheidewand der Herzkammern eine kleine Strecke eindringt, in derselben zunächst dem Endocardium der rechten Kammer ihre Lage hat, gegen die Höhle dieser Kammer etwas hervorgewölbt ist […] . Eine zweite Knorpelplatte, deren ich nirgend Erwähnung gefunden habe, kommt dicht hinter der rechten Aorta, innerhalb der unteren Wandung der rechten Herzkammer in der Gegend vor, wo diese Wandung in die äussere Wandung derselben Kammer übergeht. Sie ist ein wenig kleiner, doch nicht dünner, als die vorige, besitzt eine länglich drei eckige Form und hat eine solche Lage, dass ihre Basis nach vorn, ihre Spitze nach hinten und etwas rechtshin gekehrt ist. […] Schliesslich habe ich über beide Platten noch anzuführen, dass ihr Gewebe dasjenige der hyalinen echten Knorpel ist; und dass ihre Knorpelkörperchen, die bis 0.0005" im Durchmesser haben, sehr nahe bei einander liegen." (Rathke, 1866)

He also described differences between the detailed forms of the cartilages in different species of crocodiles. Despite the detailed description, the position and shape of the cartilages is difficult to imagine.

White (1956) provided another detailed description of the cardiac cartilage of crocodiles and included a schematic drawing (Fig. 7). He described the two 'rather complicated cardiac cartilages' with several progresses plus a small cartilage nodule at the basis of the pulmonary artery of an *Alligator mississippiensis* heart. The cartilages are in close association with the aortic valves called the central and the ventrolateral cartilage by White. While the central cartilage seems to be responsible for the stabilization of the dorsal left aortic valve and the *Foramen Panizzae*, the ventrolateral cartilage provides rigidity to the ventral left aortic valve and serves as an attachment site for the right atrioventricular valves. Together they stabilize all areas that play a role

in the redirection of blood caused by pulmonary bypass and blood flow through the *Foramen Panizzae*. Grigg and Johansen (1987) agreed on the idea that the cartilaginous support of the foraminal area might be a mechanism that is important for keeping the *Foramen* open.

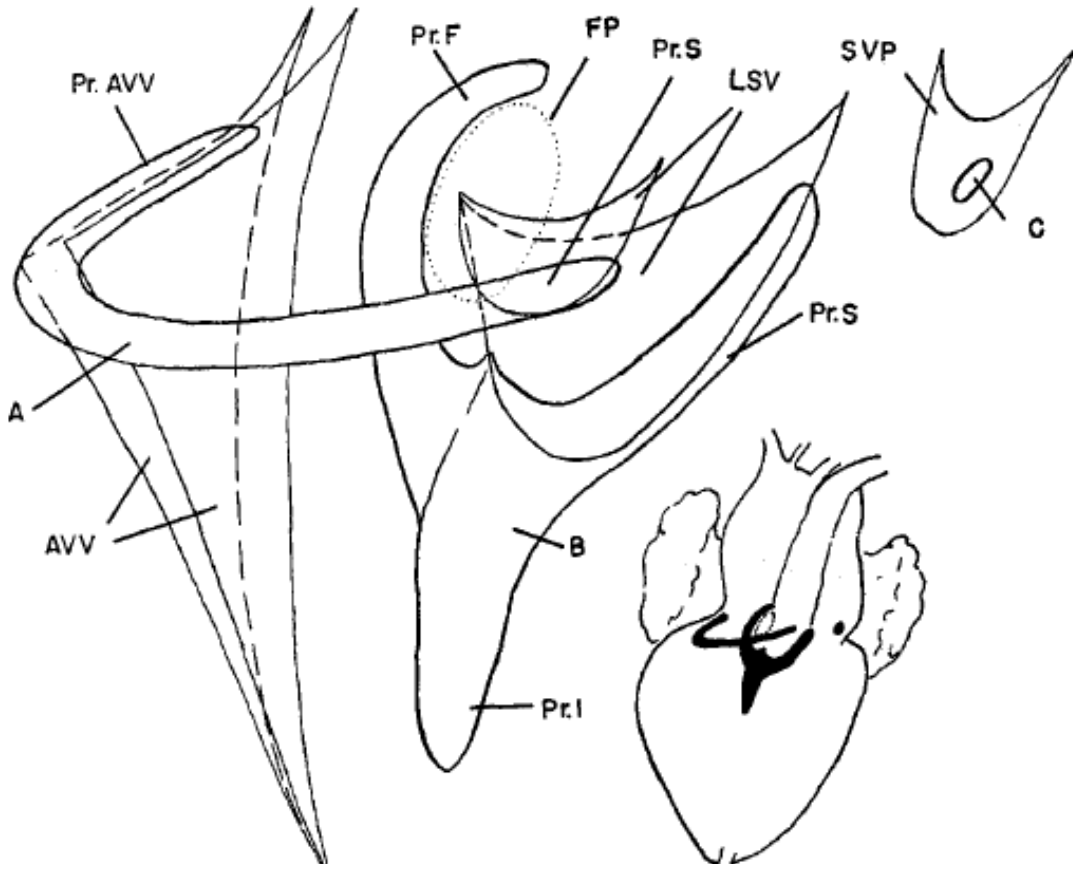

Fig. 7: The cardiac cartilages of *Alligator mississippiensis*.
Insert shows spatial relationships of cartilages to the heart. A: ventrolateral cartilage; B: central cartilage; C: small nodule in base of pulmonary artery; AVV: right atrioventricular valves; FP: *Foramen Panizzae*; LSV: semilunar valves of left aortic arch; PrAVV: process for atrioventricular valves; PrF: foraminal process; PrI: interventricular process; PrS: semilunar process; SVP: semilunar valve of pulmonary artery. White (1956, Fig. 3).

Generally, the course of the major vessels in crocodiles are similar to those found in monitor lizards and turtles. In crocodiles, blood supply of the stomach and the anterior part of the small intestine branches off from the left aorta, a pattern shared with some varanids, e.g. *Varanus niloticus* (Fig. 3). The left aorta branches off the coeliac artery and the gastrointestinal artery shortly after its connection with the right aorta, the anastomosis (see Fig. 8 and 9). Posterior to the anastomosis, the right aorta is called the dorsal aorta, while the left aorta becomes the *A. coeliaco-mesentericae* (Hafferl, 1933), providing the main supply of the digestive tract, including the esophagus, the stomach, the liver, the spleen, the small and large intestine and the rectum. A relatively small *A. mesenterica* emerges from the dorsal (right) aorta to supply the more distal segments of the small intestine. An *A. haemorrhoidales* branches off the dorsal aorta and supplies the rectum. Contrary to the rest of the digestive tract, the small intestine and rectum therefore receive oxygen-rich, carbon-dioxide-poor blood from the right aorta, a fact that has not yet been interpreted.

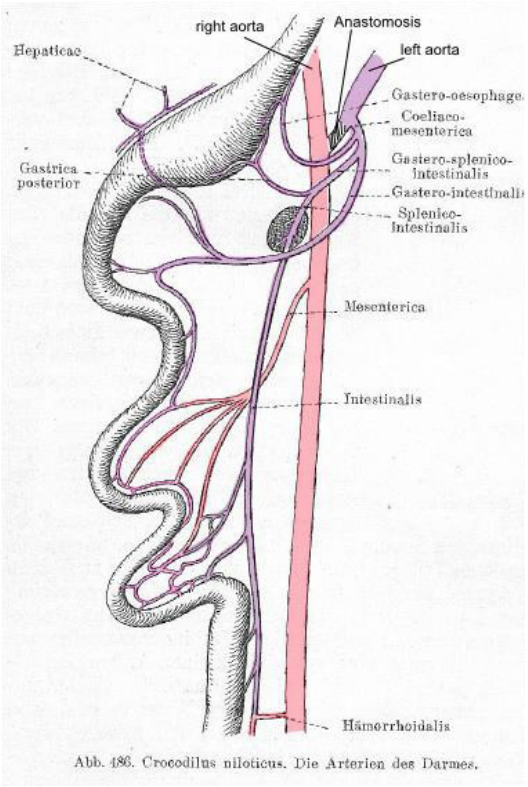

Fig. 8: Ramification pattern of the right and left aorta over the crocodilian digestive tract.
Colored and label supplemented version of a graphic from Hafferl (1933), showing that the small intestine and rectum receive blood from the right and left aorta.

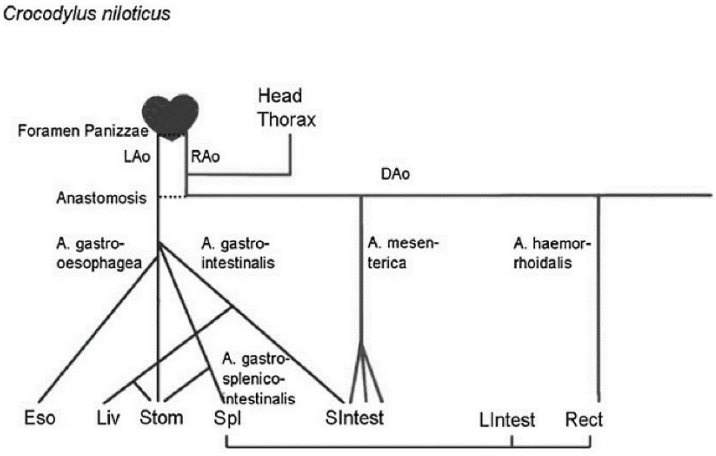

Fig. 9: Ramification patterns of the left and right aorta in crocodiles (*Crocodylus niloticus*).
Graphs combine information from Farmer (2011), Hafferl (1933), and Hochstetter (1898). Abbreviations: Lao/Rao/DAo: left/right/dorsal aorta; Eso: esophagus; Liv: liver; Stom: stomach; Spl: spleen; SIntest: small intestine; LIntest: large intestine; Rect: rectum.

1.2 Physiological relevance of bypass

In amniotes, blood transports oxygen taken up in the lungs to the oxygen consuming body tissues, and carbon dioxide produced by these tissues during cellular respiration back to the lungs, where it is exhaled. The regulation of blood volumes which contact the lung and body tissues by pulmonary or systemic bypasses, has an impact on the saturation respectively partial pressure of blood oxygen and carbon dioxide. Early physiological considerations have mainly focused on the changes that pulmonary and systemic bypass causes to oxygen delivery (without finding a consistently verifiable physiological advantage). More recent studies, however, focus on the impact of bypass on carbon-dioxide content of the blood. Because oxygen is bound to a pigment (hemoglobin) that quickly reaches a saturation, repeated circulation of blood trough the lungs (systemic bypass) is not assumed to improve oxygen transport (Burggren, 1987). Contrary, a substantial portion of the carbon-dioxide is freely dissolved in the blood, and its uptake (at the body tissues) and disposal (at the lungs) is primarily determined (and limited) by the partial pressure gradient between blood and tissue/ air. Additionally, the impact of carbon-dioxide on the hydrogen-carbonate buffer system has increasingly gained attention: Raising the percentage of carbon-dioxide to the balanced system leads to an increment of free protons (H^+) that acidify the blood and vice versa.

Hydrogen-carbonate buffer system:

$$CO_2 + H_2O \rightleftarrows H_2CO_3 \rightleftarrows HCO_3^- + H^+$$

Another change in the interpretation of the functional significance of bypass has taken place with regards to the organ systems that might profit from bypass. Earlier studies on the functional importance of pulmonary bypass have focused on its impact on blood supply of the lungs (e.g. Burggren, 1982; Eme et al., 2009; Farmer et al., 2008; Gardner et al., 2011; Jones and Shelton, 1993; Shelton and Burggren, 1976; White, 1969). The text-book paradigm is that pulmonary bypass in crocodiles supports diving by reducing

or eliminating blood flow into the unventilated lungs (e.g. Kardong, 1995). Thus, bypassing the lungs could contribute to increased oxygen delivery to the tissues, because a high carbon dioxide content of the blood decreases the affinity of hemoglobin for oxygen (*Bohr Effect*). Experimental studies on the occurrence of pulmonary bypass during diving resulted in contrasting findings: Axelsson and Fritsche (1991) and Grigg and Johansen (1987) reported that pulmonary bypass occurs during diving, while Eme et al., (2009) and Pflanzer and Wertenberger (1970) could not find any correlation between diving and the pattern of cardiovascular blood flow.

Although already suggested by Hochstetter (1898) and again proposed by Shelton and Jones (1991), the possible role of pulmonary bypass in crocodiles for digestion has gained increasing attention only during the last decade (Farmer et al., 2008; Farmer, 2011; reviewed by Campen and Starck, 2012). The left aorta receives oxygen-poor, carbon-dioxide-rich blood from the right ventricle during pulmonary bypass and supplies the digestive tract. High carbon dioxide content of the blood supplying the stomach can support gastric acid secretion from the oxyntic glands, because it improves the provision of protons. By influencing the hydrogen carbonate buffer system, it might also buffer the post-prandial alkaline tide as suggested by Jones and Shelton (1993). A study by Gardner et al. (2011) provided experimental evidence that pulmonary bypass affects acid-base balance. Farmer et al. (2008) were able to support the impact of pulmonary bypass on digestive performance.

In addition to diving and digestion, several hypotheses and ideas on pulmonary bypass in ectotherm sauropsids were summarized by Burggren (1987) and Farmer and Hicks (2002). Many of them belong to the area of apnea (introduced in section 1.2.1) and digestion (introduced in more detail in section 1.2.2), some others are provided subsequently in this thesis.

1.2.1 Ventilation, apnea, and diving

Since a pulmonary bypass has an obvious impact on blood supply of the lungs, it was often interpreted in the context of diving. As extended diving periods are most common in turtles, most research work on bypass connected with apnea ('cardiorespiratory synchrony', White et al., 1989) in non-crocodilian 'reptiles' was done on this group, as reviewed by Hicks and Krosniunas (1997). Apnea is often accompanied by bradycardia and increased pulmonary vascular resistance. Increased pulmonary vascular resistance diminishes flow into the lungs and can hence lead to the development of pulmonary bypass (Gleeson et al., 1984; Millen et al., 1964; Shelton and Burggren, 1976; Wang and Hicks, 1996a; Wang and Hicks, 1996b; White and Ross, 1966; White et al., 1989).

The oxygen binding affinity of hemoglobin is inversely related to the acidity of the blood, and blood acidity increases with increasing carbon-dioxide content of the blood. This effect is referred to as the *Bohr Effect*. Taking advantage of the *Bohr Effect*, the retention of carbon-dioxide in the systemic circulation facilitates oxygen delivery at the oxygen-consuming body tissues during diving. This theory is widely spread in textbooks (e.g. Kardong, 1995). Hicks and Wang (1996) questioned these benefits, because 1) pulmonary bypass does not provide additional benefits to oxygen exchange when the duration of apnea is within aerobic limits (oxygen transfer from the unventilated lungs to the oxygen consuming body tissues cannot be increased) and 2) carbon-dioxide can be shifted away from the lungs even without pulmonary bypass: in man voluntarily holding breath, pulmonary carbon-dioxide and gas exchange ratio are very similar to those of 'reptiles' (e.g. Douglas and Haldane, 1922). Hicks and Krosniunas (1997) summarized the conditions as follows: "*The pattern of carbon dioxide exchange during breath holding, in all air breathing vertebrates, is the result of the physicochemical properties of tissue, blood and air and does not depend on cardiac shunting*". They doubted the advantage of pulmonary bypass also for another reason, which was formulated by Hicks and Wang (1996):

3) "*Although increasing the tissue carbon dioxide will acidify the perfusing blood and thus right-shift the oxygen equilibrium curve, an R-L shunt also reduces systemic arterial oxygen levels. Thus, the benefits of a carbon-dioxide retention are only apparent when the reduction in blood oxygen affinity is greater than the reduction in arterial oxygen partial pressure resulting from R-L shunt*". Based on the measured changes in blood pH during breath holding within aerobic limits (Hicks and White, 1992; White et al., 1989), the magnitude of the Bohr shift is not large enough to offset the reductions in arterial oxygen content and oxygen partial pressure due to shunt. It is difficult, therefore, to reconcile the notion that reductions in arterial oxygen levels improve arterial oxygen delivery (Hicks and Wang, 1996).

In addition to the doubts about the theoretical benefits of pulmonary bypass during diving, there are no clear experimental results. White (1969) reported that pulmonary bypass occurs during diving. A study by Grigg and Johansen (1987) nevertheless contradicted these clear results. They studied the cardiovascular dynamics in *Crocodylus porosus* breathing air and during voluntary aerobic dives. They measured blood pressure in various vessels and found evidence for pulmonary bypass via the left aorta, occurring frequently during aerobic diving. Blood oxygen saturation in the left aorta nevertheless suggests the left aorta carries mixed blood from the right and left ventricle, with the greater portion of blood coming from the right aorta even during diving. Accordingly, the physiological relevance of a pulmonary bypass is not very substantial. Axelsson and Fritsche (1991) also studied blood flow in the salt water crocodile (*Crocodylus porosus*). They reported that short fright dives led to a decreased flow in the right aorta, the coeliac artery, and the common carotid, but could not detect clear effects on blood flow in the left aorta, contradicting the functional significance of pulmonary bypass for diving in crocodiles. Similar results for the right aorta were found in a study on *Crocodylus porosus* performed by Franklin et al. (1999). In this study, induced anoxia (in a nitrogen atmosphere, not diving) caused cerebral blood flow velocity to temporarily increase by 125%. Increased cerebral blood flow, however, indicates increased blood flow in the right, not in the left aorta. Also, Eme et al. (2009)

and Pflanzer and Wertenberger (1970) could not find any correlation between diving and the pattern of cardiovascular blood flow. Apart from the physiological implausibility of the relevance of pulmonary bypass for diving (see above), it remains unclear why also most land living sauropsids are equipped with an equally complicated heart anatomy as crocodiles and the ability to bypass the pulmonary circulation.

Burggren (1987) provided the hypothesis that pulmonary bypass saves cardiac energy during periods of apnea e.g. in turtles, but falsified this hypothesis in the same publication. The theory assumes that during proceeding apnea, lung gas partial pressures move towards pulmonary venous levels. Therefore, keeping up lung perfusion becomes increasingly less useful, while cardiac costs remain the same. Reducing pulmonary perfusion and instead using the right ventricle for supporting systemic supply during apnea could therefore save cardiac energy. Burggren (1987) refused this theory, because 1) pulmonary bypass often starts very quickly after the end of lung ventilation when oxygen partial pressure in the lungs is still high and 2) metabolic costs of pulmonary perfusion (in turtles) are so low (~0.5% of the aerobic metabolic rate) that it seems unlikely that this was the major factor in the evolution of intracardiac shunting (Burggren, 1987).

Another hypothesis also provided by Burggren (1987) assumes that the oxygen store in the lungs can be transferred to the blood and oxygen-consuming tissues more slowly and in finer doses when the rate of pulmonary perfusion is reduced during apnea. It is nevertheless questionable why a particular pattern of oxygen depletion from the lung during apnea should be more sensible than any other, because this cannot increase overall oxygen transfer to the tissues (Burggren, 1987).

Another hypothesis focuses on plasma filtration into the lungs. According to Burggren (1982), plasma flux between pulmonary capillaries and lung interstitium is proportional to pulmonary blood flow. While ‘reptilian’ plasma filtration into the lungs is 10-20 times higher than in mammalian lungs during ventilation, it is nearly completely diminished during apnea: there is a net reabsorption of fluid from lung

interstitium into the pulmonary capillaries. Burggren (1982) therefore suggested that pulmonary bypass might be a mechanism to reduce the particularly high plasma filtration into the lungs that occur in 'reptiles'. He stated that accumulation of fluid in the lung from plasma filtration may have grave consequences to gas exchange if it hinders the gas diffusion pathway. Pulmonary bypass could therefore be used to 'dry' the lungs during periods of apnea/diving to improve oxygen uptake and carbon-dioxide disposal during periods of ventilation.

Hypoxic conditions, e.g. caused by apnea/diving, lead to reduced metabolic activity in endothermic and ectothermic vertebrates, i.e. hypometabolism (Hicks and Wang, 1999). Pulmonary bypass leads to the recirculation of metabolically produced carbon-dioxide to the systemic arterial blood, increasing systemic arterial carbon-dioxide partial pressure and reducing blood pH (White, 1985). Hicks and Wang (1999) suggested that pulmonary bypass, which is often associated with diving, might trigger the development of a hypometabolic state in turtles. The reduction of metabolic activity could than contribute to the prolongation of aerobic dive times.

1.2.2 Digestion

Ectotherm sauropsids, especially "primitive" snakes from the families Pythonidae and Boidae have often been studied as model organisms of digestive regulation due to their 'intermittent' feeding pattern that is characterized by long starving periods interrupted by the intake of extraordinary large meals(Hicks et al., 2000; McCue et al., 2005; Secor, 2001; Secor et al., 1994; Starck and Beese, 2001; Starck and Wimmer, 2005). Intermittent feeding is often considerened as the contrasting feeding strategy to continuous feeding. However, at a closer look the picture becomes increasingly fuzzy because neither 'continuous' nor 'intermittent' can be clearly defined, as reviewed by Campen and Starck (2012). Although for example mammals and birds are usually considered as continuous feeding animals, they often experience periods without food uptake. Some mammals (e.g., polar bears, wolf, and reindeer) and birds (e.g. penguins, hornbills) periodically experience long fasting periods that can last up to several weeks.

Maybe some endoparasites (e.g. tapeworms, flukes, Sacculina, or unicellular blood parasites like trypanosome) feed continuously from their host during some stages of their life cycle, but even those endoparasites experience periods without feeding (e.g. as encysted persistence states in flukes and tapeworms). The same difficulties exist with the definition of the term 'intermittent feeding'. There are life cycle stages of metazoans, including also a considerable number of vertebrates that do not feed at all. They fuel their metabolism by energy stored during previous life cycle stages (e.g., numerous fish species, chelicerates, insects, etc.). 'Continuous feeding' and 'intermittent feeding' therefore rather represent two poles of a continuum than two distinct feeding strategies.

Although one must consent that all reptilian sauropsids are somehow 'intermittent feeders', it hast to be admitted that they differ significantly in the length of fasting intervals, food and energy stores quality and quantity, mass-specific energy demands, and intestinal passage times and digestive efficiency (Campen and Starck, 2012). On the one hand, there are species that feed very infrequently, most of them are sit-and-wait hunters or actively hunting predators, like boids. On the other hand, there are also frequently feeding sauropsids, often among grazing species such as many turtles. The association between feeding strategy and feeding interval can nevertheless not be consistently kept up. Among grazers we may find species that feed only during short periods of the year, and there might be sit-and-wait hunters that feed quite frequently. During migration or when they are in their nesting habitats, grazing green turtles (*Chelonia mydas*) for example experience starving periods or periods when they find only small quantities of low quality vegetable food (Carr et al., 1974; Mortimer, 1981; Tucker and Read, 2001).

As reviewed by Campen and Starck (Campen and Starck, 2012), feeding and digesting are processes that affect the cardiovascular system and it can be assumed that switching between long fasting periods and the seldom ingestion of large prey items is most challenging for the cardiovascular system. Digestion and fasting impose contrasting functional demands on the gastrointestinal tract: The gastrointestinal tract

of infrequently feeding snakes changes into a ‚quiescent' condition during fasting (Secor, 2003; Secor, 2005). This includes a reduction of intestinal mass by 50% and a reduction of rates of transepithelial nutrient transport to 30% (measured by the everted sleeve technique; Karasov and Diamond, 1983; Secor et al., 1994) compared to the digestive condition (Secor, 2005). The factors contributing to the immediate upregulation of digestive and absorptive functions after ingestion of a meal are summarized by Campen and Starck (2012) as follows: (1) enlargement of the digestive tract (including absorptive intestinal surface, e.g. microvilli length), (2) increase of the secretion of gastric acid and digestive enzymes, and (3) upregulation of the activity (and availability) of membrane-bound transporters in the intestinal mucosa. The upregulation of digestive function in pythons were described to be accompanied by increases in heart mass (Andersen et al., 2005; Slay et al., 2014), although some newer studies did not support this finding (Hansen et al., 2013; Jensen et al., 2011).

In particular the morphological changes listed above can be observed in many vertebrate species when fasting and digesting conditions are compared (Cramp and Franklin, 2005; Cramp et al., 2005; Cramp et al., 2009; Secor, 2005; Starck, 2005). Because they are most pronounced in sit-and-wait foraging 'reptilian' species with long fasting periods, these species have become popular model systems to study physiological and morphological responses to feeding (e.g. Andersen et al., 2005; Andrade, 2004; Hartzler and Munns, 2006; Lignot et al., 2005; Secor, 2008, 2003; Secor et al., 2000; Starck and Moser, 2004; Waas et al., 2010; Wang et al., 2001b, 2001a). To a lesser degree, these changes can also be observed in active hunting species like the garter snake (Secor et al., 2012; Starck and Beese, 2002).

Generally, there are two ways for organs to grow: cellular hypertrophy, meaning that existing cells increase in size thus causing organ size to increase, or by hyperplasia, meaning that cells proliferate and their multiplication leads to an increase of organ size. The morphological changes connected with fasting and digestion that can be observed in fishes, amphibians, and reptilian sauropsids are apparently largely based on intestinal cell hypertrophy. This hypertrophy is mainly achieved by the rapid

incorporation of lipid droplets (Lignot et al., 2005; Secor et al., 2002; Starck and Beese, 2001; Starck and Beese, 2002). Although the elongation of the microvilli have often been described (Lignot and Secor, 2002; Lignot et al., 2005; Secor, 2001; Secor, 2003; Secor, 2005; Secor, 2008; Starck and Beese, 2001; Starck and Beese, 2002; Starck et al., 2007), they have not yet been fully understood for reptilian sauropsids. E.g. in humans, an elongation of microvilli is based on the addition of further actin subunits to the existing actin filaments (Mooseker, 1982), meaning that microvilli elongation and increment of the absorptive surface is based on changes of the ultrastructure of the apical enterocytes (see also Campen and Starck, 2012). Several other mammals and birds differ from this pattern: in these taxa, the flexibility of the digestive tract is based on a dynamic balance of cell proliferation at the basis of the villi and cell death at the tip of the villi (Altmann, 1972; Boza et al., 1999; Dunel-Erb et al., 2001; Iwakiri et al., 2001; Karasov et al., 2004; Raab et al., 1998; Starck, 1996; see also Campen and Starck, 2012). Apart from hypertrophy of the enterocytes, gut size can also increase by intensified blood flow to the gut. According to Starck and Wimmer (2005), enterocyte hypertrophy and increased blood flow inflating the intestinal villi contribute equally (50:50) to the overall size increase in the gut of *Python regius*. This is a hint on the tight integration of the digestive tract and the cardiovascular system. Hypertrophy of cells caused by the absorption of lipids has been reported occasionally in mammals (Buschmann and Manke, 1981a; Buschmann and Manke, 1981b). However, data suggesting an integration with the cardiovascular system are only available for boid snakes. The dimensions and patterns of intestinal size changes in response to feeding and fasting of crocodiles are nevertheless similar to that of snakes (Starck, 2005; Starck et al., 2007).

The ingestion of large prey items that also often still contain fur/feathers and bones is especially challenging for the digestive system. Additionally, the food must stay longer in the stomach than if smaller meals are ingested more frequently. The oxyntic cells of the stomach must produce huge quantities of gastric acid. They dissociate protons from water and pump them into the stomach lumen. There, they

associate with Cl^- and form hydrochloric acid. Residual OH^- ions in the oxyntic cells associate with carbon dioxide forming HCO_3^- (hydrogen carbonate, also known as bicarbonate). This process is catalyzed by the enzyme carbonic anhydrase. To prevent alkalinisation, the hydrogen carbonate must be removed from the cells. When released into and dissolved in the blood, the hydrogen carbonate causes a rapid increase in blood pH, often referred to as the 'alkaline tide' (Coulson et al., 1950; Niv and Fraser, 2002).

Farmer et al. (2008) suggested that carbon dioxide diffusion into the oxyntic cells is the rate-limiting factor in gastric acid secretion. Thus, directing hypercapnic blood to the stomach could increase the rates of gastric acid secretion over what would be possible from glands perfused with arterial blood (see also Campen and Starck, 2012). As supported by Farmer et al. (2008), the pattern of blood flow to the gut is significantly correlated with digestive efficiency in alligators. This supports the meaning of the ability of ectotherm sauropsids to supply the digestive tract with carbon-dioxide-rich blood for gastric acid production.

When the chyme leaves the stomach to enter the duodenum and gastric acid production ceases, the alkaline tide ends. The liver secretes hydrogen carbonate and sodium hydrogen carbonate via the gall bladder into the duodenal lumen. This neutralizes the highly acidic chyme (e.g. Hofmann, 2011; Secor, 2008).

Hence, carbon dioxide cannot only improve gastric acid secretion, but it can also be an essential factor in regulating blood pH by contributing to the hydrogen carbonate buffer. About 50% of carbon dioxide produced by the metabolic activity of tissues binds directly to hemoglobin or is sequestered in erythrocytes as H_2CO_3/ HCO_3^-. Another 50% finally dissolves in blood plasma and contributes to the hydrogen carbonate buffer (e.g. Penzlin, 1991; Schmidt and Thews, 1980). Metabolic alkalosis can be balanced by increasing the carbon dioxide content of the blood: (1) by hypoventilation like in mammals and birds (Andrade, 2004; Hicks et al., 2000); and (2) by bypassing the

pulmonary circulation and re-directing carbon dioxide-enriched blood directly back into the systemic circulation.

Indeed, a growing body of evidence indicates that cardiovascular circuits and patterns of food ingestion are more tightly integrated than previously thought (Andrade, 2004; Busk and Overgaard, 2000; Farmer et al., 2008; Hicks and Bennett, 2004; Secor et al., 2000; Starck and Wimmer, 2005). This is mainly based on three observations, as reviewed by Campen and Starck (2012): (1) the size increment of the small intestine after feeding is partially based on increased blood flow volume and lymph flow to the gut (hydraulic pump mechanism; Starck and Wimmer, 2005); (2) the heart anatomy of reptilian sauropsids provides the possibility of central shunting, i.e., redirecting blood returning from the systemic circulation into the systemic circulation and bypassing the pulmonary circulation. Redirecting of carbon-dioxide-rich blood into the systemic circulation after feeding apparently maximizes gastric acid production and buffers alkaline tide (Farmer et al., 2008); and (3) the peripheral circuitry of blood supply of the stomach and the intestine suggests a tight integration of morphology and digestive function. In a detailed comparative morphological analysis, Farmer (2011) recently re-analyzed the pattern of major arteries in reptilian sauropsids and presented convincing functional explanations for a so far unresolved topographic pattern when digestive functions are included into the interpretations.

It is obvious that the cardiovascular arrangement of crocodiles enables for the systematic supply of the stomach with carbon-dioxide-rich blood. Resulting from the patterns of blood turbulences caused by the movement of the ventricle, it might be possible that the aortae of non-crocodilian ‘reptiles’ receive blood with different oxygen and carbon dioxide content although they both emerge from the *cavum venosum*. Deducing function from the topography of the major vessels, Hochstetter (1898) suggested that the pattern of vascular supply might bring more carbon dioxide-rich blood into the stomach. No empirical data yet has supported this hypothesis; but it is reasonable to assume that the timing of closure of the muscular ridge, the volume of the *cavum venosum*, and the dynamics of mixing blood in the ventricle may create

a pattern of blood flow that would result in carbon-dioxide-rich blood delivered to the digestive tract. Although the original hypothesis was posed more than a century ago, it has not been tested by measuring blood gas composition in the left and right aortae of non-crocodilian ectotherm sauropsids under different physiological conditions (Campen and Starck, 2012).

A functional integration of the cardiovascular system and the digestive system might be useful in particular for intermittent-feeding sauropsids. By bypassing the pulmonary circulation, the digesting individuals might respond very quickly to changes in the pH-balance connected to the alkaline tide of the blood. The alkaline tide occurs early during digestion. During this time, metabolic rates and oxygen demand are high (specific dynamic action; for review see McCue, 2006). Carbon dioxide retention and oxygen supply might therefore make contrasting demands to the cardiopulmonary system. A recent study by Malte et al. (2016) uses a modelling approach to determine whether hypoventilation or bypassing is the better strategy to supply the digestive tract with carbon-dioxide-rich blood but keep oxygen levels high enough to support increased postprandial metabolic rates. They conclude that hypoventilation is more effective for gastric carbon dioxide supply while it has only modest effects on oxygen delivery and should consequently be favoured by 'reptiles' during digestion.

However, if bypassing of the pulmonary circulation occurs, as assumed by Campen and Starck (2012), more on a beat-by-beat basis than for periods of several hours, it may still buffer the alkaline tide yet also provide sufficient oxygen to tissues. This short-term response has not been verified experimentally, but it would explain why the studies published so far led to such contrasting results. Former studies suggest that pulmonary or systemic bypass occurs for extended periods in the range of hours or even days. If we assume that bypass might only last for (maybe repetitive) periods of a few beats or minutes, former studies might have (in parts) missed bypass episodes. The greatest challenge for the detection of short-time bypass will nevertheless be to detect a measurable physiological signal that triggers the response (i.e., blood pH). Evidence for the integration of digestive and cardiovascular performance comes from studies on

pythons and crocodiles, both known for their long fasting periods and large meal sizes. Campen and Starck (2012) reviewed the studies that indicate a tight connection between digestion and the cardiovascular system: (1) Starck and Wimmer (2005) and Secor (2008) both measured increased blood flow volume into the gastrointestinal tract in pythons. Starck and Wimmer (2005) measured significantly increased blood flow in the liver portal vein (3-fold increase) and the mesenteric artery (ca. 30% increase) compared to predigesting values in pythons. Secor (2008) measured only the superior mesenteric artery and reported an 11-fold increase in blood flow volume in pythons. From the results of these studies it remains unclear whether this increase in blood supply of the digestive tract is a result of pulmonary bypass or of generally increased cardiac output, because blood flow measurements were performed on peripheral blood vessels. (2) Jones and Shelton (1993) suggested that bypass might play a role for digestion balancing blood pH during the crocodilian alkaline tide, but unfortunately they did not test this idea. (3) Axelsson and Fritsche (1991) could not explain the significant permanent pulsatile blood flow they measured in the coeliac artery in fasting *Crocodylus porosus*, because blood flow in the left aorta was very low. They concluded that right aortic blood enters the left aorta through the *Foramen Panizzae* and that during fasting most of the blood in the coeliac artery comes from the right aorta through the anastomosis. This blood would be oxygen-rich and carbon-dioxide-poor. After feeding, blood flow in the left aorta and coeliac artery increased and right aortic blood flow decreased. This supports the idea that carbon-dioxide-rich, oxygen-poor blood is pumped into the left aorta to supply the stomach and the anterior part of the small intestine in digesting animals. (4) According to Farmer et al. (2008) pulmonary bypass increased after feeding in *Alligator mississippiensis.* Alligators that could bypass the pulmonary circulation digested bones faster than animals that were surgically disabled to bypass the pulmonary circulation. (5) Structural changes in the digestive tract after feeding in *Caiman latirostris* are identical to those in pythons, which partly depend on increased blood flow. Starck et al. (2007) therefore suggested that blood flow into the mucosa of the small intestine of *Caiman latirostris* increases

during digestion. (6) The elevated metabolic rates in *Varanus exanthematicus* and pythons associated with digestion result in enhanced cardiac activity (Hicks et al., 2000; Secor et al., 2000). A 40% increase in ventricular wet mass was measured in *Python molurus* following feeding (Andersen et al., 2005). Increased levels of mRNA for cardiac myosin heavy chains after feeding suggest cardiac muscle protein was synthesized. Riquelme et al. (2011) report that ventricular growth after digestion in pythons is accompanied by increased activity and expression of the cardioprotective enzyme superoxide dismutase and increased transport and oxidation of special fatty acids.

Of course, all these results do not inform about a targeted navigation of blood into the digestive organs. They nevertheless underscore the importance of the integration the cardiovascular system with the digestive system.

1.2.3 Thermoregulation

Ectotherm sauropsids depend on their environment to regulate their body temperature. External heating sources like the sun or warm substrates are indispensable for them to reach a sufficiently high body temperature. One source of heat loss is via the expired air. Bypassing the lungs might therefore reduce heat loss over the lungs and the respiratory air (Tucker, 1966). Based on a study on *Iguana iguana* and *Tupinambis nigropunctatus*, Baker and White (1970) suggest that pulmonary bypass might reduce heat-loss. Heating was not only accompanied by increased ventricular output into the systemic circulation (by a factor of 2.3), but three iguanas and one tegu showed also pulmonary bypass. According to Farmer et al. (2008), crocodiles also prefer higher temperatures when they digest, which can be accompanied by pulmonary bypass. However, they might also prefer higher temperatures because it upregulates enzymatic activity during digestion.

1.2.4 Exercise

As reviewed by Campen and Starck (2012) the integration of pulmonary bypass in other functional systems affecting the acid–base system might be expected, if it is also

related to regulating post-feeding acid–base balance. Anaerobic exercise is another physiological condition that has an impact on acid-base balance. The production of lactate leads to a rapid acidification of the muscles and blood (Hicks and Bennett, 2004). Because in particular ectotherm sauropsids possess only small aerobic muscular capacities, they rely on anaerobic muscle power output. In numerous species of ectotherm sauropsids, more than one half of the energy required for intense muscle work is derived from glycolysis (Bennett, 1994; Bennett and Licht, 1972; Bennett et al., 1975; Gatten, 1984; Ruben, 1976). Lactate production and acidification of muscle cells and blood coincide (Robergs, 2004), although the protons leading to a decreased pH in the muscle and blood do not originate from the lactate itself (Lindinger, 2005), as one would expect. During anaerobic exercise of mammals, acidification of skeletal muscles is buffered mainly by the amino acid histidine and to a lesser extent by the dipeptide carnosine (β-alanine and histidine; Jones et al., 2004).

The carbon-dioxide buffer system is not important for exercising humans and they are not able to bypass the pulmonary or systemic circulation, but they do not work anaerobically to the same extent as ectotherm sauropsids. Both the carbon-dioxide buffer system and systemic bypass could help balancing the exercise-induced acidosis of reptilian sauropsids. If blood is increasingly directed into the lungs, this could improve carbon-dioxide disposal and thus antagonize the metabolically induced acidosis by a cardiac and respiratory induced alkalosis. Indeed a recent study by Filogonio et al. (2016) measured a systemic bypass in *Crotalus durissus* during activity at lower temperatures (15%), but not at higher temperatures. As the oxygen-carrying capacity of the snakes' blood is decreased at lower temperatures, they suggest that systemic bypass is connected to improved oxygen uptake during exercise. The possibility to support balancing an exercise-induced acidosis was unfortunately not discussed. Also, they did not discuss the fact that the snakes were able to induce systemic bypass despite the vagotomy, suggesting that an additional possibility to regulate systemic bypass must exist, e.g. versus systemic vasoconstriction or the timing of the closure of the muscular ridge.

Because of the heart anatomies, systemic bypass is only possible in Chelonia, Rhynchocephalia, and Squamata, but not in Crocodylia. Therefore, crocodiles cannot conter an exercise-induced acidosis by systemic bypass and have to rely on other compensation mechanisms, as hyperventilation (Hartzler et al., 2006).

1.2.5 Triggering of hypometabolism

Hicks and Wang (1999) showed that metabolic depression (hypometabolism) in freshwater turtles is triggered by a certain level of decreased blood oxygen of arteria and that this level is reached after the onset of pulmonary bypass in diving turtles. According to the authors, this condition suggests that the onset of pulmonary bypass might function as a trigger to the rapid onset of a hypometabolic state and might therefore contribute to increased aerobic diving times. Platzack and Hicks (2001) confirmed that systemic oxygen transport rather than arterial oxygen partial pressure triggers a metabolic downregulation. According to Pritchard (2002) this acute metabolic depression is caused by modulation of mitochondrial aerobic metabolism, not by pulmonary bypass.

1.3 Blood volume distribution in the crocodilian body caused by pulmonary bypass and blood flow through the *Foramen Panizzae* and the aortic anastomosis.

In all ectotherm sauropsids bypassing one or the other circulation does not only have an impact on blood gas levels, but also changes the blood volumes that reach certain organ systems or body regions per time unit. The possibility for cross-over washout shunts in Chelonia, Rhynchocephalia, and Squamates enables changes of blood oxygen and carbon dioxide content without differences in the volumes of blood that both circulations receive per time unit. As a consequence of the different cardiovascular arrangement, crocodiles differ in this respect. Blood volumes of the bypassed pulmonary circulation are added to the output into the systemic circulation. Further points to regulate the distribution of blood volume in the crocodilian body are the *Foramen Panizzae* and the aortic anastomosis. All in all, there are three sites of the crocodilian heart and outflow tract to regulate volumes of passing blood: (1) The distribution of right ventricular outflow to the pulmonary artery (regulated by the cog-teeth-like valves) and the left aorta. (2) Blood flow through the Foramen Panizzae which is determined by the diameter or area of the *Foramen Panizzae*, respectively, the degree by which it is overlapped by the left and right aortic valves, and the pressure difference between the aortae. (3) Finally, blood flow through the aortic anastomosis, which is mainly determined by the anastomosis' diameter/ cross section area and pressure differences between the aortae.

Wang and Hicks (2002, 1996) developed a model to predict maximum oxygen uptake in sauropsids with the ability to bypass the lungs and tidally ventilated lungs. This model fits well for non-crocodilian 'reptiles' in which both aortae receive blood with the same or a very similar blood gas composition and transport it to all areas supplied by systemic vessels because both aortae emerge from the *cavum venosum* (Burggren, 1987; White, 1968). In crocodiles, the aortae emerge from different ventricles and

therefore receive blood with different blood gas content. Additionally, blood exchange between the aortae is possible through the *Foramen Panizzae* and the aortic anastomosis. Consequently, the crocodilian cardiovascular morphology adds some extra difficulties to the prediction of maximum oxygen uptake by different body compartments. Based on the cardiac morphology of crocodiles and their vascular arrangement (Farmer, 2011; Hafferl, 1933; Hochstetter, 1898), four gross supply areas may receive blood with different blood gas composition (see Fig. 10): the anterior body, the posterior body, the digestive tract, and the lungs. To predict oxygen supply and carbon-dioxide disposal it is necessary to understand the distribution of blood volumes to these supply areas in dependence from pulmonary bypass and blood exchange between the aortae.

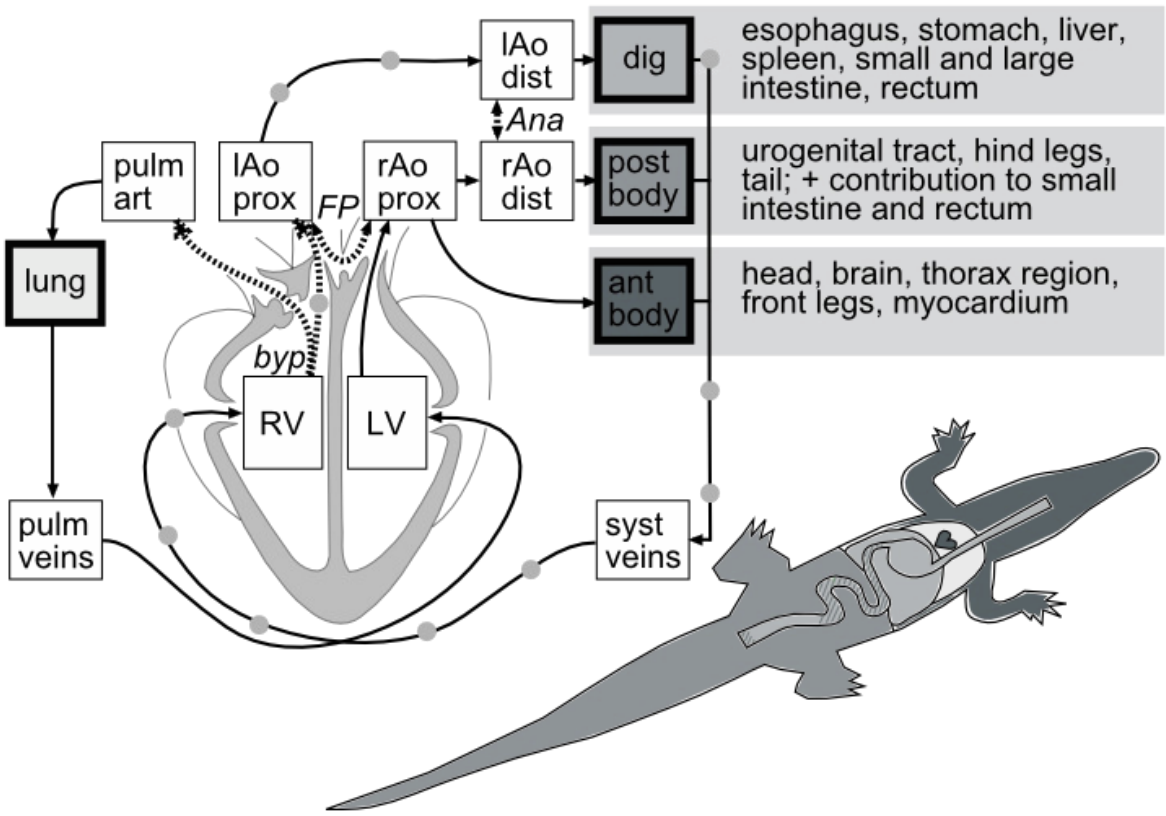

Fig. 10: Schematic illustration of the compartments (boxes), their connections (solid arrows) and the connections manipulated in the computational simulation (dotted arrows).
The connection between the right ventricle and the pulmonary artery/ left aorta (byp), the *Foramen Panizzae* (FP) and the aortic anastomosis (Ana). Capillary beds/ supply areas are highlighted by bold boxes. The route supplied during complete pulmonary bypass without flow through the *Foramen Panizzae* and the aortic anastomosis is marked with grey dots. Vascular topography is based on anatomical descriptions and drawings by Hafferl (1933) about *Crocodylus niloticus*. Compartments: LV/RV: Left/ right ventricle; lAo/rAo prox: proximal left/ right aorta; lAo/ rAo dist: distal left/ right aorta; pulm art: pulmonary arteries; dig: digestive tract; post body: posterior body; ant body: anterior body; lung: lung; syst veins: systemic veins; pulm veins: pulmonary veins.

The blood volume passing a vascular connection like the *Foramen Panizzae* or the aortic anastomosis in a certain time unit is called the volumetric flow through this connection. It depends on pressure differences between the two interconnected vessels and flow resistance following the Ohm law based formula

$$\mathbf{I = \Delta p / R}$$

With I = volumetric flow; Δp = pressure difference; R = flow resistance

Consequently, two main factors determine how much blood can flow from a vessel or vascular section to another: (1) Blood pressure differences between the vessels involved: Following physical laws, flow direction e.g. through the *Foramen Panizzae* and the aortic anastomosis must be along the pressure gradient: from the aorta with the higher pressure into the one with the lower pressure (Axelsson and Franklin, 2001; Axelsson et al., 1997), while flow will be faster with increasing pressure differences. (2) Flow resistance R which is, according to the Hagen-Poiseuille law, determined by the connection's cross section area (which can be reduced by vascular valves and vasoconstriction), the length of the vascular connection and fluid viscosity:

$$R = 8 L \eta / \pi r^4$$

with r = inside radius of the vessel, L = vessel length, and η = blood viscosity and R= Δp/ I.

However, the Hagen-Poiseuille law is only applicable for an incompressible and Newtonian fluid flowing through a cylindrical pipe in laminar flow. Flow dynamics may additionally be influenced by turbulances caused by vascular curvature and branching, vascular valves and they will differ at an opening between two blood vessels like the *Forman Panizzae*, as flow velocity at the walls of cylindrical walls is zero. Additionally, phylogenetic and ontogenetic anatomical differences might have an impact on the flow dynamics and consequently on blood distribution. To be able to model the impact of different blood flow volumes through the left aorta, the *Foramen Panizzae*, and the aortic anastomosis, a "flow coefficient" of the vascular connection in percent was introduced which is high if flow resistance is low and vice versa. This flow coefficient describes the percentage of blood that can pass the vascular connection, independent from the factors influencing this (like turbulences). Introduction of this flow coefficient enabled mathematical modelling of the degree of pulmonary bypass and blood flow through the *Foramen Panizzae* and the aortic anastomosis. For example, when the cog-teeth-like valves are entirely closed, the pulmonary circulation is completely bypassed (in the simulation: a flow coefficient of 0% of the pulmonary artery), whereas left aortic flow coefficient is maximal (100%). I assume that every degree of partial pulmonary

bypass can be achieved by incompletely closed cog-teeth-like valves. I used the flow coefficient of the connection between the proximal right and left aorta as a measure for the potential flow through the *Foramen Panizzae*. The flow coefficient of the connection between the distal right and left aorta served likewise as a measure for the potential flow through the aortic anastomosis (Fig. 10). Additionally, the introduced model operates under the simplified assumption that in vascular departments of the same size fill levels differences equal pressure differences neglecting the possibility of different wall elasticity.

Several studies indicate that the dimension of the respective structure is regulated actively, having an impact on the degree of pulmonary bypass, and blood flow through the *Foramen Panizzae* and the aortic anastomosis. A regulatory mechanism for pulmonary bypass could be the β-adrenergic tone of the heart, having an impact on the muscle constricting the cog-teeth-like valves (Axelsson and Franklin, 2001; Axelsson et al., 1997). A recent study by Joyce et al. (2014) showed that cardiac purinoceptors are ubiquitous across ‘reptiles’ and that purinergic regulation may play an important and, so far, underappreciated role in ‘reptile’ cardiovascular physiology. Adenosine and ATP might consequently have an impact on the muscle surrounding the cog-teeth-like valves and weaken the contraction force of the muscle fibers. According to Axelsson and Franklin (2001), Axelsson et al. (2001), Grigg and Johansen (1987), and Karila et al. (1995), the diameters of the *Foramen Panizzae* and the aortic anastomosis are regulated by neurotransmitters, vasoactive molecules and intestinal polypeptides. For the interpretation of the results of the simulation, it must be kept in mind that if the cross-section area of the vascular connection is assumed to be the main factor determining the flow through it apart from pressure differences, only a doubling of the radius of a vascular connection is necessary to achieve a 16-fold increase in flow through it according to the Hagen-Poiseuille law (if the pressure difference stays constant).

1.4 Research questions

1.4.1 Detailed morphology of the heart and bypass related structures of ectotherm sauropsids

In Chelonia, Rhynchocephalia, and Squamata, the extent and direction of pulmonary and systemic bypass depend on the detailed anatomy of various cardiac structures. Likewise important is the timely integration of the action of these structures, as the timing of the opening and closing of the atrioventricular valves, the anatomical structure and timing of closure of the muscular ridge, and the capacity of the *cavum venosum* and *cavum pulmonale*. In crocodiles, the extent of bypass depends on the ability of the cog-teeth-like valves to increase pulmonary vascular resistance so that blood volumes are ejected into the left aorta. The degree of blood flow through the *Foramen Panizzae* is caused by its diameter and the length of the aortic valves that might overlap it during ventricular systole. I used a variety of methodologies, two histological methods, magnetic resonance imaging (MRI), X-ray micro-computed tomography (µCT), and virtual 3D reconstruction to examine and illustrate the detailed anatomy of different bypass-related structures in snakes and crocodiles. MRI was performed in cooperation with Dr. Marcus Settles from the Institute of Radiology of the Klinikum rechts der Isar der TU München. Dr. Bernhard Ruthensteiner from the Zoological State Collection München conducted X-ray micro-computed tomography (µCT) on some crocodile hearts. I chose snakes as a representative taxon from the Chelonia, Rhynchocephalia, and Squamata, because most physiological and morphological work on the heart and circulatory system was conducted on snakes.

The morphological part of the thesis contributes to following open questions concerning **snakes**:

- How long are the atrioventricular valves of various species of snakes in comparison to the size of the interventricular canal and do the valves overlap

the canal? Can blood streams from the right and left atrium be effectively separated during ventricular diastole?

- How are the muscular ridge and the 'bulbuslamelle' positioned? Do they enable complete separation of the *cavum venosum* and *cavum pulmonale* during systole? Is pressure separation between the systemic and pulmonary circulation possible?
- How are the relative sizes of the three cava? Does the *cavum venosum* enable large washout shunts?
- How do these morphological features differ in snakes from various taxa, and can a connection to the species' ecology or phylogeny be identified?

I tried to answer the following questions concerning **crocodilian** cardiac anatomy:

- How long are the aortic valves? Can they completely overlap the *Foramen Panizzae* during systole, when they are pressed against the aortic walls by the blood stream?
- How is the cranial part of the myocardium arranged in relation to the cog-teeth-like valves? Could it press the cog-teeth-like valves together, increasing pulmonary vascular resistance and initiating pulmonary bypass?
- How is the cartilage clasp surrounding the *Foramen Panizzae* structured three-dimensionally?

1.4.2 Blood volume redistribution caused by pulmonary bypass and blood flow through the *Foramen Panizzae* and the aortic anastomosis in crocodiles

In cooperation with Prof. Dr. Dirk Metzler and Dr. Meike Wittmann (Statistical Genetics Group) and Dr. Philipp Rautenberg (German Neuroinformatics Node GNode), all of the Biocenter of the Ludwig-Maximilians-Universität München, I developed a computational simulation model of blood flow. This model should spend light on the

effects of regulation of blood volume by the left aorta, the *Foramen Panizzae*, and the aortic anastomosis. I aimed to understand the effect of these blood flows on:

- blood supply of the different regions of the crocodilian body
- left and right ventricular return
- physiological parameters used in experimental studies, like stroke volume, a key component of cardiac output, and the ratio of pulmonary blood flow (Q_{pul}) to systemic blood flow (Q_{sys})
- volume and flow direction of blood flowing through the *Foramen Panizzae* and the aortic anastomosis.

2 Material and Methods

2.1 Morphology of bypass-related structures in the heart of ectotherm sauropsids

2.1.1 Material

All species /organs used for the morphological part of the thesis are listed in Table 1.

Photos, short descriptions and a phylogeny of the species are given in Fig. 11 and 12.

2.1.2 Classical histology, H&E stain

The alcohol stored heart of a juvenile *Crocodylus niloticus* (material no. 10) was embedded in paraffin and cut into 10 µm thick sections. H&E staining was performed on deparaffined and in descending alcohol dehydrated sections following the standard protocol as given in Aescht et al. (2010). To photograph the images, the covered sections were placed on a stereomicrotome (SZX7, Olympus, Tokio, Japan) with a microscope camera (DP20, Olympus, Tokio, Japan). Photographs were taken using cellSens Imaging Software, Version 1.7. (Olympus, Tokio, Japan), with a resolution of 1200 x 1600 pixels.

Table 1: Animal material used for the morphological part of the thesis.
All material was stored in EtOH 70% at study start. Earlier storage is uncertain. The following abbreviations are used for the location of storage: *ZSM*: Bavarian Natural History Collections, The Bavarian State Collection of Zoology, Section for Herpetology; *LMU Bio*: Ludwig-Maximilians-University of Munich, Department Biology II, Functional Morphology Group.

Species	Material No.	Storage	Source	Cataloging no./ Former microchip no.	Object	Developm. stage	Sex	Body mass (g)	Date and location of death	Imaging method
Serpentes										
***Aphrotyphlops punctatus* LEACH 1819**	**01**	ZSM	H. Mühle leg.	ZSM 60/1985	entire animal	adult	unknown	unknown	01/ 1985: Tansania, near Geita (south of Lake Victoria)	MRI
***Bogertophis subocularis* BROWN 1901**	**02**	ZSM	presumably animal trade	uncatalogued	entire animal	adult	unknown	unknown	unknown	MRI
***Crotalus culminatus* KLAUBER 1952**	**03**	ZSM	animal trade	ZSM 89/1988	entire animal	adult	unknown	unknown	Before 1986; Mexico	MRI
***Pantherophis guttatus* LINNAEUS 1766**	**04**	LMU Bio	private property of the Vohberger family, Hilgertshausen	uncatalogued	entire animal	adult	unknown	unknown	06/2011; Hilgertshausen	MRI
***Python molurus* LINNAEUS 1758**	**05**	LMU Bio	animal trade	Python molurus 3/ 66CD6FB	heart	adult	unknown	4500	07/2006; Planegg-Martinsried	MRI

Species	Material No.	Storage	Source	Cataloging no./ Former microchip no.	Object	Developm. stage	Sex	Body mass (g)	Date and location of death	Imaging method
Crocodilia										
Caiman crocodilus **LINNAEUS 1758**	**06**	ZSM	presumably animal trade	uncatalogued	heart	juvenile	unknown	unknown	unknown	µCT
Caiman crocodilus **LINNAEUS 1758**	**07**	ZSM	presumably animal trade	uncatalogued	heart	juvenile	unknown	unknown	unknown	µCT
Caiman crocodilus **LINNAEUS 1758**	**08**	ZSM	presumably animal trade	uncatalogued	heart	juvenile	unknown	unknown	unknown	µCT
Crocodylus niloticus **LAURENTI 1768**	**09**	LMU Bio	animal trade	Croco 5/ 66BFF72	heart	juvenile	female	2200	11/2008; Planegg-Martinsried	histology
Crocodylus niloticus **LAURENTI 1768**	**10**	LMU Bio	animal trade	Croco 6/ 670F54A	heart	juvenile	female	3000	11/2008; Planegg/ Martinsried	histology
Crocodylus niloticus **LAURENTI 1768**	**11**	LMU Bio	animal trade	Croco 8/ 66BEDB1	heart	juvenile	unknown	2322	09/2008; Planegg-Martinsried	µCT
Crocodylus porosus SCHNEIDER 1801	**12**	LMU Bio	Donation of Chris Tracey, University of Melbourne	uncatalogued	heart	adult	unknown	unknown	05/2009; Australia	MRI + µCT

Afrotyphlops punctatus LEACH 1819

Higher taxa: Typhlopidae (Afrotyphlopinae), Typhlopoidea, Serpentes

Distribution
S Mauritania ?, Senegal, Gambia, Guinea Bissau, S Mali, Ivory Coast, Burkina Faso, Ghana, Togo, Benin, Nigeria, SW Chad, Central African Republic, Cameroon, Uganda, SW Ethiopia, Bioko = Fernando Po I, N Democratic Republic of the Congo (Zaire), Sierra Leone, Guinea, Sudan

Characteristics
- non-venomous
- feeding on ants and termites
- ground-dwelling
- blind
- body lenght: up to 50 cm

Bogertophis subocularis BROWN 1901

Higher taxa: Colubridae, Colubrinae, Lampropeltini, Colubroidea, Serpentes

Distribution
USA (S New Mexico, W Texas), Mexico (NE Chihuahua, Coahuila, NE Durango)

Characteristics
- non-venomous
- feeding on small vertebrates
- nocturnal
- lifes on desert flats and brushy slopes
- oviparous
- body length: up to 150 cm

Crotalus culminatus KLAUBER 1952

Higher taxa: Viperidae, Crotalinae, Serpentes

Distribution
Southwestern USA, Mexico (Michoacan, Oaxaca, Morelos)

Characteristics
- venomous
- feeding on small vertebrates
- lives in the open savannah
- viviparous
- body length: up to 150 cm
- sit-and-wait predator

Pantherophis guttatus LINNAEUS 1766

Higher taxa: Colubridae, Colubrinae, Lampropeltini, Colubroidea, Serpentes

Distribution
USA (Arkansas, Mississippi, Alabama, South Carolina, North Carolina, Kentucky, Tennessee, Virginia, Maryland, Delaware, West Virginia, New Jersey, Florida, Texas, Louisiana, Georgia), Cayman I, US Virgin Islands, Anguilla, Antigua, St. Bartélmy

Characteristics
- non-venomous
- feeding on small vertebrates
- lives in forests and meadows
- viviparous
- body length: up to 150 cm
- nocturnal sit-and-wait predator

Python molurus LINNAEUS 1758

Higher taxa: Pythonidae, Henophidia, Pythonoidea, Serpentes

Distribution
Pakistan, India (Assam, Himachal Pradesh, Gujarat, Madhya Pradesh, Kerala, Tamil Nadu, Andhra Pradesh, Karnataka, Maharashtra, Punjab, Nepal, Bhutan, Myanmar, Vietnam, Sri Lanka, USA (introduced and established in Florida

Characteristics
- non-venomous
- feeding on vertebrates
- lives terrestrial and arboreal, sometimes semi-aquatic in forests
- viviparous
- body length: up to 300 cm
- nocturnal sit-and-wait predator

Caiman crocodilus LINNAEUS 1758

Higher taxa: Alligatoridae, Crocodylia

Distribution
Brazil (incl. Mato Grosso), Colombia, Costa Rica, Ecuador, El Salvador, Guatemala, Honduras, Mexico, Nicaragua, Panama, Peru (Pasco etc.), Surinam, French Guiana, Guyana, Tobago, Trinidad, Venezuela, BoliviaCuba (introduced), Isla de Juventud (=Isla dePinos; introduced), Puerto Rico (introduced), Lesser Antilles (introduced ?),USA (introduced to Florida, Texas)

Characteristics
- feeding on snails and arthropoda, fishes and other vertebrates
- lives semiaquatic in wetland and rivers
- aestivation during harsh environmental conditions
- oviparous
- body length: up to 300 cm

Crocodylus niloticus LAURENTI 1768

Higher taxa: Crocodylidae, Crocodylia

Distribution
Angola, Benin, Botswana, Burkina Faso, Burundi, Cameroon, Central African Republic, Chad, Congo, Egypt, Ethiopia, Equatorial Guinea, Gabon, Gambia, Ghana, Guinea, Guinea Bissau, Ivory Coast, Kenya, Liberia, Madagascar, Nosy Faly, Malawi, Mali, Mozambique, Namibia, Niger, Nigeria, Rwanda, Senegal, Sierra Leone, Somalia, South Africa, Sudan, Swaziland, Tanzania, Togo, Uganda, Zaire, Zambia, Zimbabwe.

Characteristics
- feeding on arthropoda up to vertebrates of all sizes
- lives semiaquatic in lakes, rivers, freshwater swamps, brackish water
- oviparous
- body length: up to 600 cm
-

Crocodylus porosus SCHNEIDER 1801

Higher taxa: Crocodylidae, Crocodylia

Distribution
Australia, Bangladesh, Brunei, Myanmar (= Burma), Cambodia, China, India (including Andaman Islands, Nicobar Islands), Indonesia (Java, Sulawesi, Komodo), Malaysia, Palau (Caroline Islands) , Papua New Guinea, Philippines, Singapore, Sri Lanka, Solomon Islands, Thailand, Vanuatu (Banks Islands), Nauru?, Micronesia, Vietnam.

Characteristics
- feeding on arthropoda up to vertebrates of all sizes
- lives semiaquatic in brackish water around coastal areas and in rivers
- oviparous
- body length: up to 600 cm

Fig. 11: Distribution and ecology of the species used for the morphological part of the work.
All information on the distribution and systematics comes from www.reptile-database.org (16.09.2014). The rare information on the ecology of Typhlopidae/ *Afrotyphlops punctatus* comes from Akani et al. (2008) and Wallach and Ineich (1996), on *Bogertophis subocularis* from Rhoads (2008), on *Crotalus culminatus* from Campbell and Lamar (2004), on *Pantherophis guttatus* from Köhler (2005), on *Python molurus* from Walls (1998), and on all crocodilian species from Ross (2002).

Snakes

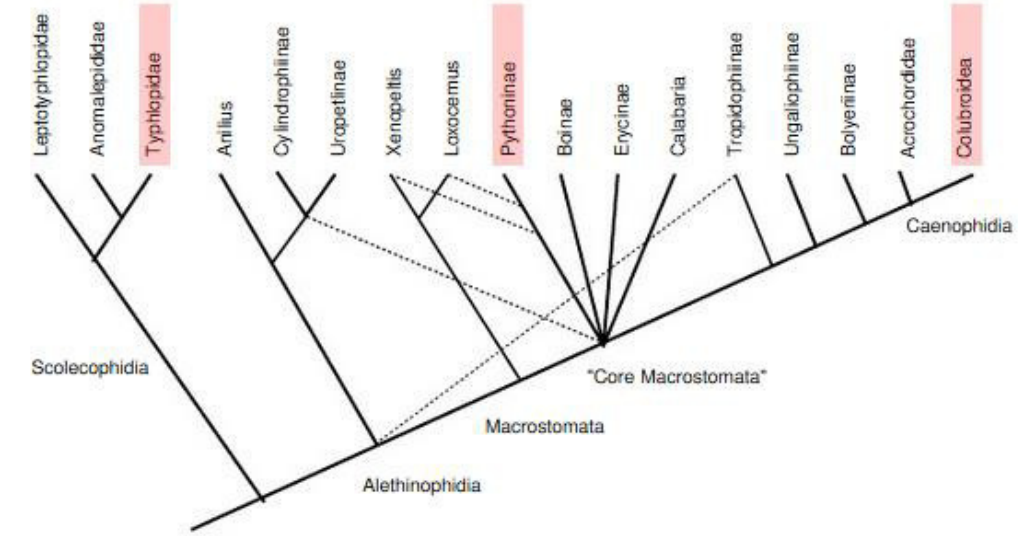

Crocodiles

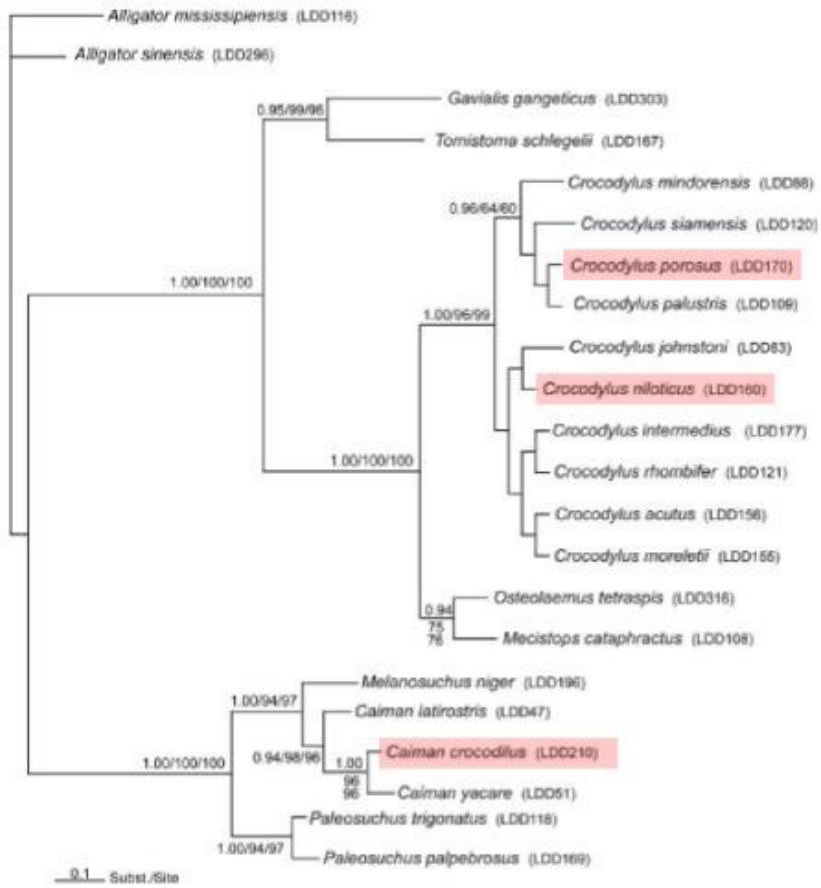

Fig. 12: Phylogenetic classification of the examined snake and crocodile species.
The examined families (snakes) or species (crocodiles) are marked in red. Snakes: Typhlopidae: *Afrotyphlops punctatis*; Pythonidae: *Python molurus*; Colubroidae: *Bogertophis subocularis*, *Crotalus culminatus*, *Pantherophis guttatus*. The phylogeny of snakes and crocodiles is continuously revised. The presented phylogeny of snakes is from Lee et al. (2007), the phylogeny of crocodiles by Willis (2009).

2.1.3 Sliding microtome planer method

This method was inspired by the 'Heidelberger Hobel' (Denk and Horstmann, 2004) and invented by myself to avoid shrinking and deformation of the material, a problem that often occurs during histological cutting and staining processes in organs with large cava. I used the heart of a juvenile *Crocodylus niloticus* for this method (material no. 09) and embedded it in paraffin. The block was fixed in a sliding microtome. A stereomicroscope (SZX7, Olympus, Tokio, Japan) with a microscope camera (DP20, Olympus, Tokio, Japan) was positioned on a custom-made wooden pedestal and fixed with bar clamps (Fig. 13). It was adjusted to a position and height that enabled to produce focused and centered photos of the paraffin block surface after being cut by the knife of the slide microtome. I cut slices of 10 µm. After every fourth section (every 40 µm), the surface of the block was stained using methylene blue soaked cotton wool wrapped around forceps. The methylene blue was allowed to work for around 3 seconds on the organ cut surface. Spare methylene blue was then removed with clean cotton wool and wool fibers stuck to the surface were removed carefully. A photograph was taken with the microtome using cellSens Imaging Software, Version 1.7 (Olympus, Tokio, Japan), with a resolution of 1200 x 1600 pixels. As the microtome knife height is fixed while the paraffin block is gradually lifted, the surface of the block remained at the same distance from the camera. Thus, no new focusing was necessary and no consequent increase or decrease of the object's size on the photographs caused by different distances from the camera occurred. The 10 µm thick ‚planing chips' were collected and could be processed into the normal H&E staining procedure (see 2.1.2) during which most of the methylene blue stain is eluted.

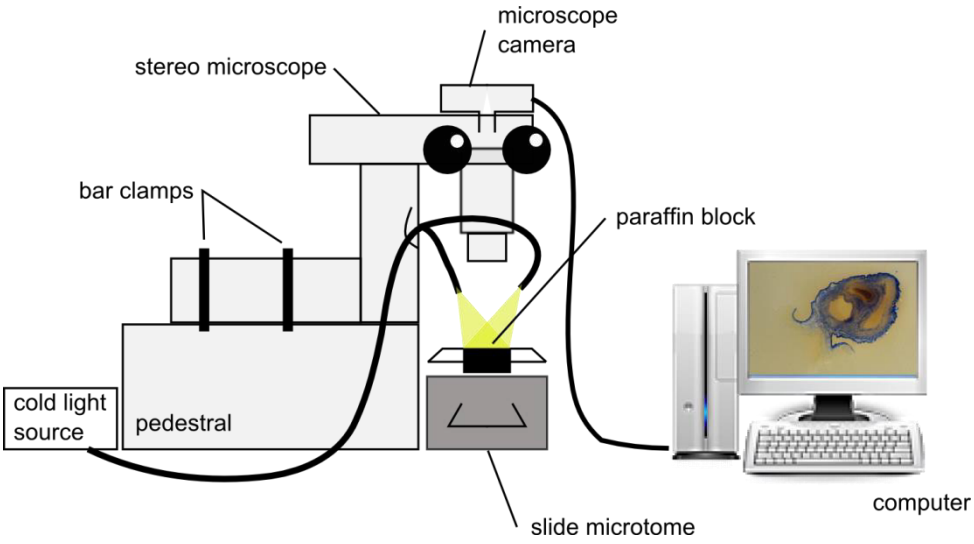

Fig. 13: Schematic illustration of the organization of technical components used for the 'Sliding microtome planer method'.

2.1.4 Magnetic resonance imaging (MRI)

MR imaging was performed on a 1.5 Tesla Philips Achieva clinical scanner (Best, the Netherlands) equipped with the Nova Dual gradient system at the Institute of Radiology at the TUM Klinikum rechts der Isar, München, Germany. I scanned the heart when isolated organs were available, and the heart region in complete specimens where the hearts could not be removed (rare and valuable collection material). I scanned isolated hearts in a closed plastic bin of a suitable size in 70% EtOH. Complete specimens were wrapped in plastic film to prevent them from drying-out during scanning. Different scan times are owed to the different degrees of capacity utilization of the clinically used MRI scanner. I did not use any contrast agents for MRI. The following species were scanned with the given settings and configurations:

***Afrotyphlops punctatus* (material no. 01):** We used a 3D turbo spin echo sequence with a spatial resolution of 0.13 mm isotropic, a repetition time TR of 1000 ms together with a DRIVE pulse, an echo time TE of 95 ms, an echo train length of 9, four averages and a total scan time of 22 h 2 min. The 47 mm Microscopy coil was used for signal reception.

***Bogertophis subocularis* (material no. 02):** We used a 3D turbo spin echo sequence with a spatial resolution of 0.13 mm isotropic, a repetition time TR of 1000 ms together with a DRIVE pulse, an echo time TE of 95 ms, an echo train length of 9, two averages and a total scan time of 14 h 15 min. The 47 mm Microscopy coil was used for signal reception.

***Crotalus culminates* (material no. 03):** We used a 3D turbo spin echo sequence with a spatial resolution of 0.20 mm isotropic, a repetition time TR of 1000 ms together with a DRIVE pulse, an echo time TE of 95 ms, an echo train length of 11, three averages and a total scan time of 11 h 21 min. The 4-channel Wrist coil was used for signal reception.

***Pantherophis guttatus* (material no. 04):** We used a 3D turbo spin echo sequence with a spatial resolution of 0.10 mm isotropic, a repetition time TR of 1000 ms together with a DRIVE pulse, an echo time TE of 95 ms, an echo train length of 9, two averages and a total scan time of 14 h 55 min. The 23 mm Microscopy coil was used for signal reception.

***Python molurus* (material no. 05):** We used a 3D turbo spin echo sequence with a spatial resolution of 0.13 mm isotropic, a repetition time TR of 1000ms together with a DRIVE pulse, an echo time TE of 95 ms, an echo train length of 9, four averages and a total scan time of 22 h 2 min. The 47 mm Microscopy coil was used for signal reception.

***Crocodylus porosus* (material no. 12):** We used a 3D turbo spin echo sequence with a spatial resolution of 0.25 mm isotropic, a repetition time TR of 1000 ms together with a DRIVE pulse, an echo time TE of 95 ms, an echo train length of 11, six averages and a total scan time of 25 h 12 mins. The 2-channel SENSE FlexS coil was used for signal reception.

2.1.5 X-ray micro-computed tomography (µCT)

2.1.5.1 Contrasting

Before scanning, the hearts (stored in 70% ethanol) were contrasted with various alcoholic iodide solutions (see Table 2) following standard protocols. I used various compositions of the staining agents to test the impact of different proportions of H_2O and EtOH in the contrast agent on scanning results.

Table 2: Iodide solutions used for contrasting before µCT.

No.	Composition	Used for material no.
(1)	1 g I_2 + 100 ml EtOH 100%	08, 11
(2)	1 g I_2 + 100 ml EtOH 80%	06, 12
(3)	80 ml (1) + 20 ml (4)	07
(4)	Degenhardt's Logol Iodide: 10 g KI + 5 g I_2 + 100 ml H_2O, diluted 1:3 in H_2O and saturated with I_2	

2.1.5.2 Scanning

Scanning was performed on a Phoenix Nanotom m (GE Measurement & Control, Wunstorf, Germany) cone beam CT scanner at The Bavarian Zoological State Collection, München, Germany. The following species were scanned with the given settings and configurations:

***Caiman crocodilus* (material no. 06):** We scanned at a voltage of 120 kV and a current of 120 mA for a total scan time of 12 mins with 1440 projections and a spatial resolution of 0.0107 mm isotropic.

***Caiman crocodilus* (material no. 07):** We scanned at a voltage of 120 kV and a current of 120 mA for a total scan time of 12 mins with 1440 projections and a spatial resolution of 0.0088 mm isotropic.

***Caiman crocodilus* (material no. 08):** We scanned at a voltage of 120 kV and a current of 120 mA for a total scan time of 8.3 mins with 1000 projections and a spatial resolution of 0.0071 mm isotropic.

***Crocodylus niloticus* (material no. 11):** We scanned at a voltage of 70 kV and a current of 120 mA for a total scan time of 96 mins with 1440 projections and a spatial resolution of 0.0188 mm isotropic.

***Crocodylus porosus* (material no. 12):** We scanned at a voltage of 100 kV and a current of 90 mA for a total scan time of 12 mins with 1440 projections and a spatial resolution of 0.0470 mm isotropic.

2.1.6 3D reconstructions

The image series were converted from RGB color to grayscale and contrast enhanced with GIMP 2.8.1 (GNU Image Manipulation Program, http://www.gimp.org). The preprocessed images were loaded into Amira® 5.6 (FEI Visualization Sciences Group, Berlin, Germany), aligned, and segmented. The segmentation process included the manual selection of the profiles of organs or other structures from every photographed histological slice, MRI or X-ray microtomography image and their assignment to different anatomical structures (‘materials’). Interpolation between slices was used to bridge missing or damaged slices from histology and to generate a smoother 3D surface. On basis of the different materials, surfaces were rendered, smoothed and displayed under any defined angle, color, transparency, and material composition. Selected views of the digital 3D-models were virtually “photographed” using the software-integrated snapshot tool.

2.2 Computational simulation

The crocodilian blood circulatory system was modeled as a number of inter-connected compartments of various size (Fig. 10). Each one of these compartments receives blood from one or more donor compartments and, in turn, passes blood to one or more acceptor compartments. The simulation model tracks, how the current fill level of each compartment changes over time. Transfer is regulated by the model parameters: the minimum and maximum volumes of each compartment and a matrix of flow coefficients that regulates the distribution of blood volumes in cases where there is more than one acceptor compartment (see Fig. 14).

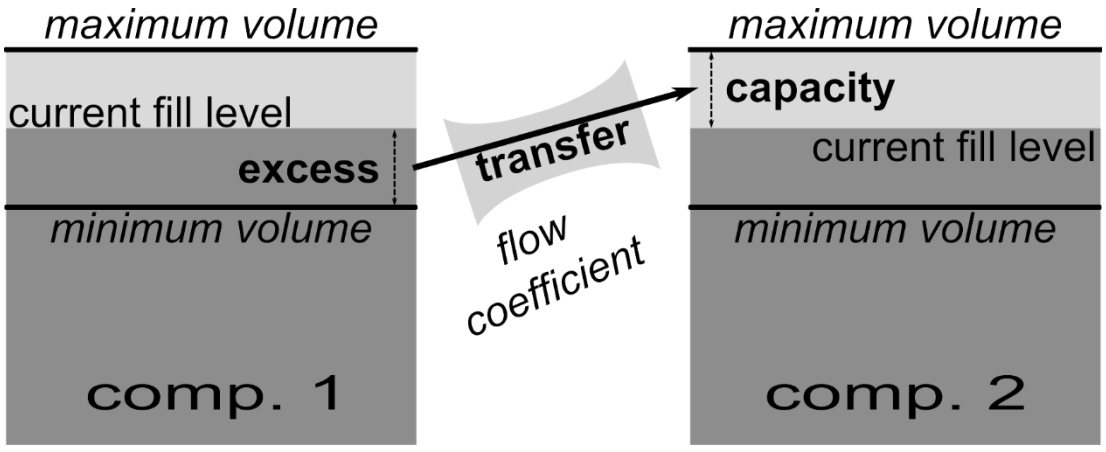

Fig. 14: Visualization of the transfer of blood volumes from one compartment to the next. Fixed parameters are the compartments minimum and maximum volume and, within one scenario, the flow coefficient of the connections. The compartments current fill level changes depending on transfer of blood volumes to and from the compartment. The compartment's excess and capacity depend on its current fill level. Excess, capacity, and the flow coefficient of the specific connection together determine the transferred blood volume.

2.2.1 Model parameters

The model parameters had to be deduced from the closest data available, since data on inner volumes of vascular beds are currently not available in the literature for crocodiles. Table 3 summarizes the chosen default model parameter settings for compartment sizes. The numbers result from a combination of crocodilian organ masses from Hoffman et al. (2000), complemented by values that were extrapolated from human vascular bed inner volumes or blood volume distribution from Elad and Einav (2004). Table 4 includes background information on the values and how I adapted them. To allow fill levels to function as an approximation to pressure differences, I assigned equal volumes to the anterior and posterior left and right aortae. Based on the relative compartment sizes, I obtained minimum compartment volumes by subtracting a certain percentage of the compartment size, and maximum volumes by adding the same percentage. I used various percentages for arteries (15%), capillaries (25%), and veins (35%), to represent differences in vascular compliance. I chose larger values for veins than for arteries, because in humans (and thus supposedly also in crocodiles), venous compliance is larger than arterial compliance (e.g. Gelman, 2008).

2.2.2 Definitions

I defined a compartment's capacity as the difference between maximum volume and current fill level, and its excess volume as the difference between current fill level and minimum volume (Fig. 14). Blood flow was simulated by subtracting a transfer volume from the donor compartment's excess volume and adding it to the acceptor compartment's fill level. Consequently, transfer volume is restricted by two numbers: by the donor compartment's excess and the acceptor compartment's capacity, together representing pressure differences between the compartments. The simulation algorithm is documented as an appendix at the end of this thesis.

Table 3: Distribution of total blood volume in the compartments at the start of the simulation, compartment type and subsequent minimum and maximum volumes.
Start blood volumes equal compartment sizes with exception of the ventricles (see text). Start blood volumes add up to 100% total blood volume.

Compartment	Compart-ment type	Compartment minimum volume	Distribution of blood volumes at the beginning of the simulation	Compartment maximum volume
			[% of total blood volume]	
Left ventricle	Ventricle	1.000	3.000	3.000
Right ventricle	Ventricle	1.000	3.000	3.000
Proximal right aorta	Arteries	3.825	4.500	5.175
Proximal left aorta	Arteries	3.825	4.500	5.175
Distal right aorta	Arteries	3.825	4.500	5.175
Distal left aorta	Arteries	3.825	4.500	5.175
Pulmonary arteries	Arteries	1.700	2.000	2.300
Lung	Capillaries	2.250	3.000	3.750
Anterior body	Capillaries	3.000	4.000	5.000
Posterior body	Capillaries	3.375	4.500	5.625
Digestive tract	Capillaries	3.375	4.500	5.625
Pulmonary veins	Veins	2.600	4.000	5.400
Systemic veins	Veins	35.100	54.000	72.900
SUM			**100.000**	

Table 4: Estimation of total blood volume distribution in the compartments at the start of the simulation based on human and crocodilian data. The relative inner volumes of the used sections of vascular beds are not available for crocodiles. Here, I summarize how I deduced compartment sizes from a combination of blood volume distribution in humans (Elad and Einav, 2004) and crocodilian organ masses (Hoffman et al. 2000) and which adaptations were conducted.

Compartment	Distribution of blood volumes at the beginning of the simulation (% of total blood volume)	Reference values	Species	Adaptation/Comment
left ventricle/ right ventricle	3.0 / 3.0	7% of blood volume in the heart (both atria and both ventricles)	Humans	7 % - 1% (assumed atrial volume is small when ventricles are filled), further explanation in the text
proximal right aorta/ proximal left aorta/ distal right aorta/ distal left aorta	4.5 / 4.5 / 4.5 / 4.5	13% of 84% (≈ 11%) of total blood volume in all systemic arteries	Humans	Increased to 18% because of presence of two aortae in crocodiles; volumes of larger arteries branching off the aortae are included into this volume; all sections of the aortae were assigned the same volumes to allow fill levels to function as approximation for pressure
pulmonary arteries/ lung/ pulmonary veins	2.0 / 3.0 / 4.0	9% of total blood volume in all pulmonary vessels	Humans	Adopted as it stands; veins were assigned larger volume than arteries because veins contain larger volume also in the systemic circulation
digestive tract/ anterior body/ posterior body	4.5 / 4.0 / 4.5	7% of 84% (≈ 6%) of total blood volume in **all** systemic capillaries, suggesting a distribution of 2% of total blood volume for each the digestive tract, the anterior body, and the posterior body of crocodiles	Humans	Compromise between human capillary blood volumes (arteriole and venule volumes missing) and crocodilian organ masses; crocodilian organ masses suggest a relatively even distribution of around 15% of body mass for each of these supply areas; Bones and fat of anterior and posterior body probably relatively low perfused; Attribution of volumes to all other compartments left 13% of total blood volume for the three systemic supply areas. We distributed these 13% relatively evenly to the systemic supply areas. The posterior body was chosen to contain slightly more blood than the anterior body due to the muscular tail of crocodiles.
		Digestive tract: Mass of liver, gastrointestinal tract und gut fat is 12.3% of total body mass (spleen and pancreas probably missing); Mass of **Anterior and posterior body:** Mass of both compartments together is 34.3% of total body mass (without bones, fat and skin);	Nile crocodiles	
systemic veins	54.0	64% of 84% (≈ 54%) of entire blood volume in the systemic veins	Humans	Adopted as it stands

2.2.3 Calculation of blood distribution

If a compartment is connected to more than one acceptor compartment, blood distribution is weighted by excess and capacity of the compartments involved as usually (representing pressure differences), but is additionally weighted by the flow coefficient of the connection between the compartments (representing different diameters of the vascular connection and possible additional factors like turbulences). Flow coefficients of connections can range between 0% and 100%. All flow coefficients of a donor compartment to its acceptor compartments add up to 100%. The flow coefficient of the connection between proximal right aorta and anterior body was set to 20% for all simulations. At the sites where regulation of blood flow distribution is possible, i.e. where a donor compartment was connected to more than one acceptor compartment, flow coefficients of the connections were manipulated to test their impact on parameters of interest. This is at the right ventricle and between the proximal and distal right and left aortae (see Fig. 10).

2.2.4 Implementation of cardiac dynamics

To allow for parameter changes within the heart cycle and thereby approximate cardiac dynamics, the time span of one heartbeat was subdivided into 100 time steps. A proportion p of the excess volume is assumed to be transferred to the next compartment in each of the 100 time steps. This would lead to a geometric (approximately exponential) decay of the excess volume, reducing it by a factor thousand over the time of one heartbeat if there was no input into the compartment.

To simulate ventricular pumping, the 100 time steps per heartbeat were assigned to systole and diastole. During diastole (time steps 1-70), ventricular input was allowed, but output was prohibited and vice versa during systole (time steps 71-100). The chosen relative duration of systole and diastole resembles human cardiac dynamics: At a heart rate of 70 bpm, the durations of diastole and systole in humans are 0.5 and 0.3 seconds, respectively (Elad and Einav, 2004). This results in a diastole:systole ratio of

1.7. Relative diastolic duration increases with decreasing heart rates. Crocodilian heart rates are temperature-dependent, but generally lower than 70 bpm, often around 40 bpm (Altimiras et al., 1998; Davies et al., 1951; Munns et al., 2005; Zhao-Xian et al., 1991). Therefore, relative diastolic duration is probably longer than in humans with 70 bpm. Consequently, I increased relative diastolic duration, resulting in a diastole:systole ratio of 2.3. When these relative durations of systole and diastole are compared with the relative duration of blood flowing from the contracting ventricles into the large pulmonary and systemic vessels, e.g. as recorded by Eme et al. (2009), it is realistic that diastole is approximately twice as long as systole. This is also in agreement with observations of the pumping crocodile heart under echocardiographic observation performed in our lab (unpublished data).

The maximum volume of each ventricle was set to 3% and the minimum volume of each ventricle to 1% of total blood volume. Consequently, every ventricle could pump maximally 2% of total blood volume per heartbeat, resulting in 4% for both ventricles. Elad and Einav (2004) reported that the human heart (both ventricles and both atria) contain a mean of 7% of total blood volume. Since the atria were not modelled in the simulation, it seems realistic that maximum cardiac stroke volume is 4% of total blood volume.

2.2.5 Simulated scenarios

I simulated 396 different scenarios that are characterized by all combinations of flow coefficients of the left aorta (11 different flow coefficients, from 0-100% left aortic flow coefficient in steps of 10%), the *Foramen Panizzae* (6 different flow coefficients, from 0-50% *Foramen Panizzae* flow coefficient in steps of 10%) and the aortic anastomosis (6 different flow coefficients, from 0-50% aortic anastomosis flow coefficient in steps of 10%). I decided to simulate maximum *Foramen Panizzae* and aortic anastomosis flow coefficients of 50%, meaning the flow coefficient (as well as the diameter and the cross section) of the *Foramen Panizzae* and the following aortic section are equal. This includes all values reported in literature. It must be kept in mind that due to $P = \pi * r^2$,

a doubling of the inner radius r of a vascular connection leads to a fourfold increase in its inner cross section area P.

Because the aortic valves overlap the *Foramen Panizzae* during systole and consequently obstruct flow (Axelsson et al., 1997; Webb, 1979; morphological part of this thesis), blood flow through the *Foramen Panizzae* was limited to diastole. As there are no heart-cycle dependent obstructions to blood flow, flow through the aortic anastomosis was allowed throughout the heart cycle.

500 heartbeats, i.e. 500 times 100 time steps, were simulated for each scenario, starting with fill levels set to the respective compartment size. The main analyses are based on the dynamics during the last heartbeat of the simulation (heart beat 500). I graphed the input into the capillary beds of the lungs, the anterior and posterior body regions, and the digestive tract, as well as net blood flow through the *Foramen Panizzae* and the aortic anastomosis, total cardiac stroke volume and the ratio of Q_{pul}/Q_{sys}.

3 Results

3.1 Morphology

3.1.1 Results achieved with the different methods used for heart anatomy imaging

3.1.1.1 Classic histology, H&E staining

Classical histology and H&E staining delivers contrast-rich images with a very high spatial resolution that is only limited by the human eye, the used microscope and digital camera. Haematoxilin stains acidic structures, therefore nuclei become blue/violet. Eosin stains intracellular or extracellular proteins like cell plasma in a pinkish color. The resulting images of HE-staining are highly detailed and contrast-rich, being suitable for the quantification of cells and nuclei and their spatial density as well as contrast-rich survey views of organs (Fig. 19 D). It is easy to distinguish different tissue types including cartilage. The high resolution is of advantage for the 3D reconstruction of fine structures like the aortic valves. The disadvantage is, however, that the organ is physically destructed during the cutting process (but the slides can be stored). Additionally, the histological preparation process, even if carefully conducted, can lead to shrinkage, deformation or destruction, especially in organs with large cavities, like hearts and vessels. This makes 3D reconstruction difficult, because deformed sections cannot be aligned in a way that produces a smooth surface reconstruction (Fig. 20 D). Interpolation of severely deformed sections is possible in Amira, but it also reduces reliability of the reconstructed surfaces if used too often.

3.1.1.2 Sliding microtome planer method

I developed the sliding microtome planer method to avoid the deformation of the sections occurring during classical histology and to increase the reliability of the 3D reconstructions. The method reached this goal producing images that can be aligned

perfectly. However, the method revealed also some disadvantages concerning the identifiability of the surfaces in contrast to the organ structures deeper in the nearly transparent paraffin block, especially if they were dark. The unstained heart and vessels in the depth of the paraffin block appear yellowish and can therefore be well distinguished from the blue-stained surface. Illumination of the block from the sides with a mobile cold-light source brightens up the heart in the paraffin block and improves the contrast. However, remaing blood volumes in the heart cavities are problematic, because they appear as brown-black blurs that poorly contrast to the dark blue stained material surface. This impedes the identification of the material surface for segmentation during 3D reconstruction. To avoid this effect, I tried to make the paraffin block nontransparent by admixing the lipophilic dye Sudan Black and leave the block surface unstained. However, I did not find a mixture that was sufficiently nontransparent black without also staining the complete embedded organ. Sudan Black infiltrates the heart with the paraffin, staining it greyish, thus not increasing the contrast between the organ and the paraffin as intended.

3.1.1.3 Magnetic resonance imaging (MRI)

MRI (as well as µCT) leave the scanned organ undestroyed and produce a perfectly aligned three-dimensional image stack. Slice shrinking or deformation, missing slices or accidental diagonal shifting of the aligned images are excluded by this method.

Two conflicting demands had to be met by the chosen receptor coil: 1) the resolution should be as good as possible, but 2) the coil had to cover a sufficiently large scan area to image the whole heart. We chose the coil that met both these demands as good as possible.

The 23 and 47 mm microscopy coils, clinically used for finger/skin/eye scanning, were used for the smallest and thinnest complete specimen (*Afrotyphlops punctatus*, material no. 01, 47 mm microscopy coil; *Bogertophis subocularis*, material no. 02, 47 mm microscopy coil; *Pantherophis guttatus*, material no. 04, 23 mm microscopy coil). In *Afrotyphlops punctatus*, *Pantherophis guttatus,* and *Crotalus culminatus* it was not

possible to obtain scanning results with a sufficiently high resolution for a 3D reconstruction and many anatomical details could not be evaluated (see Fig. 17 B and C and 18 B). It was not possible to increase scanning times further, as the scanner was clinically used during the week and in cases of emergency. As the hearts were not isolated, it was not possible to free their insides from clotted blood and to remove the surrounding tissue. Clotted blood delivers a signal very similar to the signal of the myocardium and the vessels. Accordingly, the tissues surrounding the heart could not be distinguished clearly from the surrounding tissue that also delivers a very similar signal when fixed.

In contrast, the isolated hearts of *Python molurus* and *Crocodylus porosus* delivered very good scanning results with a sufficiently high resolution for reconstruction even of thin structures like the aortic valves and a good contrast (see Fig. 15 A, 16, and 18 A). I scanned the heart of *Python molurus* with the 47 mm microscopy coil and the *Crocodylus porosus* heart with the 2-channel SENSE FlexS coil. This is the smallest of the SENSE coils and usually used for scanning carotid arteries in humans, orbits, and smaller joints. Both hearts were isolated and could therefore be mostly freed from clotted blood before scanning. This highly improved the identifiability of the tissues of interest from the surrounding, however, it was not possible to identify cartilage.

3.1.1.4 X-ray micro-computed tomography (µCT)

µCT produced the best resolution results after histology (see Fig. 15 B and 19 A and B). Even the very small hearts of the *Caiman crocodilus* specimen were depicted with a very high resolution (Fig. 19 A and B). The identification of cartilage was easily possible. Scanning times were short with around 20 minutes compared to MRI scanning times. Computed volume rendering is a quick and easy way to get an idea about the scanned objects outer surface (Fig. 15 B). It shows the high resolution of the pictures computed with µCT. The treatment of the heart with the alcoholic iodide solution nevertheless led to further shrinking and partial collapse of the ventricular chambers. Fig. 15 shows the same heart of *Crocodylus porosus* which was first examined with MRI (A) and later

contrasted and scanned with µCT (B). The collapsed ventricles that resulted from treatment with alcoholic iodide solution are clearly visible.

I could not find any significant differences between the µCT images of hearts treated with various alcoholic iodide solutions (Table 2), neither concerning the contrast, nor the brightness or any other parameter.

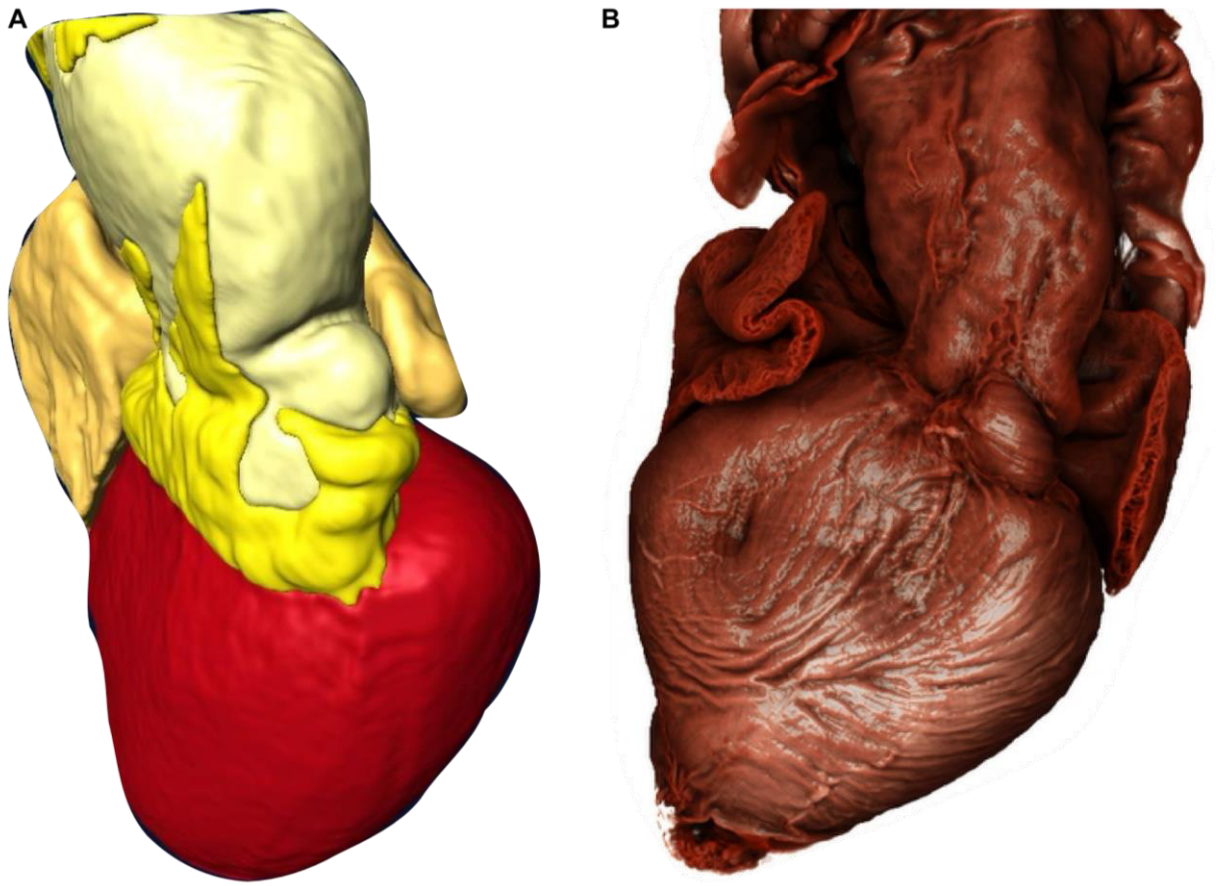

Fig. 15: 3D reconstruction of the same heart of *Crocodylus porosus* with two different methods. A: MRI: Surface rendering of the heart of *Crocodylus porosus* (material no. 12) after manual segmentation, dorsal view. B: µCT: Automatic volume rendering of the same *Crocodylus porosus* heart (after contrast enhancement with alcoholic iodide), ventral view.

3.1.2 Bypass-related structures in snakes

3.1.2.1 The muscular ridge and the 'bulbuslamelle'

The muscular ridge could be identified easily in all examined species except for *Afrotyphlops punctatus* (Fig. 17B). It is a massive muscular wall that emerges ventrally from the outer ventricular wall at the basis of the horizontal septum (Fig. 16 C and F and 17 A-E). From purely anatomical considerations, the muscular ridge is sufficiently long to reach the opposing ventricular wall in all examined specimen. The *Bulbuslamelle* is a double-layered protuberance of the vascular wall opposite to the muscular ridge (Fig. 16 C, 17 A-E). It rests on the ventricular wall and could sometimes not be clearly distinguished from it (Fig. 17 A-D).

3.1.2.2 The atrioventricular funnel and the interventricular canal

The atrioventricular funnel was only visible in *Python molurus*. Fig. 18 A shows the left atrioventricular funnel of *Python molurus,* a solid muscular structure. The atrioventricular valves could not be identified in any of the scans. The interventricular canal has a diameter of approximately 5% of the length of the ventricle in both specimens. Resulting from its minor size, only two MRI scans had a sufficiently high resolution to see the interventricular canal. Figs. 16 A and B show the horizontal septum and the interventricular canal of *Python molurus* and *Afrotyphlops punctatus*.

3.1.2.3 The size and other characteristics of the three ventricular cava

In all examined species, the *cavum arteriosum* and the *cavum pulmonale* appeared larger than the *cavum venosum* (Fig. 16 B-F and 17 A-D), reaching further to the tip of the ventricle and having larger and more cavities between the trabeculae. Due to the heterogeneous shrinkage of structures and bad resolution in some MRI scans, no comparative quantitative volume measurements were conducted.

It is a unique characteristic of *Python molurus* that the *cavum venosum* was surrounded by very dense cardiac muscle compared to the other cava (Fig. 16 E and F). In all other

species examined the density of the myocardium including the horizontal septum and the muscular ridge looked homogeneous.

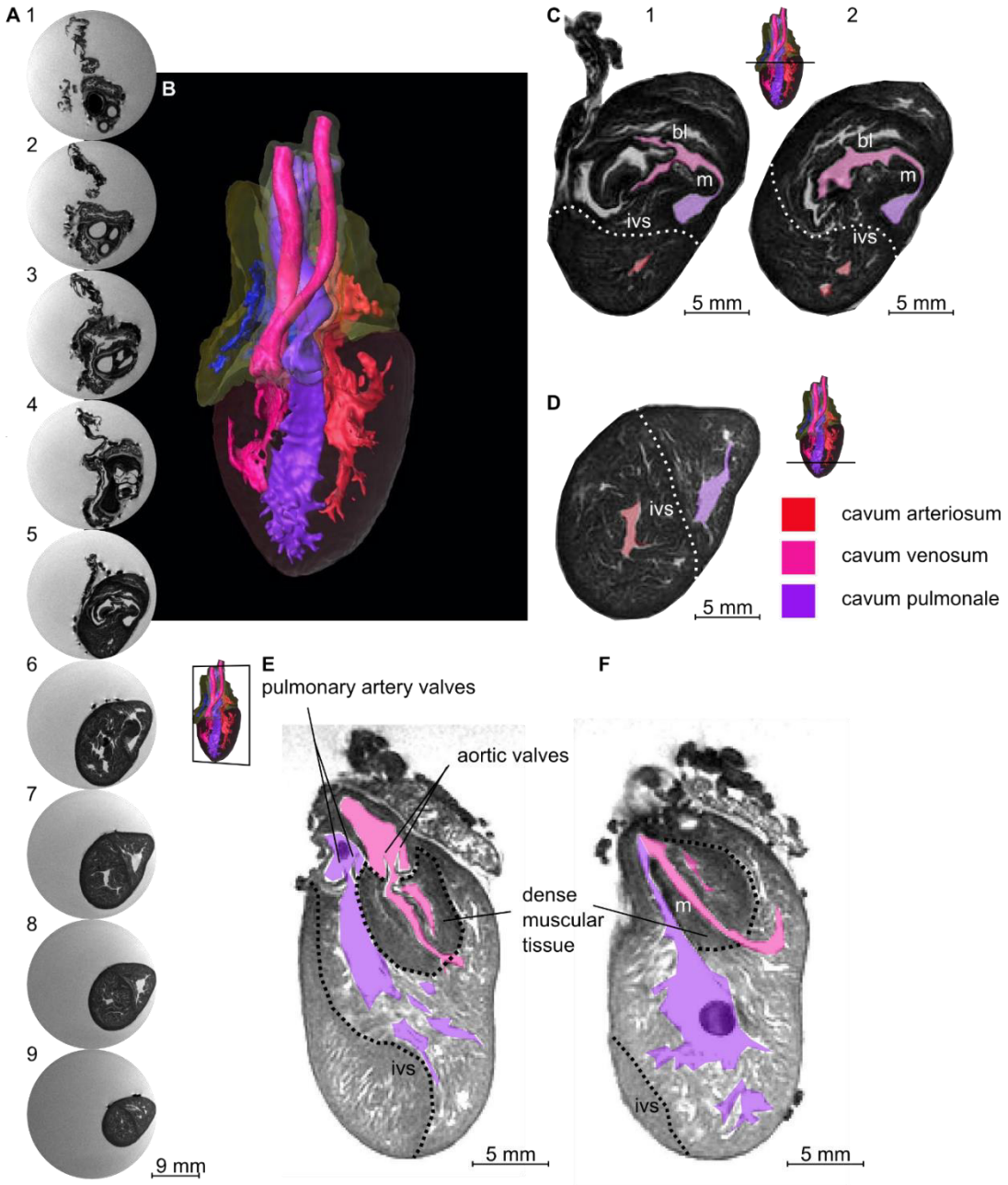

Fig: 16: The heart of *Python molurus* examined with magnetic resonance imaging.
All images from material no. 5. A 1-9: Serial cross sections from cranial (1: large arteries) to caudal (9: tip of ventricle). Distance between the images: 3.25mm. B: 3D reconstruction of the heart. The myocardium and the vascular walls are semi-transparent, blood streams within are solid. C: Cross section through the heart positioned between A 5 and A 6 showing the horizontal septum and the muscular ridge between the *cavum venosum* and *cavum pulmonale* and the *bulbuslamelle* opposite to it. D: Cross section on the level of A 8. E: Longitudinal section showing a diagonal cut through the *cavum venosum* and the *cavum pulmonale* at the basis of the large arteries. The *cavum arteriosum* is surrounded by much more solid muscular tissue than the *cavum pulmonale*. The muscular tissue of the cavum arteriosum is intermediately compact. F: Longitudinal section showing the muscular ridge from another angle. Hs: horizontal septum; m: muscular ridge; bl: bulbuslamelle.

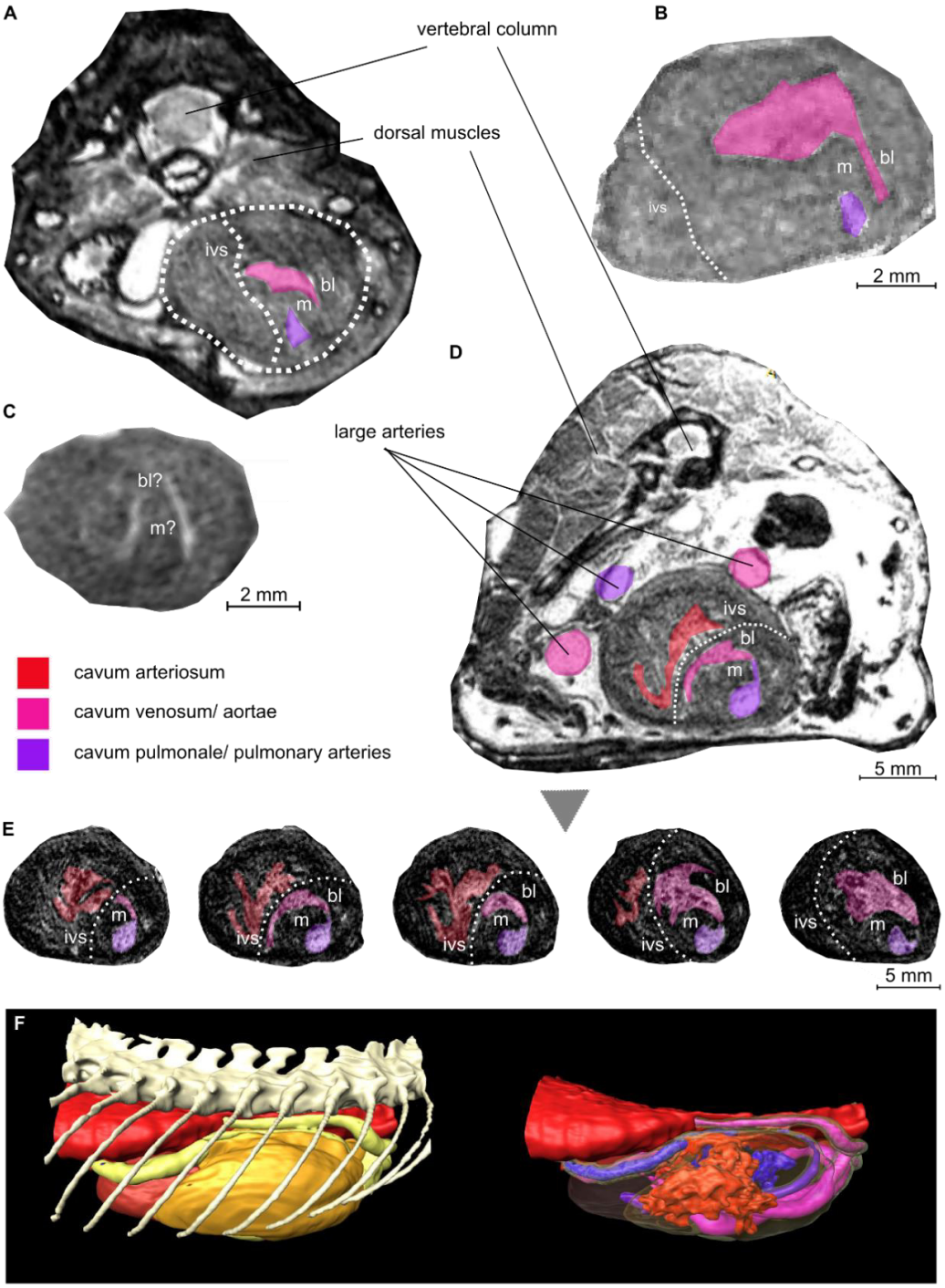

Fig. 17: The anatomy of the muscular ridge in different snake species based on MRI.
A: Cross section through a complete specimen of *Pantherophis guttatus* on the level of the ventricle. B: Cross section through the heart of *Crotalus culminatus* on the level of the muscular ridge. C: Cross section through the heart of *Afrotyphlops punctatus*. Due to the very bad resolution of the scan, the muscular ridge and 'bulbuslamelle' cannot be identified. D: Cross section through complete specimen of *Bogertophis subocularis*. The pictures relative position in the series E is indicated by the arrow. E: Serial cross sections through the heart of *Bogertophis subocularis*. Distance between sections: 0.65 mm. F: 3D reconstruction of *Bogertophis subocularis*. Left: The heart (ventricle: light red, atria: dark yellow), major vessels (light yellow), a part of the lung (red), and the vertebral column with ribs (white). Right: the same view with removed vertebral column and ribs and semitransparent ventricle, atria, and vascular walls. Cranial: right.

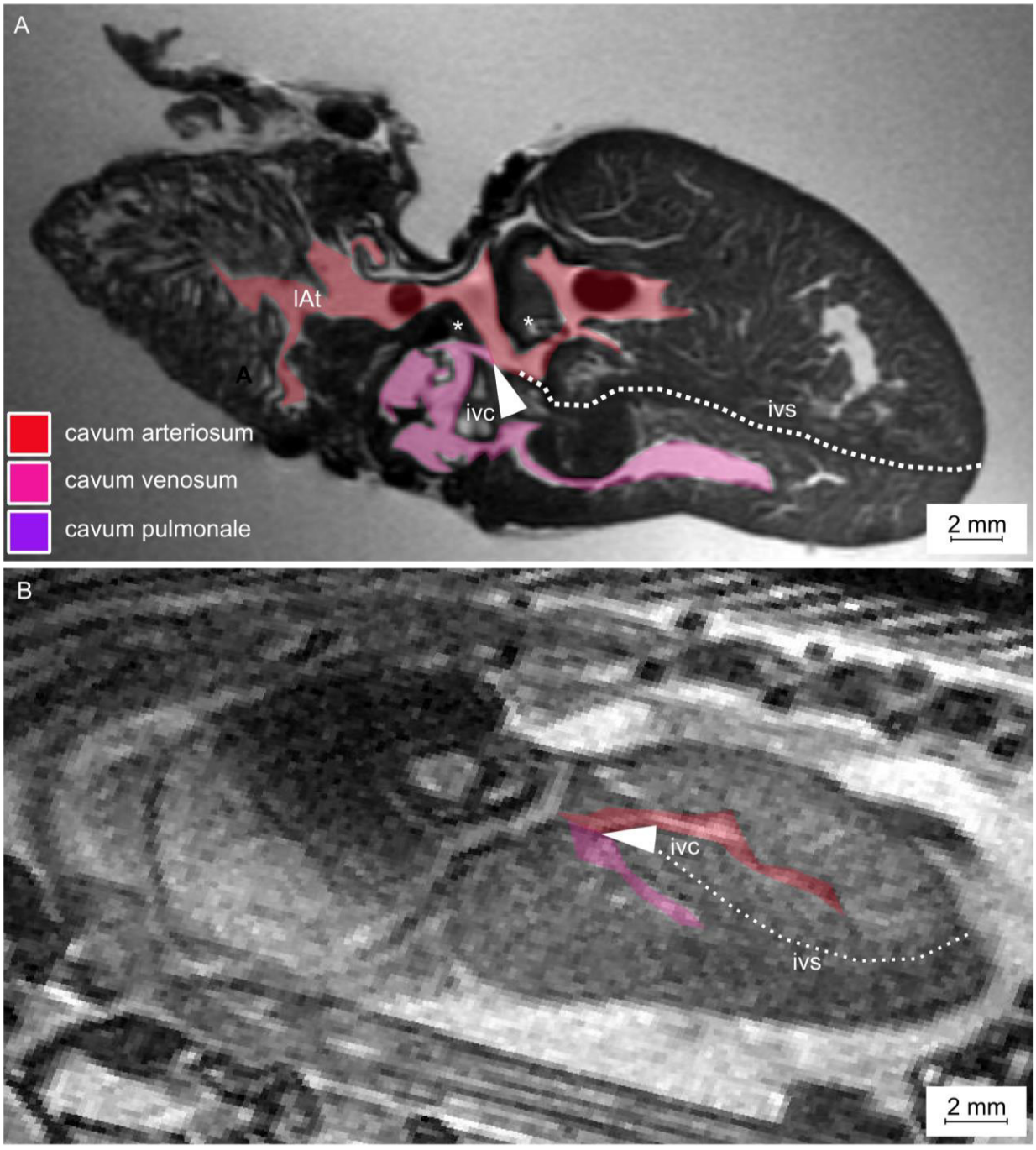

Fig. 18: The interventricular canal between the *cavum arteriosum* and *cavum venosum* and the atrioventricular valves.
A: MRI: Longitudinal cut through the heart of *Python molurus*. B: MRI: Longitudinal cut through an intact *Afrotyphlops punctatus* specimen, with the heart in the center of the picture. The cutting plane does not enable to show the interventricular canal and the connection to the left atrium at the same time. The resolution is too poor to show the atrioventricular valves. lAt: left atrium; Asterisks: Atrioventricular funnel; Arrow/ivc: Interventricular canal; ivs: interventricular septum. Cranial: left.

3.1.3 Pulmonary bypass-related structures in crocodiles

3.1.3.1 The Foramen Panizzae and the bicuspid aortic valves

The *Foramen Panizzae* is positioned in the shared wall of the aortae (see Fig. 19). The bicuspid aortic valves possess an inner (i.e. positioned closer to the *Foramen Panizzae*) and an outer cusp. The inner cusp is overlapping the *Foramen Panizzae* in all examined species (Fig. 19). Fig. 19 E shows serial sections through the *Foramen Panizzae* of *Crocodylus niloticus*. The complete inner cusp of both the right and the left aorta overlap the lower part of the *Foramen Panizzae* (Fig. 19 E 1 and 2), whereas it is only overlapped by its margins further distally (Fig. 19 E 3-7). Due to its position at the side of the bicuspid aortic valves, it is nevertheless fully covered by them. From Fig. 19 E 8 on the sections are positioned above the upper margin of the *Foramen Panizzae*, while the margins of the bicuspid aortic valves still continue, showing that the aortic valves overlap the *Foramen Panizzae* over its entire length. This is supported by Fig. 20 E.

Comparing the diameters of the *Foramen Panizzae* and the aortae, the *Foramen Panizzae* is small, reaching not more than 20% of the right aorta's diameter (Fig. 19 and 20) in all examined crocodile species, this means for a circular Foramen that is has only around 4% of the area the cross section of the right aorta has. Fig. 20 A shows a 3D reconstruction of the heart of *Crocodylus porosus*. Blood streams are colored to identify left and right aortic and pulmonary arterial blood. The *Foramen Panizzae*, i.e. the connection between the violet left aortic and red right aortic blood stream in Fig. 20 A, is 10-20% the radius of the right aorta.

3.1.3.2 Form and position of the pulmonary artery in crocodiles cranial of the cog-teeth-like valves

Fig. 20 A, F, G, and H show that the pulmonary artery is not a separate vessel with a circular diameter cranial of the cog-teeth-like valves, but is flattened and wrapped around one half the aortic bases like a double-layered envelope. Fig. 20 F, G, and H show how the pulmonary artery could collapse when the left aorta is inflated with blood, e.g. during pulmonary bypass, and vice versa.

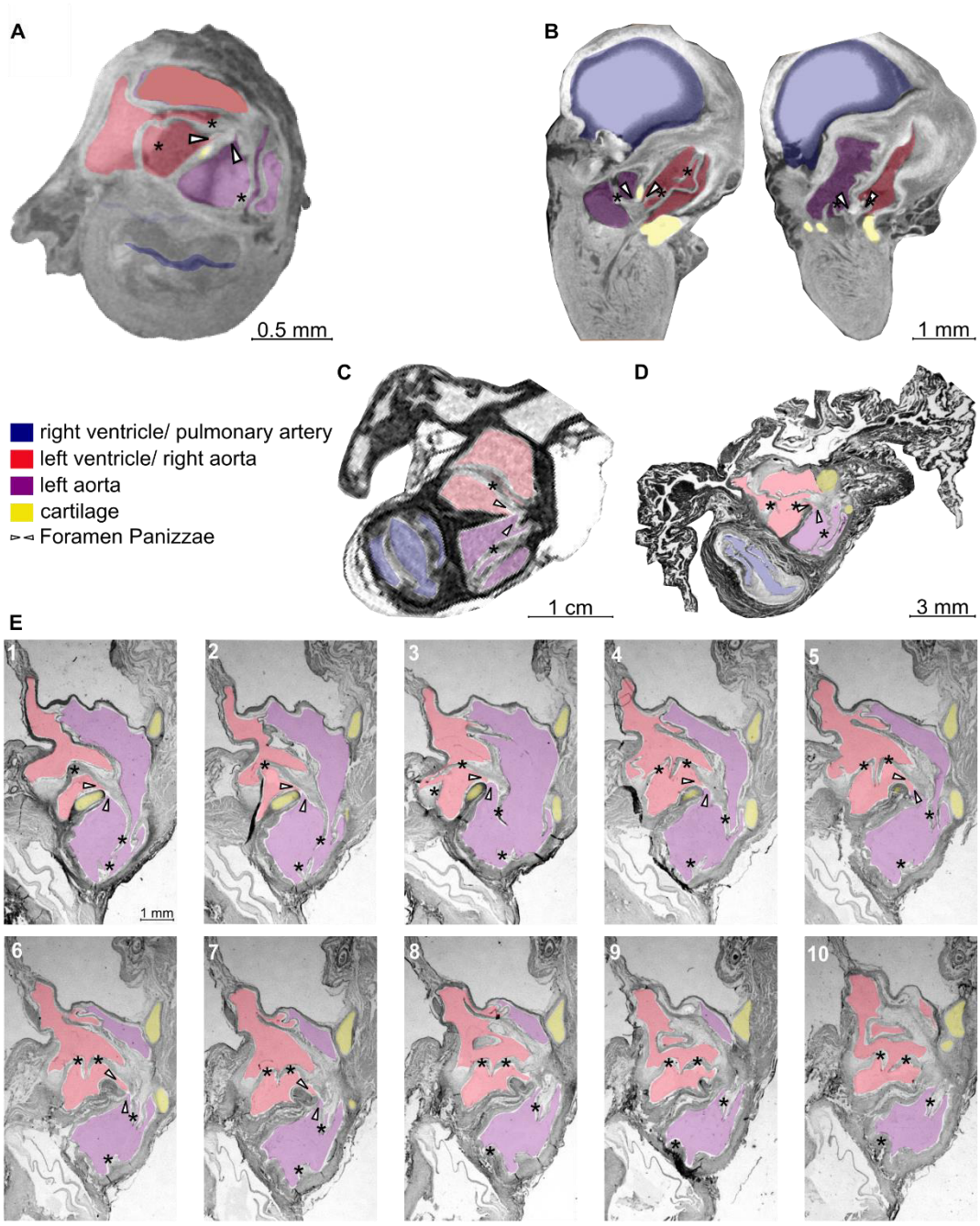

Fig. 19: Morphology of the *Foramen Panizzae* and the bicuspid aortic valves of crocodiles, I.
A: µCT: Cross section through the heart of *Caiman crocodilus* (material no.7) cranial of the *Foramen Panizzae*. B: µCT: Slightly diagonal sagittal sections of the heart of *Caiman crocodilus* (material no. 6). C: MRI: Cross section of the heart of *Crocodylus porosus* (material no. 12) at the level of the *Foramen Panizzae*. D: Histology: Greyscale photograph of a cross section through the heart of *Crocodylus niloticus* (material no. 10) stained with H&E stain. E: Histology: serial cross sections of the heart of *Crocodylus niloticus* (material no. 9) from caudal to cranial. Distance between sections: 80 µm. Arrows direct on the *Foramen Panizzae*, asteriscs indicate the left and right bicuspid aortic valve that is positioned close to the *Foramen Panizzae* and might overlap it during systole.

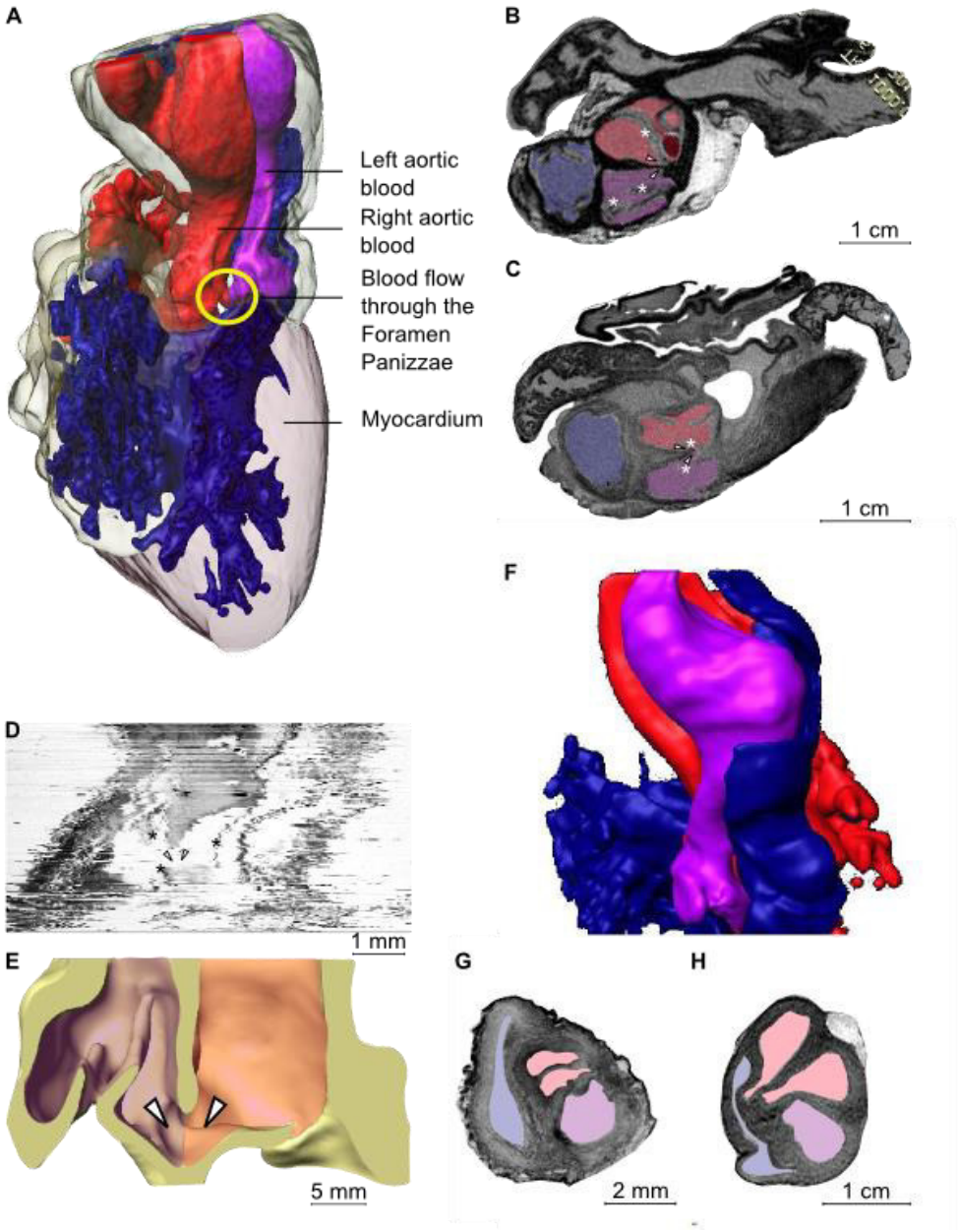

Fig. 20: Morphology of the *Foramen Panizzae*, the bicuspid aortic valves, and the pulmonary artery of crocodiles, II.
A: MRI: 3D reconstruction of the heart of *Crocodylus porosus* (material no.12) from the image series of B: MRI: cross section of the heart of *Crocodylus porosus* (material no. 12) on the level of the *Foramen Panizzae*. C: µCT cross section of the heart of *Crocodylus porosus* (material no. 12) on the level of the *Foramen Panizzae*. D: Histology: Digital reconstruction of a cut perpendicular to the original cutting axis through a staple of H&E stained slices from the heart of *Crocodylus niloticus* (material no. 10). E: MRI: 3D reconstruction of a sagittally cut bases of the aortae of *Crocodylus niloticus* showing the *Foramen Panizzae* and sections of the bicuspid aortic valves of Crocodylus porosus (material no.12). F: MRI: 3D reconstruction of the heart of *Crocodylus porosus* (material no.12), showing only the blood streams within the aortae and pulmonary artery without the surrounding vascular wall. G & H: Cross section through the bases of the aortae and the pulmonary artery of *Crocodylus niloticus* from slices produced with the sliding microtome planer method (G; material no. 9) and of *Crocodylus porosus* produced with MRI (H; material no. 12). Color coding as in Fig. 19.

3.1.3.3 The cog-teeth-like valves and the constrictor muscle

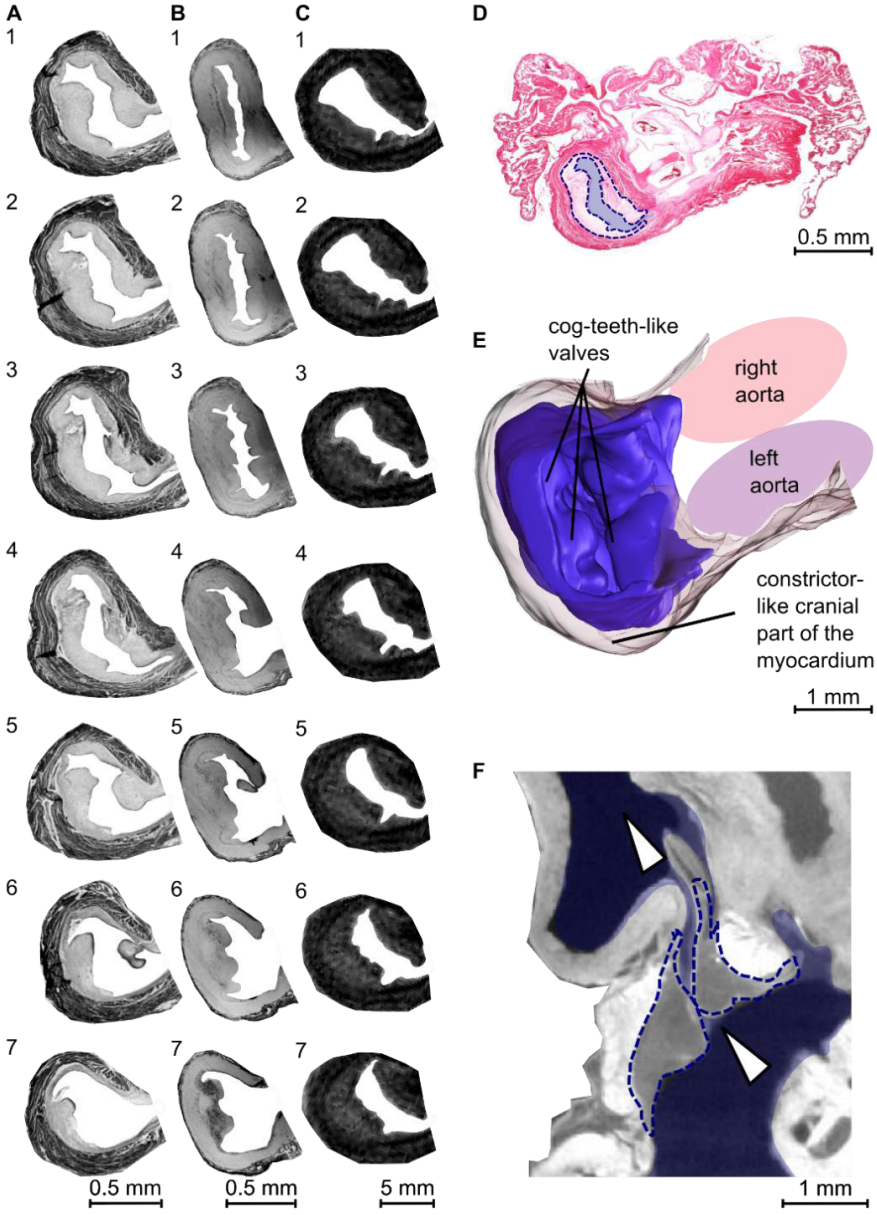

Fig. 21: Morphology of the cog-teeth-like valves.
A: Histology: Cropped greyscale photographs of histological serial cross sections through the cog-teeth-like valve of *Crocodylus niloticus* (material no. 10) stained with H&E stain. Distance between sections: 50 µm. B: Sliding microtome planer method: Cropped greyscale serial photographs of the methylene-blue stained paraffin. Cross sections through the heart of *Crocodylus niloticus* (material no. 9). Distance between sections: 50 µm. C: MRI: Cropped slices from the heart of *Crocodylus porosus* (material no. 12), cross sections through the cog-teeth-like valves. Distance between sections: 250 µm. D: Histology: Originally colored photograph of a cross section through the heart of *Crocodylus niloticus* (material no. 10) stained with H&E stain. The pulmonary artery and the cog-teeth-like valves are highlighted in blue. E: 3D reconstruction based on the serial sections partly shown in (B). View from the center of the heart to the pulmonary artery. F: µCT: Cropped longitudinal slice through the cog-teeth like valves of *Crocodylus niloticus* (material no. 11). The cog-teeth-like valves are highlighted by dotted lines. Arrows indicate the direction of blood flow. Color-coding as in Fig. 19.

The cartilaginous cog-teeth-like valves are anatomically similar built in all crocodile species examined (Fig. 21 A-C). They consist of an outer half-circle that lines the outer surface of the myocardium and arterial basis. This half-circle is opposed by a smaller cartilaginous part that is positioned at the transition of the *cavum pulmonale* and the pulmonary trunk. Both parts consist of several cartilaginous nodules that can interlock with the nodules on the opposing part (Fig. 21 D, E, and F). The cranial part of the myocardium surrounds the basis of the pulmonary artery. Its fibers are arranged circularly around the pulmonary trunk (Fig. 21 D).

3.1.3.4 The cartilage clasp

The cardiac cartilage is composed of various parts. In *Crocodylus niloticus* there are three cartilages (Fig. 22 C): (1) The ventrolateral cartilage is positioned in the ventricular muscle close to the *Foramen Panizzae* and opposite to the pulmonary trunk. (2) The central cartilage is positioned between the pulmonary trunk and the two aortae. One of its processes reaches into the shared wall of the aortae and ends directly at the *Foramen Panizzae* (Fig. 22 C, foraminal process). Another process of the central cartilage reaches into the interventricular wall in the middle of the triangle of the three large arterial bases (Fig. 22 C, interventricular process). (3) A small round cartilage nodule is only attached to the rest of the central process by a thin connection and reaches into the right aorta close to the basis of the right aortic valves. A separate cartilage nodule is positioned close to the ventrolateral cartilage in the aortic wall (Fig. 22 C, cartilage nodule). The cartilage clasp of *Caiman crocodylus* was not 3D reconstructed. Inferred from the µCT images (Fig. 19 B), the 3D structure appears very similar to that of *Crocodylus niloticus*, with a central cartilage with a foraminal process, a ventrolateral cartilage and a cartilage nodule. Fig. 22 D shows that the central cartilage can stabilize the *Foramen Panizzae* being positioned in the aortic wall and reaching around the oval *Foramen* being semilunar shaped. The other part of the cartilage clasp is also semilunar shaped and positioned on the other side of the

Foramen Panizzae. The *Foramen Panizzae* is therefore surrounded by an interrupted ring-like cartilage structure.

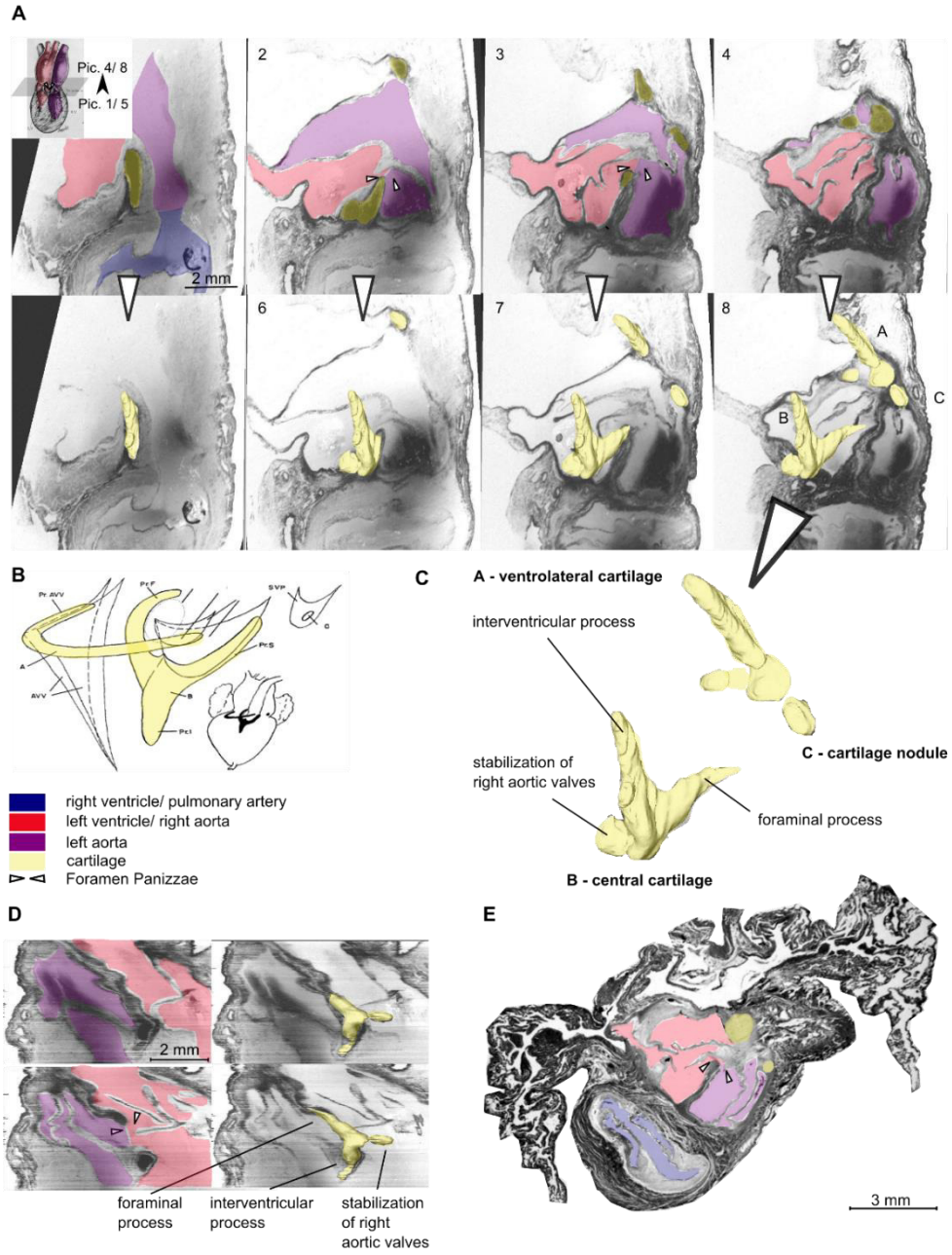

Fig. 22: The cartilage clasp of *Crocodylus niloticus*.
A: Sliding microtome planer method: Series of cross sections through the *Foramen Panizzae* region of the heart of *Crocodylus niloticus* (1-4) and the same slices with an included 3D reconstruction of the cartilage clasp (5-8). Distance between cuts: 40 µm. B: Schematic drawing of the cartilage clasp of *Alligator mississippiensis* by White (1956), see Fig. 7 for details. C: The cartilage clasp in *Crocodylus niloticus* as 3D reconstruction from the images in A with an attempt to re-identify the structures described in B. D: Sliding microtome planer method. Left side: Digital reconstruction of a longitudinal cut through the bases of the aortae (perpendicular to the original cutting axis) through a staple of images obtained by the sliding microtome planer method from the heart of *Crocodylus niloticus* (material no. 9). Right side: The same images including the 3D reconstruction of the cartilage clasp. E: Histology: Greyscale photograph of a cross section through the heart of *Crocodylus niloticus* (material no. 10) stained with H&E stain showing a similar section as 20 A 3 produced with another method, including sections through cartilage part A and C.

3.2 Computational simulation

3.2.1 Dynamics and equilibration

Examples for typical dynamics of input to the supply areas at the beginning of the simulation are shown in Fig. 23. The exact number of heartbeats being necessary for equilibration depends on the compartment and the scenario chosen, but input, output and fill level of all compartments reach an equilibrium after less than ten heartbeats. Fig. 23 A and C show that without pulmonary bypass, blood input into the four distinguished supply areas has equilibrated after eight heartbeats, while Fig. 23 B and D show that equilibration is finished after three heartbeats after start of the simulation when the lungs are completely bypassed. Afterwards, inputs follow the same dynamics during each heartbeat. Therefore, the values from heartbeat 500 that are used for the remaining analyses (Fig. 24) represent equilibrium values.

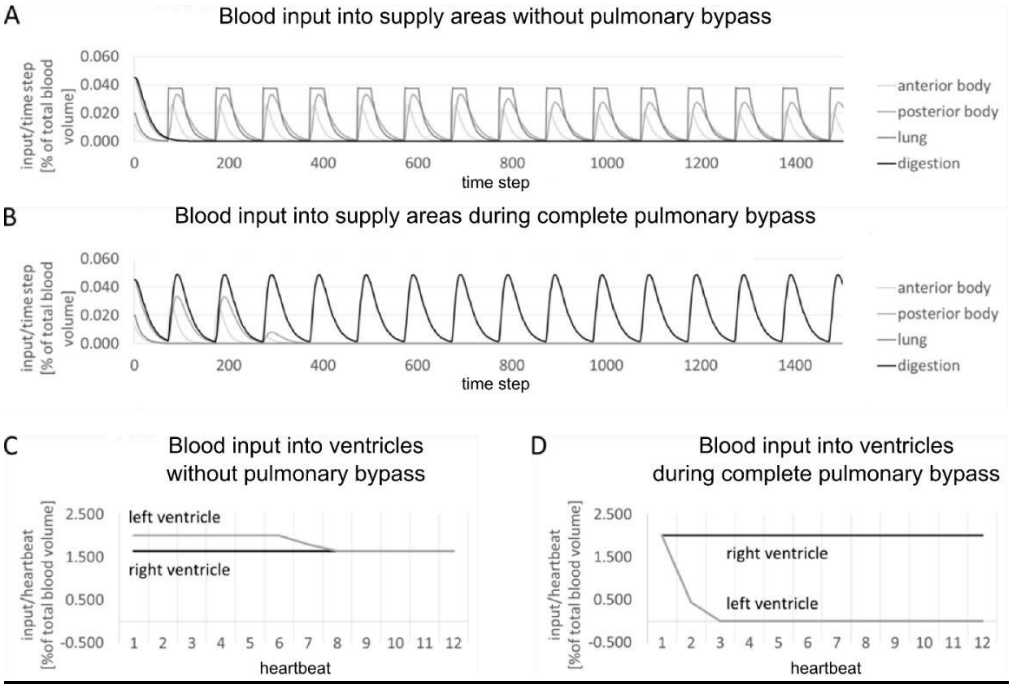

Fig. 23: Dynamics of balancing of blood input into different compartments after the start of the simulation from starting values (as given in Table 3).
I show the dynamics of two scenarios: without (A and C) and during complete (B and D) pulmonary bypass. Both scenarios assume a completely constricted *Foramen Panizzae* and aortic anastomosis here. After less than 10 heart beats, all inputs equilibrate and follow the same dynamics during every heartbeat. A and B show the input dynamics of the four supply areas that were distinguished in the simulation during every time step. C and D show total input values into the two ventricles summed up over one heartbeat.

3.2.2 Impact of pulmonary bypass on the supply areas of the crocodilian body

The simulation results (Fig. 23 and 24) show that without pulmonary bypass and with an impermeable *Foramen Panizzae* and aortic anastomosis, all compartments receive blood with exception of the digestive tract (Fig. 23 A and 24 D). When the flow coefficient of the left aorta increases (increasing pulmonary bypass), this leads to decreasing blood supply of the lungs (Fig. 24 A), the anterior body (Fig. 24 B), and the posterior body (Fig. 24 C). Simultaneously, blood supply of the digestive tract increases (Fig. 24 D).

Blood supply of the lungs declines to zero during complete pulmonary bypass. This also applies to the anterior and posterior body regions but only if in addition there is no blood flow through the *Foramen Panizzae* and the aortic anastomosis.

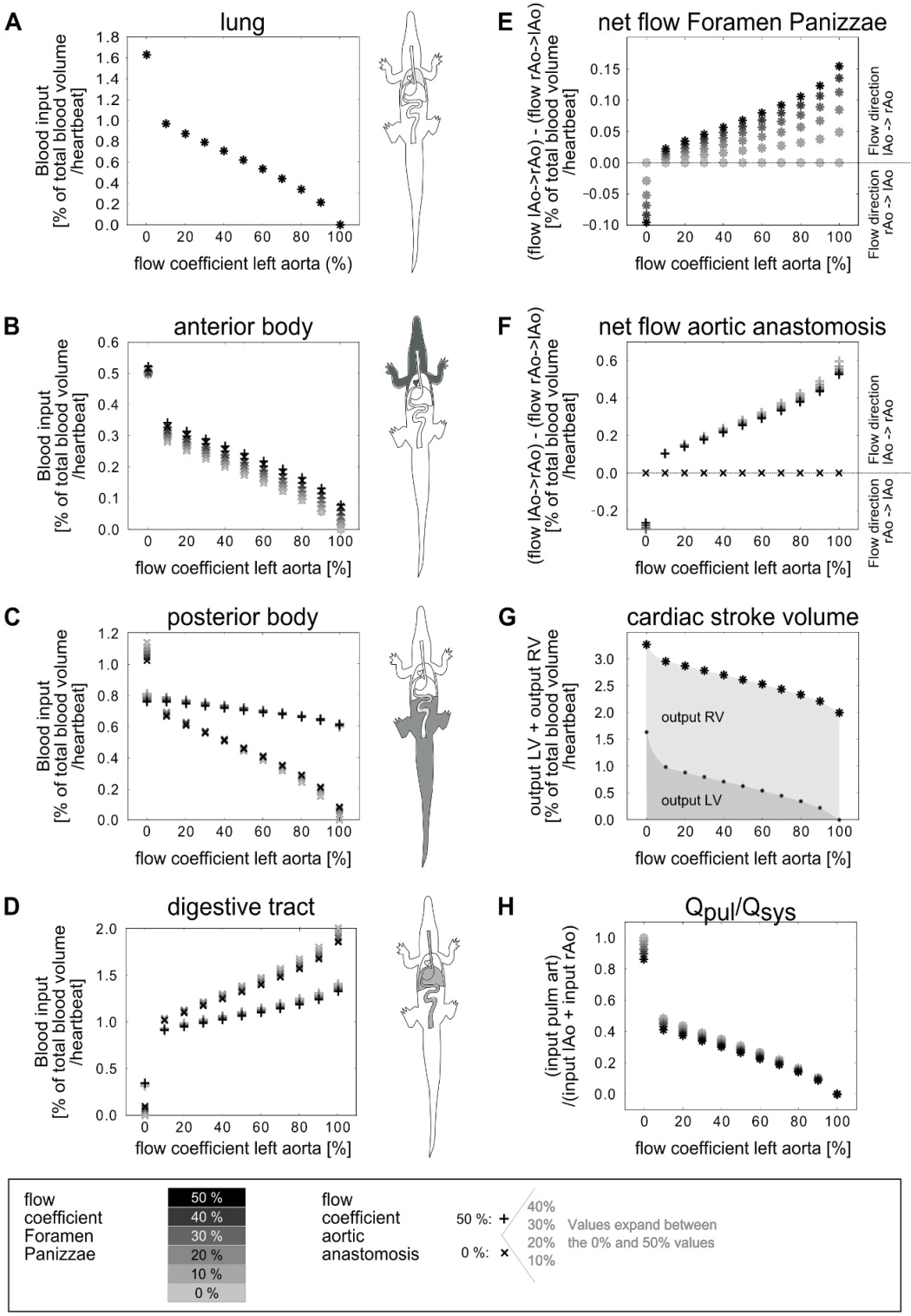

Fig. 24: Impact of the flow coefficient of the left aorta, the *Foramen Panizzae* and the aortic anastomosis:
On blood supply of the lung (A), the anterior body (B), the posterior body (C) and the digestive tract (D), net blood flow through the *Foramen Panizzae* (E) and the aortic anastomosis (F), right and left ventricular stroke volume and their contribution to total cardiac stroke volume (G) and the ratio of pulmonary to systemic blood flow Qpul/Qsys (H). LAo/rAo: left/right aorta; LV/RV: left/right ventricle; pulm art: pulmonary arteries.

3.2.3 Blood flow direction through the *Foramen Panizzae* and the aortic anastomosis and impact of this flow on blood supply of blood supply of the crocodilian body

Without pulmonary bypass (left aortic flow coefficient is zero), net blood flow through both the *Foramen Panizzae* and the aortic anastomosis is from the right into the left aorta. When the lungs are bypassed, blood flows from the left into the right aorta, increasing with the flow coefficient of the *Foramen Panizzae*/ the aortic anastomosis (Fig. 24 E and F). Blood flow through the *Foramen Panizzae* has an impact on net blood flow through the aortic anastomosis, but not vice versa (Fig. 24 E and F). Without a *Foramen Panizzae* (flow coefficient between the proximal aortae is zero), blood flow through the aortic anastomosis is larger (Fig. 24 F).

Supply to all areas of the crocodilian body except for the lungs is affected by blood flow through the *Foramen Panizzae* and the aortic anastomosis (Fig. 24 B-D). Increasing flow coefficient of the *Foramen Panizzae* leads to increased blood supply of the anterior body (Fig. 24 B). Blood supply of the posterior body exhibits a more complex relationship with the flow coefficient of the *Foramen Panizzae* (Fig. 24 C). For little or no pulmonary bypass, an increase in the flow coefficient of the *Foramen Panizzae* leads to slightly reduced blood supply of the posterior body. At intermediate degrees of pulmonary bypass, the *Foramen Panizzae* has minor impact on blood supply of the posterior body. When the lungs are nearly or completely bypassed, the blood supply of the posterior body slightly increases with an increasing *Foramen Panizzae* flow coefficient. Concerning the digestive tract, an increasing flow coefficient of the *Foramen Panizzae* leads to increased blood supply only in the complete absence of pulmonary bypass. As soon as there is some pulmonary bypass, increasing the flow coefficient of the *Foramen Panizzae* reduces blood supply of the digestive tract (Fig. 24 D). The impact of blood flow through the *Foramen Panizzae* is most pronounced for the anterior body.

The effect of changes in the flow coefficient of the aortic anastomosis on the posterior body (Fig. 24 C) is more pronounced than its impact on blood supply of the anterior body (Fig. 24 B). Increasing the flow coefficient of the anastomosis reduces blood supply of the posterior body in the absence of pulmonary bypass and increases it during pulmonary bypass. Blood flow through the aortic anastomosis increases blood supply of the digestive tract in the absence of pulmonary bypass and decreases it during pulmonary bypass (Fig. 24 D).

3.2.4 Impact of pulmonary bypass on ventricular input and output

Without pulmonary bypass, both ventricles equilibrate at an input (Fig. 23 C) and output (Fig. 24 G) of 1.6% of total blood volume. During complete pulmonary bypass, right ventricular input and output is maximal with 2% of total blood volume (Fig. 23 D and 23 G). Under the same conditions, left ventricular input and output goes to zero within three heartbeats. Consequently, total cardiac stroke volume declines with increasing pulmonary bypass. The flow coefficients of the *Foramen Panizzae* and the aortic anastomosis have no impact on left or right ventricular stroke volume.

3.2.5 Impact of blood volume redistribution on Q_{pul}/Q_{sys}

Without pulmonary bypass and without blood flow through the *Foramen Panizzae*, Q_{pul}/Q_{sys} is 1, meaning that pulmonary and systemic blood flow are balanced (mammalian/ avian situation; see Fig. 24 H). With increasing flow coefficient of the left aorta, Q_{pul}/Q_{sys} rapidly declines to values around 0.5, then declines more slowly at medium flow coefficient values, and again more sharply near complete pulmonary bypass. Blood flow through the *Foramen Panizzae* enhances this decline.

4 Discussion

4.1 Evaluation of the used imaging techniques

The best method for the 3D-imaging of the heart anatomy of crocodiles and snakes (and probably for many other large 'reptiles' as well) depends on several parameters and the respective goals of the study to evaluate the importance of the advantages and disadvantages of each method. Parameters to be considered are:

1. the necessary resolution for the structures of interest
2. the size of the specimen resp. the heart
3. wheather or not the heart is left in situ or removed from the body
4. wheather or not the heart may be stained or destructed by sectioning or if it must remain intact
5. wheather or not the heart under study should be permantently deposited
6. the time available for the examination process
7. wheather or not 3D reconstructions are planned

The necessary resolution depends on the structures that shall be made visible. If cellular structures must be visible, histology or even ultrastructural techniques are the only possible method, but it modifies/destructs the intact organ. The method is therefore not applicable for rare or valuable collection material (e.g., type specimens). Histology with standard laboratory equipment is only possible up to a certain size of the organ. To use photographs from histological sections as a basis for 3D reconstruction may cause certain problems: The histological preparation process and the placement of the slices on the object holder can result in deformation and heterogenous shrinkage, especially in organs with large cavities like hearts and vessels. Alignment can therefore be difficult or unreliable (Fig. 20 D shows a virtual staple of histological images and shows quite irregular images despite of careful alignment). In addition, histological probe preparation is very time-consuming and can take weeks.

If a detailed overview anatomy is sufficient, all other methods are applicable. The sliding microtome planer method has a large advantage over classical histology: no deformation and easy alignment for 3D reconstruction. The resolution is theoretically very good (if the camera resolution is high enough), but the image quality is reduced by reflections of the surface and heterogeneous illumination of the paraffin block. Additionally, not only the block surface, but also the remaing heart in the block is visible. Cellular structures cannot be distinguished because of unspecific and low contrast. I did not test wor not en bloc staining of the whole organ before paraffin embedding improves the results. This method is by far the most time-consuming method of all methods described here.

The following evaluations of MRI and µCT are based on the technical equipment I worked with. Medical imaging technologies are continuously improved, therefore disadvantages stated herein might be overcome in the future.

MRI is a good method for large hearts, especially if they are removed from the body so their lumen can be rinsed and freed from clotted blood, and surrounding tissues can be removed. The hearts of crocodiles and snakes are surrounded by a pericardium that can be tightly conjoined with the large arteries. The bases of the large arteries may be surrounded with massive fat reservoirs, contrasting reports by Jensen et al. (2014) . If these tissues can be removed before scanning, it facilitates the interpretation of the images. Long scanning times (up to hours or days), a high-resolution MRI with a strong magnetic field (high Tesla numbers) and a suitable reception coil can lead to very good results. The scans can be performed without contrasting and in 80% EtOH, which is the medium tissue samples are often stored in. Therefore, the probes do not have to be prepared and can remain in the body of the animal. A low resolution prescan to identify the position of the heart might then be necessary. The generated image stack is three-dimensional and therefore perfectly aligned. It can be imported into 3D reconstruction software like AMIRA without any problems.

The same advantages with respect to 3D reconstruction apply for µCT imaging, but the resolution is much better and the scans last shorter. It is therefore a recommended method also for smaller hearts. For the scanning of soft tissues contrasting is necessary, therefore the hearts must be removed from the bodies in animals to large to be contrasted intactly. If the hearts are removed, it is possible to remove clotted blood and surrounding tissue, but the method is not applicable for rare or valuable collection material that may not be contrasted or sectioned. Additionally, contrasting increases the danger of collapse of cavities like a heart. I would therefore not recommend the method if it is planned to measure cavity volumes quantitatively.

In general, fresh material should be preferred. Fixation and long-term storage of the material e.g. in ethanol inevitably leads to tissue changes and deformation and valuable information is lost. Jensen et al. (2011) suggests to perfuse the beating heart of freshly dead animals with heparinized saline, followed by cardioplegic solutions containing Ca^{2+} ligands such as ethylene glycol tetraacetic acid (EGTA). They obtained completely clean hearts in a diastole-like condition. However, this equires the availability of living animals and does not enable the examination of specimen under nature protection or collection material.

Some new bioimaging techniques have promising results that might be able to combine the advantages of the methods I used. Jensen et al. (2014) used nuclear magnetic resonance imaging (NMR) producing high-resolution images including all advantages of scanning technologies for 3D reconstruction.

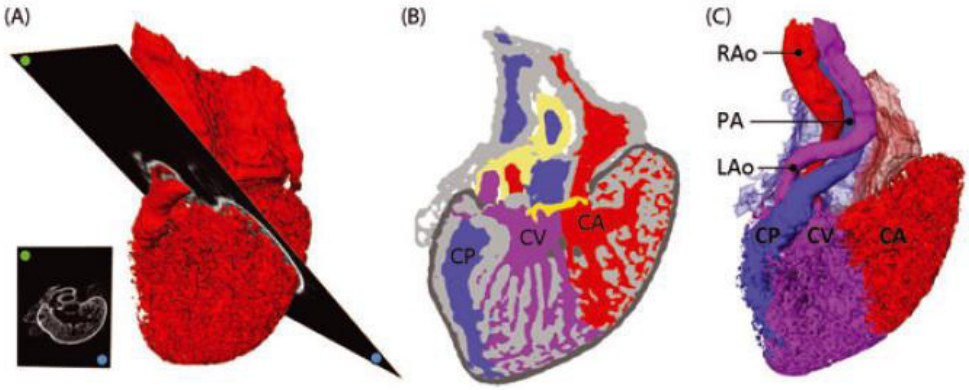

Fig. 25: Volume rendering from nuclear magnetic resonance imaging of a heart of *Eunectes notaeus*.
A: volume rendering with one image. B: Slice of the 3D model. C: Volume rendering of the annotated lumina. CA: *Cavum arteriosum*; CV: *Cavum venosum*; CP: *Cavum* pulmonale; rAo/ lAo: right/ left aorta; PA: pulmonary artery. Fig. 9 from Jensen et al. (2014).

4.2 Pulmonary and systemic bypass in Chelonia, Rhynchocephalia, and Squamata

4.2.1 Pressure separation, bypass, and the role of the muscular ridge

During the past few years, it became increasingly obvious that there is a clear distinction between the 'standard' squamate heart and the heart of (at least some, since not all species have been examined) pythons and varanid lizards (Burggren and Johansen, 1982; Jensen et al., 2010a; Jensen et al., 2010b; Wang et al., 2002; Wang et al., 2003). These two groups maintain different blood pressures between the systemic (high pressure) and pulmonary (low pressure) circulation similar to mammalian pressures, whereas the 'standard squamate heart' generates more or less equal pressures in the pulmonary and systemic circulation. Mammals and birds developed pressure separation in connection with their high metabolic rates that are related to endothermy. As in crocodiles, pressure separation is achieved by a complete separation of the two circulations within the ventricle during systole. The increased oxygen demand of the tissues of endothermic animals has to be met by increased blood flows and high systemic pressures. Conversely, gas exchange in the lungs needs to become more effective. This can be achieved by weakening the blood-air barrier by a thin lung epithelium. A thin lung epithelium nevertheless does not tolerate high blood pressures which would lead to edema. The pulmonary blood pressure therefore has to be kept low, while systemic blood pressures still need to be high (e.g. Burggren, 1982; Jensen et al., 2010a). If lung epithelia are thin, then blood pressures in the lung must be kept low throughout the heart cycle. Consequently, the muscular ridge and the 'bulbuslamelle' must be shaped in a way that enables them to completely separate the *cavum venosum* from the *cavum pulmonale* completely throughout systole, which means during all phases of ventricular contraction. Well-developed atrioventricular valves can effectively separate blood streams coming from the atria during ventricular diastole. This might be supported by the ventricular trabeculae that direct the blood

within the ventricular cava. The hearts of some pythons and varanid lizards combine these features (Jensen et al., 2010a; Jensen et al., 2014b).

It is important to note that pulmonary or systemic bypass and pressure separation are *per se* independent features. Pulmonary and systemic bypass can occur with or without pressure separation. Both scenarios differ regarding the factors that decide over blood distribution into the two circulations: (1) Without pressure separation during systole (meaning that the connection between the *cavum venosum* and *cavum pulmonale* remains open even during systole), the blood streams are distributed by the vascular resistance of the systemic and pulmonary circulation (this is sometimes called a pressure shunt, e.g. Hicks and Malvin (1992)). In this case, pulmonary or aortic vasoconstriction could induce bypass of the one or the other circulation (e.g. pulmonary vasoconstriction via the vagus nerve: Taylor et al., 2009). (2) With pressure separation during systole: blood distribution in the ventricle at the moment the muscular ridge closes is decisive for the distribution into the circulations: All blood volumes in the *cavum arteriosum* and *cavum venosum* will go into the aortae, all blood volumes in the *cavum pulmonale* into the pulmonary arteries, independent of vascular resistance of the two circulations (washout shunt, e.g. Hicks and Malvin (1992)). A muscular ridge that does not close at the beginning of systole, but a bit later, would cause the combination of these two mechanisms. This could be the case in species with a shorter muscular ridge and 'bulbuslamelle': they might close when ventricular contraction has advanced (see Fig. 26). Additionally, the velocity of the contraction of the ventricle in relation to complete systole duration might have an impact, but this was not examined yet. Several studies have measured considerable degrees of bypass accompanied by unequal blood volume distribution into the circulations in species with high systemic pressures (Berger and Heisler, 1977; Campen, 2009; Starck, 2009).

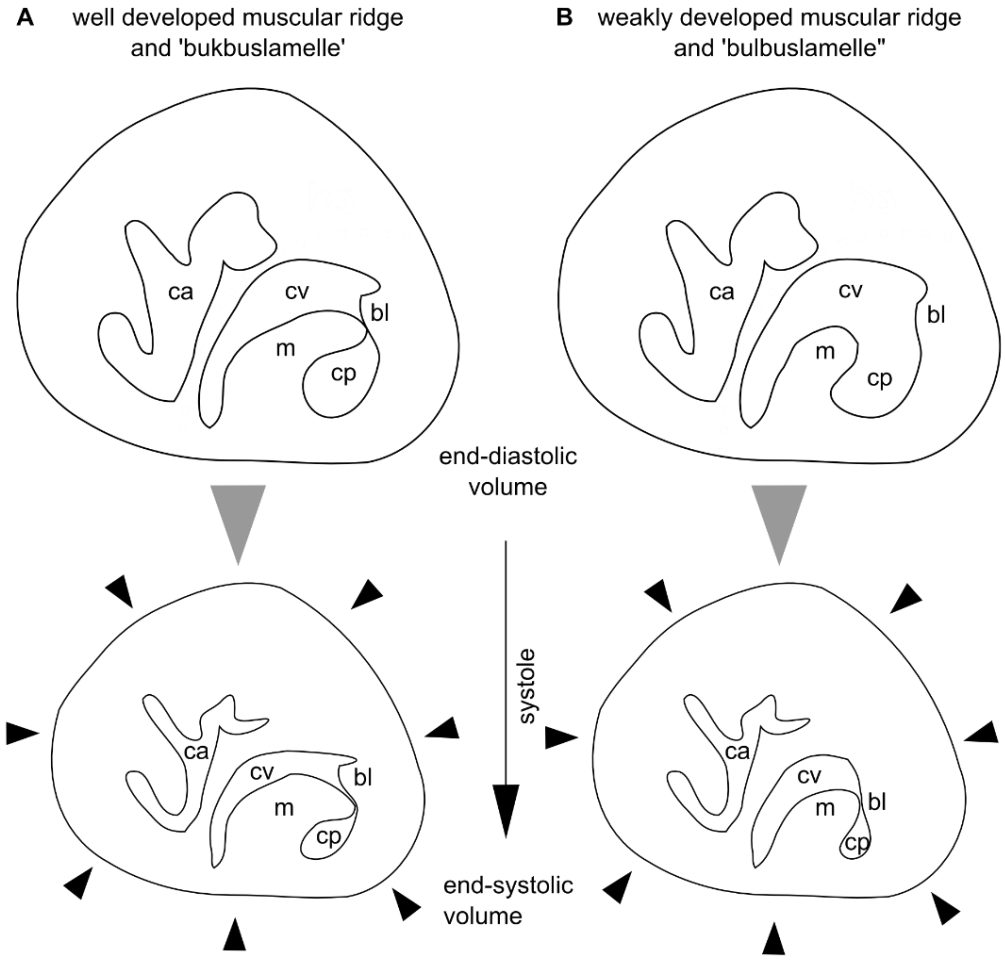

Fig: 26: Schematic drawing of a ventricular cross section explaining the possible connection between the size of the muscular ridge and the time point of separation of the cavum venosum and the cavum pulmonale.
ca: *cavum arteriosum*; cv: *cavum venosum*; cp: *cavum pulmonale*; bl: bulbuslamelle; m: muscular ridge.

Oxygen delivery and carbon dioxide disposal are especially efficient, if pressure separation is accompanied by the division of oxygen-rich/ carbon-dioxide-poor and oxygen-poor/ carbon-dioxide-rich blood streams within the ventricle. This does not disagree with the statement that pulmonary (or systemic) bypass might be of advantage during certain temporary physiological circumstances, e.g. if oxygen consumption or carbon dioxide removal is limited by external factors (like during diving), or if the disadvantages of reduced oxygen delivery might be outweighed by the advantages of the retention of carbon dioxide (e.g. during digestion). These special

physiological conditions are discussed in section 4.3.8 together with those of crocodiles.

Fig. 27 shows cross sections through the ventricles of several species of Chelonia, Rhynchocephalia, and Squamata showing the size and position of the muscular ridge in relation to the *cavum venosum* and *cavum pulmonale*. The muscular ridge and the *cavum venosum* and *cavum pulmonale* are very heterogeneously shaped within all depicted species. Decisive for the possible degree of shunting and for pressure separation is the length relatively to the cava and the shape of the muscular ridge to separate the *cavum venosum* and the *cavum pulmonale* effectively from each other. However, a constant pattern correlateing the shape of the cava and the muscular ridge with their ability for pressure separation could not be detected. Contrary, the various species show a variety of muscular ridge and 'bulbuslamelle' forms combined with very inhomogeneous ventricle shapes and cava sizes.

Chelonia mydas is not able to generate different pressures in both circulations, although the relatively thin muscular ridge should be able to reach the opposite wall (Fig. 27 B). *Varanus* spec. has a massive muscular ridge and is able to separate pressures fitting very well into the proposed logic. According to Kashyap (1950), the muscular ridge of Typhlopidae is exceptionally weakly developed and even smaller than their 'bulbuslamelle' (Jensen et al., 2014b). The present results can neither support nor deny this hypothesis, because the MRI scan produced images with a very bad resolution and nearly unidentifiable detail structures (Fig. 17 C, 27 D). This might be due to the 30 years of storage of the specimen in formol and ethanol and because the blood fixed inside the heart could not be removed. Both depictions of *Python molurus* (Fig. 27 E and F) show a relatively well developed muscular ridge in an apparently differently strong contracted ventricle, and indeed pressure separation is possible in this species. Another examined specimen from the Boidae family, *Liasis amethistinus,* has a quite short and thin muscular ridge (Fig. 27 G). In contrast, the muscular ridge of *Boa constrictor* (Fig. 27 H), a close relative of the pythons with a very similar ecology and way to feed (large prey animals with an accompanying large

post-prandial increase in metabolic rate), has a long and well developed muscular ridge, but is not able to generate separate pressures. The same is true in all studied Colubridae and Viperidae: Their muscular ridge is sufficiently well developed to reach the 'bulbuslamelle', but probably none of them accomplishes pressure separation. Differences concerning various aspects of ecology also appear irrelevant: The present material does not allow for a distinction between land-living and aquatic species, as the only aquatic species examined is the turtle. However, there are examples of land-living species with and without pressure separation. It is probably a functional coincidence that the aquatic *Chelonia mydas* and the largely aquatic anaconda *Eunectes notaeus* (Jensen et al., 2014b) both have no pressure separation. There are sit-and-wait predators with low activity levels that have pressure separation (*Python molurus*) and others that do not (*Boa constrictor, Bogertophis subocularis, Pantherophis guttatus*). The picture is similar fuzzy when looking at toxicity, ovo- and viviparity, body mass or length, level of activity, or prey size. The ability to generate different blood pressures in the systemic and pulmonary circulation cannot be unequivocally correlated to any of these parameters nor to high post-prandial or general metabolic rates (compare also Jensen et al. (2014)). The pure morphological shape alone is apparently not sufficient to judge the ability of the muscular ridge to close the gap between the *cavum venosum* and *cavum pulmonale* pressure-tight throughout the cardiac cycle. According to Jensen et al. (2010b), a muscular ridge consisting of dense myocardium is an indicator of pressure separation, but this could not be examined here.

It has not been described yet that the *cavum venosum* of pythons is surrounded by exceptionally dense myocardial tissue that is denser than the myocardium of the other two cava (Fig. 16 E and F). According to Webb et al. (1971), the *cavum arteriosum* and *cavum venosum* are both equipped with equally compact musculature. It would be interesting to examine the ventricular wall of the three cava in other pressure-separating species to see whether this is a repetitive pattern. Maybe, the differently shaped trabeculae and strands in the snake ventricle that appear to

contribute to the directioning of blood within the ventricular chambers have a higher impact on blood flow directioning than previously considered, see also Jensen et al. (2014b). Examinations of these flow dynamics require living animals and thus are beyond this study.

4.2.2 The size of the different cava

The results show that the *cavum venosum* is smaller than the *cavum arteriosum* and the *cavum pulmonale* in all examined species. However, the difference for pythons is not as striking (see Fig. 16 B) as described by Jensen et al. (2010b; 2014), who reported the volume of the *cavum venosum* being one tenth of the *cavum arteriosum*. According to these studies, the very small *cavum venosum* limits the blood volumes available for pulmonary bypass in pythons, resulting in an almost complete (mammalian-like) separation of blood streams within the heart. This statement is debateable: Bypass in pythons has been measured in several studies. Starck (2009) measured an increase of Q_{pul}/Q_{sys} from 0.72 to 0.52 in digesting pythons, indicating that systemic blood flow increased compared to pulmonary blood flow during digestion (and that systemic blood flow always exceeded pulmonary blood flow). In my diploma thesis I examined central cardiac shunting in *Python regius* using Doppler-echocardiography and respirometry (Campen, 2009). I measured different degrees of pulmonary bypass during fasting and resting, digestion, and exercise in *Python regius*. While the fraction bypassing the systemic circulation was smaller during exercise compared to rest, and larger during digestion compared to fasting. The data suggests that bypass might help balancing metabolic alkalosis (increased pulmonary bypass) and acidosis (lower pulmonary bypass) caused by digestion and exercise, but disagrees with the hypothesis that pythons cannot bypass one or the other circulation.

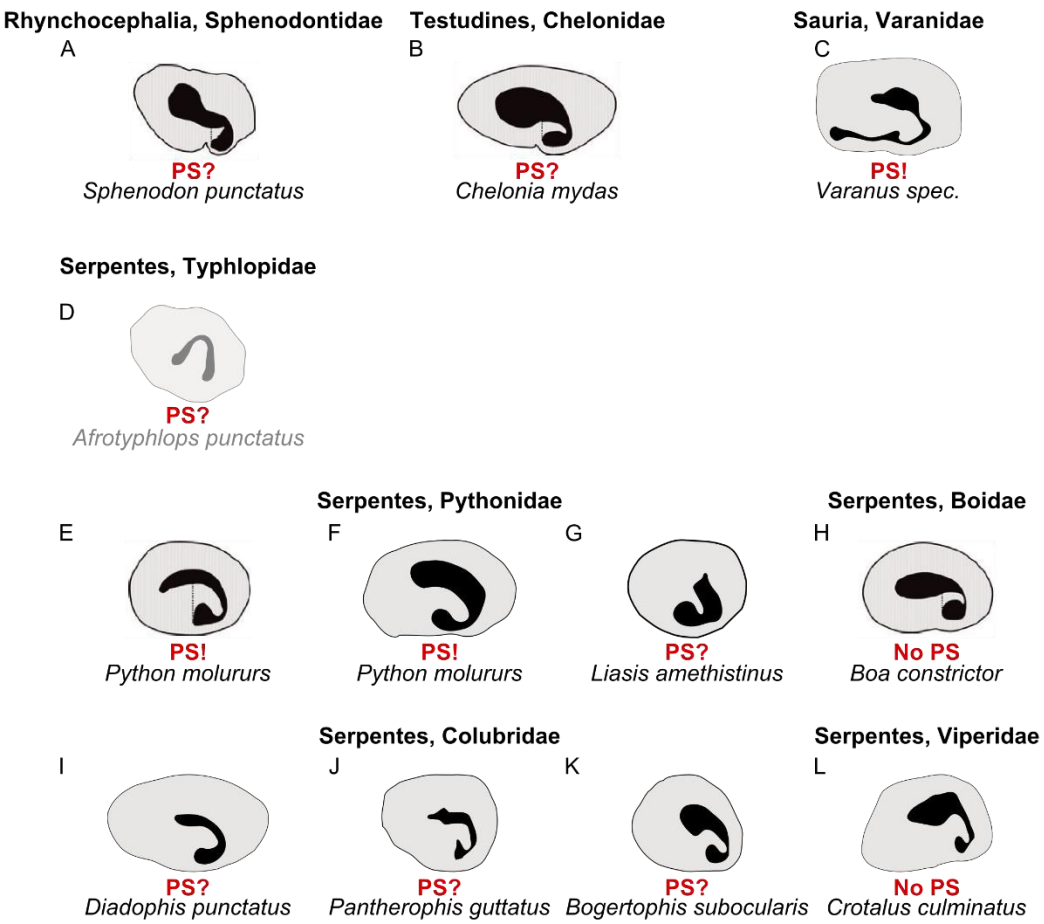

Fig. 27: Cross sections through the ventricles of several species of Chelonia, Rhynchocephalia, and Squamata showing the size and position of the muscular ridge in relation to the *cavum venosum* and *cavum pulmonale*.
Pictures A, B, E, and H are from Jensen et al. (2014), C is based on an anatomical drawing of a cross section from Mathur (1944), G is based on an anatomical drawing by Webb et al. (1974), I is based on an anatomical drawing of a cross section from White (1959), D, F, J, K, and L are based on my own material. The *Afrotyphlops punctatus* image (D) is kept semitransparent, because the interpretation of the scan is uncertain due to a very bad resolution. Grey: myocardium incl. muscular ridge; Black: *cavum venosum* (above muscular ridge), *cavum pulmonale* (under muscular ridge). PS: Pressure separation has been measured. The state of contraction of the ventricle at the time point of fixation is unknown except for D and H showing a diastolic ventricle, and E showing a mean value of differently contracted ventricles.

4.2.3 Further morphological structures with an impact on bypass capacity

The identification of further bypass-related structures other than the muscular ridge was often hindered by the resolution obtained: The atrioventricular funnel was only visible in *Python molurus*. The atrioventricular valves could not be identified in any

scan, possibly because they lie too close to the wall of the atrioventricular funnel. Since the aortic and pulmonary artery valves are visible for example in *Python molurus,* although they are very thin, resolution is probably not the reason, why the atrioventricular valves could not be identified. Also Jensen et al. (2014, Fig. 4), could not identify the atrioventricular valves, although they used nuclear magnetic resonance imaging with a higher resolution. I can therefore not confirm whether or not the atrioventricular valves are long enough and suitable shaped to cover the interventricular canal and separate blood streams from the atria effectively during ventricular diastole. However, several studies on blood streams in the beating python heart suggest that this is the case (e.g. Campen, 2009; Jensen et al., 2014; Starck, 2009). The length of the atrioventricular valves in various snake species in relation to the interventricular canal should be reassessed using histology and flow measurements in the indisturbed beating hearts to clear up the matter.

4.3 Pulmonary bypass, and blood flow through the *Foramen Panizzae* and the aortic anastomosis in crocodiles

4.3.1 Anatomical structures with an impact on blood flow distribution in the crocodilian circulation

The cog-teeth-like valves decide about the degree of bypass. For complete pulmonary bypass, the cog-teeth-like valves must close the pulmonary trunk pressure-tightly, so that all blood from the right ventricle is ejected into the left aorta. My results indicate that the cog-teeth-like valve can achieve this function (Fig. 21). As described by Axelsson et al. (1996), the tissue nodules on both sides are positioned and shaped so they can interlock like the cogs of a cog-wheel. The cranial part of the myocardium is positioned around the pulmonary trunk structured in a way that allows it to act as a constrictor muscle, pressing the tissue nodules of the cog-teeth-like valves together, as already suggested by White (1969). Depending on the contraction of the constrictor-like arranged myocardium, all degrees of pulmonary bypass are probably possible. Accordingly, I tested them all in the simulation model.

The cog-teeth like valves where depicted for *Crocodylus* species, but no images of their structure in alligators is available yet: Images are available for *Crocodylus rhombifer* (Axelsson et al., 1996) and *Crocodylus porosus* (Franklin and Axelsson, 2000; Webb, 1979), herein I contribute further images of the cog-teeth-like valves of *Crocodylus porosus* and *Crocodylus niloticus* (Fig. 27). The pictures obtained by different imaging methods differ greatly, but these differences are not correlated with the species. In the in-situ-perfused hearts of *Crocodylus porosus* (age unknown, Fig. 28 A) and *Crocodylus rhombifer* (probably adult, Fig. 28 B), the cogs appear cubic. The histology-based 3D reconstruction of the hearts of juvenile specimen of *Crocodylus niloticus* (Fig. 28 C and D) and the MRI of an adult *Crocodylus porosus* (Fig. 28 F) show the cog-teeth-like valves as a continuing ridge with some thicker nodes but without any real gaps in between them. A photograph of the cog-teeth-like valves of a dissected

heart of an adult *Crocodylus porosus* (Fig. 28 E) shows cog-teeth-like valves with a mushroom-like shape, with the nodules sitting on thin 'stipes'. This very different shape might be caused by drying out of the cogs after dissection of the heart, but the circumstances of the dissection are unknown. The shape of the cog-teeth-like valves are apparently less homogeneous than previously thought and can be deformed by imaging techniques. This should be further explored.

Downstream, the next structure influencing blood flow direction is the *Foramen Panizzae*. My results indicate that the *Foramen Panizzae* is positioned under the long margins of the bicuspid aortic valves in a way that makes the valves overlap the *Foramen Panizzae* completely (Fig. 19 and 20). This hypothesis is supported by studies that indicate that both (Greenfield and Morrow, 1961) or at least the right (Axelsson et al., 1996) aortic valves are long enough to overlap the *Foramen Panizzae* during ventricular systole, effectively preventing blood flow between the aortae.

Axelsson and Franklin (2001) examined the reaction of the *Foramen Panizzae* to vasoactive substances. They showed that the *Foramen* dilates when exposed to vasoactive intestinal peptides while it constricts when exposed to adrenaline. The diameter of the *Foramen Panizzae* might therefore be actively controlled. The *Foramen Panizzae* of the alcohol-stored specimen I used was oval, while Axelsson et al. (1996) show images of a completely round, probably fully dilated *Foramen*. My histological sections show the short diameter of the oval *Foramen Panizzae*, which is never more than 5-10% of the diameter of the right aorta. However, its length might be around 20% of the diameter of the right aorta. Both diameters are smaller than the 35-40% measured by Axelsson et al. (1996) using angioscopy in a perfused *Crocodylus rhombifer* heart.

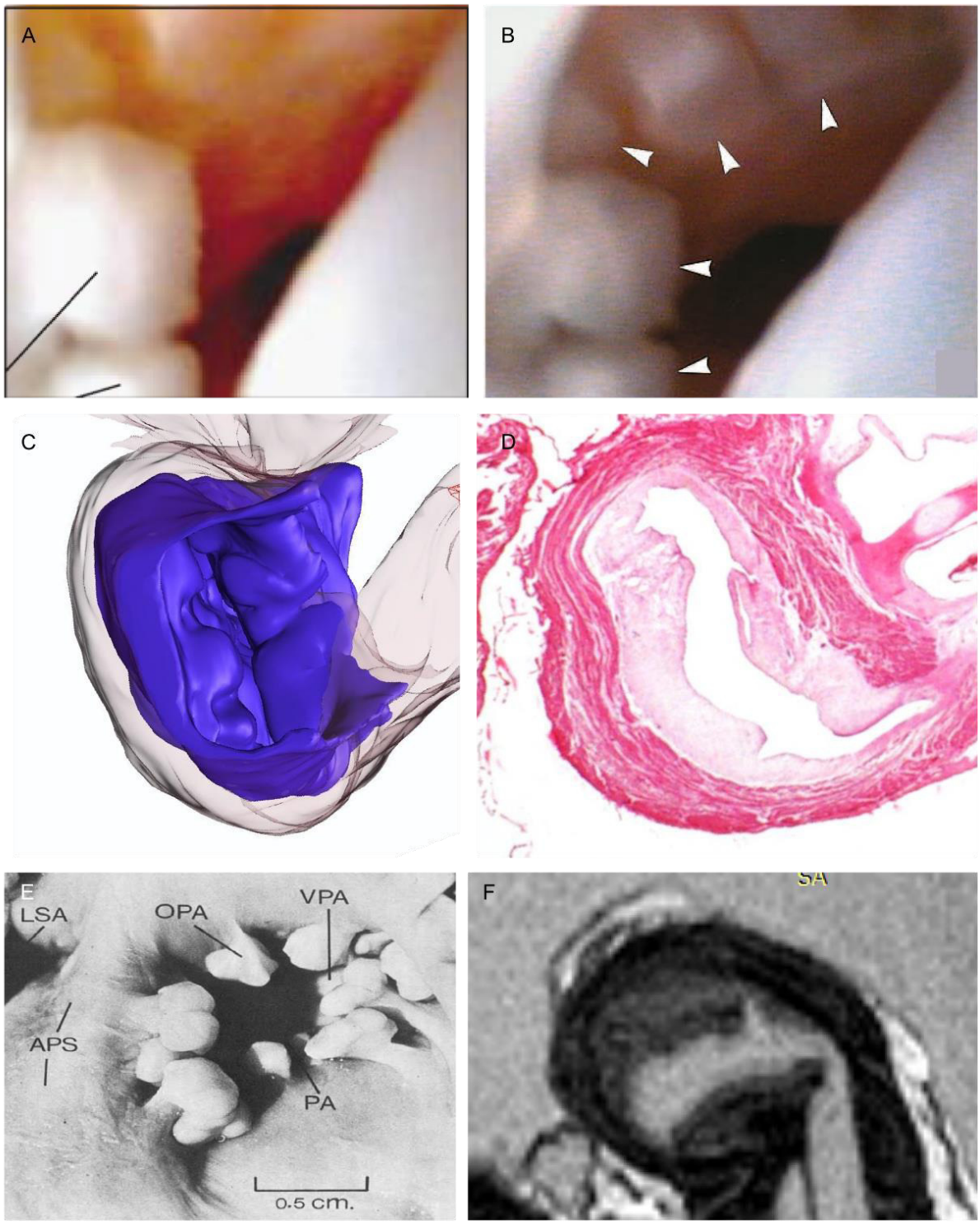

Fig. 28: The cog-teeth-like valves in various crocodile species.
A: Single cog from an in-situ perfused heart of *Crocodylus porosus* (Franklin and Axelsson, 2000). B: Row of cogs from the cog-teeth-like valve of an in-situ perfused heart of *Crocodylus rhombifer* (Axelsson et al., 1996). C: From Fig. 21 E, 3D reconstruction based on the serial sections of the heart of *Crocodylus niloticus*. D: From Fig. 21 E: Originally colored photograph of a H&E stained cross section through the heart of *Crocodylus niloticus* showing also the arrangement of the muscular fibers of the constrictor muscles. E: Photograph of the cog-teeth-like valves of an adult *Crocodylus porosus* (Webb, 1979). F: MRI scan of the cog-teeth-like valve of an adult *Crocodylus porosus*, from the scan shown in Fig. 21 C. Scale bars in the original publications and Fig. 21 of this thesis.

Axelsson and Franklin (2001) proposed that the *Foramen Panizzae* might be dilated during pulmonary bypass (diastole and systole) to enable blood flow from the left into the right aorta to supply the brain with oxygen-rich blood (see simulation results in Fig. 24 B, higher *Foramen Panizzae* flow coefficients increase blood supply of the anterior body including the brain). With respect to the morphological results shown in Fig. 19 and 20, I can nevertheless not confirm that even the dilated *Foramen Panizzae* enables for significant blood exchange between the aortae during systole. However, changes in the size of the *Foramen Panizzae* have an effect during diastole when the *Foramen Panizzae* is not overlapped by the aortic valves (Fig. 23 B, see also section 4.2.5). The aortic anastomosis is important for the distribution of blood volumes, but being a vascular connection without special attributes it was not examined in the morphological part of this thesis, but studied by the simulation model.

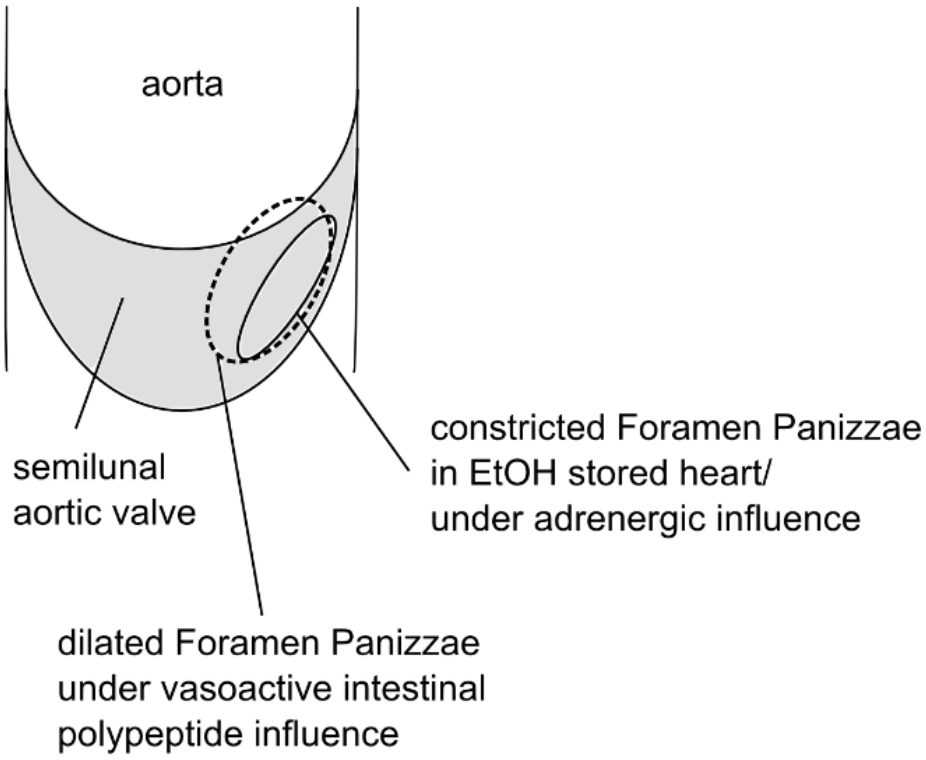

Fig. 29: The potential influence of dilation of the *Foramen Panizzae* on blood flow through it during ventricular systole.
While the constricted *Foramen Panizzae* is completely overlapped by the medial cusp of the semilunar shaped aortic valve, its margin might not be overlapped by the aortic valve when it is in a dilated state.

Another functionally not fully explored part of the cardiovascular systems of crocodiles is the multipart cartilage clasp. Cardiac cartilages, or a cartilage cordis also occur in mammals, e.g. in hamsters (Durán et al., 2004), in turtles (López and Durán, 2003), and in snakes and monitor lizards (Young, 1994). In the turtle *Mauremys leprosa*, the cardiac cartilage is a derivative of the neural-crest and part of the horizontal septum and the right aortic wall (López and Durán, 2003). In snakes, a cardiac cartilage was found in 11 of 42 species examined, positioned near the basis of the aortae and the pulmonary trunk. According to Young (1994), there is no connection between the presence of a cartilage and body size, taxonomy, or habitat. He therefore suggested that the presence of cartilage in the snake heart just reflects the potential for chondrification that is present in the connective tissue of the aorticopulmonary septum without playing a functional role. Rathke (1866) and Beddard and Mitchell (1894) described a hyaline cartilage in the heart of crocodiles, and Sabatier (1873) stated that the tight association of the cartilage with the left aortic arch provides high rigidity. Only one study (White, 1956) deals with its detailed structure. The 3D structure of the cartilage in *Crocodylus niloticus* (Fig. 22) differs so much from the schematic drawing of White (1956) for *Alligator mississippiensis*, that is was partly impossible to transfer his terminology for the various parts of the cartilage clasp: The drawing of White (1956) shows a kind of two-dent fork with the individual forks positioned around the *Foramen Panizzae* plus a semilunar shaped part reaching around the *Foramen* from the same side, but more horizontally. In contrast, the cartilage clasp in *Crocodylus niloticus* (and, according to the µCT scans, also in *Caiman crocodilus*) is shaped like an interrupted ring surrounding the *Foramen*. White (1956) described a small cartilage nodule positioned at the basis of the pulmonary trunk. This nodule could not be found in *Crocodylus niloticus*, but there is another nodule, which is positioned at the opposite (distal from the pulmonary artery) basis of the right aortic valves. Additionally, in *Alligator mississippiensis* there is no elongated process on the ventrolateral cartilage that reaches far into the ventricle (Fig. 22 C, part A). This arrangement seems more suitable to stabilize the aortic valves around the *Foramen Panizzae* and the bases of

the aortic valves. It would be interesting to examine the cartilage shapes of different crocodilian species in connection with the extent of dilation and constriction of the *Foramen Panizzae*.

4.3.2 Possible explanations for the heterogeneousity in the results of former studies on living animals

As summarized by Campen and Starck (2012), experimental studies on the 'reptilian' heart are dominated by highly invasive studies, including open heart surgery, vagotomy, large vessel ligation, or perfused heart models. While those studies provide important basic information, it is unclear how much they reflect a regular physiological condition. Another problem occurs in studies performed in animals under anaesthesia. In former studies, capillary filtration rate and the role of the lymphatic system as a carbon dioxide sink have been neglected. The movement of lymph against gravity is closely connected to movements of skeletal muscles and the lung. Anesthesia, disrupting locomotive muscle movement and reducing lung movement leads to drastically reduced backflow of lymph to the lymph hearts and therefore into the systemic vein in frogs (Hillman et al., 2010). If this is also case in ectothermic sauropsids, anesthesia during experiments would not only disturb normal flow and shunting because of general depression of the cardiovascular system. Lymph storage uncouples oxygen and carbon dioxide and thereby influences blood gas composition: Around 50% of the carbon dioxide produced in tissues is dissolved in the plasma, thus carbone dioxide can leave the blood vessels and can be temporarily stored in the lymph system. In contrast, oxygen is for the most part bound to hemoglobin and thus remains in the blood vessels. Consequently, less blood volume and fewer carbone dioxide would return to the left ventricle with implications for blood and carbone dioxide distribution in the body. I acknowledge the difficulty of measuring patterns of blood flow by non-invasive methodology is difficult, nevertheless application of these methods as far as possible should be encouraged. Another possibility is the application of simulation models. Always being a simplification of nature, these models must be

validated by physiological studies. Both methods must therefore go hand in hand (see also Burggren et al. (2013).

4.3.3 Current limitations of the simulation model

The simulation model did not consider that the sizes of the various vascular compartments may change over time as a result of vasodilation and vasoconstriction. It has been shown that vasoactive substances influence vascular resistance in many sauropsids (Axelsson et al., 2001; Galli et al., 2005; Galli et al., 2007; Skovgaard et al., 2005; Skovgaard et al., 2017; Stecyk, 2004). Also, Kagstrom et al. (1998) could show that various neuropeptides cause vasodilation of gastrointestinal vessels or increased gut movement or both. In further studies, the algorithm could be applied to study the role of varying vascular compartment sizes and vascular resistance during pulmonary bypass.

Crocodiles have large lymphatic vessels. Apart from passive transport by body movements, lymph is actively transported by two posteriorly situated lymph hearts (e.g. McCauley, 1956). The lymphatic vessels transport significant fluid volumes and are closely linked to the blood-transport system. Smits and Lillywhite (1985) reported that snakes have large interstitial fluid volumes that can be quickly shifted into the blood vessels. Nevertheless, I decided not to include the impact of lymph flow in the simulation, as lymph flow takes place in parallel to the veins, starting at the systemic capillary beds and ending in the large systemic veins. Lymph transport does therefore not directly affect the sites relevant for the results I am interested in. Nevertheless, fluid volumes and carbone dioxide might be stored temporarily in the lymphatic vessels, having an impact predominantly on the timing of right-ventricular return.

For a physiological interpretation of the results one should keep in mind that the crocodilian cardiovascular anatomy can redirect blood flow into the systemic circulation without changing the oxygen content of the blood. Thus, a higher blood volume distributed to a body region does not necessarily increase the oxygen supply

to that region. The model simulates the redistribution of blood volumes in the crocodilian body, but is not suited for quantitative statements about the blood gas contents of these blood volumes. Wang and Hicks (1996b) used a two-compartment model to calculate arterial oxygen contents depending on pulmonary bypass and lung ventilation. Their results show that arterial oxygen content is influenced by the degree of pulmonary bypass and lung ventilation, but additionally by variables like the rate of oxygen uptake, blood oxygen carrying capacity, and the level of hypoxia.

Important factors for deducing hypotheses about oxygen supply and carbon-dioxide disposal from blood supply are unexplored so far: It is unknown, for example, whether blood that has already passed the systemic circulation once contains enough rest oxygen to contribute to organ supply and there is probably no clear answer, as this depends on the metabolic activity of the tissues it has passed already. Crocodilian blood has a relatively high oxygen carrying capacity (Wells et al., 1991), while metabolic rates in ectotherm sauropsids are relatively low compared to endotherm animals. Blood that has already passed the systemic circulation might therefore contain enough oxygen to contribute to tissue oxygen supply. Apart from oxygen saturation of the blood and the volume of blood passing the organs, there are internal factors influencing oxygen delivery to tissues, e.g. the Bohr Effect. All these factors make it a challenge to estimate the blood gas content or saturation on the basis of volume shifts.

Although the simulation model is largely simplified and includes uncertainties concerning the correct parameter values, the results of the simulation support physiological assumptions and experimental results in many points. Further fine-tuning of the algorithm and adjustment of parameter values is possible and desirable, when new experimental data become available.

4.3.4 The non-linear relationship between left aortic aperture and parameters tested in the simulation model

The relationship between the flow coefficient of the left aorta and the parameters tested has a characteristic, non-linear shape: it changes sharply between flow coefficients of 0% and 10% (Fig. 24 A-D), then approximately linearly at intermediate coefficients and more sharply again near complete pulmonary bypass. This characteristic shape would probably also occur in reality as it reflects the impact of pressure differences between the vessels (approximated by the comparison of the departments' excess volumes in the model). Pressure differences between two equally sized interconnected vessels are maximal, if the difference between blood volumes inside them is maximal. This is the case between the right ventricle and a nearly empty left aorta during systole at very low bypass levels (e.g. left artic flow coefficient of 10%). When fill levels balance, the pressure difference loses impact.

4.3.5 Q_{pul}/Q_{sys} as a measure for pulmonary bypass in crocodiles

With increasing flow coefficients of the left aorta, blood input into the pulmonary circulation decreases. As a consequence, also the ratio of pulmonary to systemic blood flow Q_{pul}/Q_{sys} decreases. According to the simulation results, this decline is non-linear resulting from fill level changes in the large outflow vessels. As expected, the simulation results show that Q_{pul}/Q_{sys} is 1 with a non-permeable left aorta and *Foramen Panizzae*, representing a balanced right and left ventricular output as it is standard in birds and mammals (e.g. Klabunde, 2005). Q_{pul}/Q_{sys} is also influenced by the flow coefficient of the *Foramen Panizzae* (see Fig. 24 H). The reason is the impact of the acceptor compartments capacity on transfer volumes. Flow from the left into the right aorta through the *Foramen Panizzae* increases left aortic capacity. This enables increased flow from the right ventricle into the left aorta instead of the lungs, increasing overall systemic flow and decreasing Q_{pul}/Q_{sys}. This increase is physiologically relevant: In real life, the volumetric flow from the right ventricle

depends on the diameter/ cross-section area of the vascular connection (cog-teeth-like valves) and the pressure in proximal aortae. Flow from the left into the right aorta decreases this pressure with the consequence of higher input from the right ventricle.

In experimental studies Q_{pul}/Q_{sys} is often used to characterize the degree of pulmonary or systemic bypass in ectotherm sauropsids, with a ratio below 1 indicating pulmonary bypass, and above 1 indicating systemic bypass (Axelsson and Franklin, 1997; Galli et al., 2005; Starck, 2009; Wang et al., 2002). However, the simulation results show that values of Q_{pul}/Q_{sys} for different flow coefficients can be relatively close to each other in crocodiles, especially at intermediate degrees (Fig. 24 H). Moreover, the aperture of the *Foramen Panizzae*, which has not yet been quantified in studies synchronously with the measurement of Q_{pul} and Q_{sys}, has an impact on Q_{pul}/Q_{sys} as the simulation shows. Hence, experimentally determined values of Q_{pul}/Q_{sys} with a certain error can result from a broad range of degrees of pulmonary bypass. Accordingly, Q_{pul}/Q_{sys} may not be a good value to quantify pulmonary bypass in crocodiles (whereas it ia acceptable in all other ectotherm sauropsids). It is therefore important to develop a more informative value.

4.3.6 Is the duration of complete pulmonary bypass limited?

A still unexplored consequence of crocodilian vascular topography is that complete pulmonary bypass not only shuts off the lung, but also the left ventricle and consequently all compartments supplied by the latter, i.e. the anterior and posterior body regions (Fig. 23 D and 24 B and C). In this case, blood circulation exclusively takes place via the right ventricle/left aorta (see Fig. 10, circulation route highlighted by grey dots), while left ventricular output comes to rest as a result missing left ventricular return. In this case, the anterior and posterior body compartments can only be supplied via the *Foramen Panizzae* and the aortic anastomosis. However, because the *Foramen Panizzae* and the aortic anastomosis are positioned posterior to the heart and only allow blood exchange between vessels that lead to the right ventricle, their blood flow cannot contribute to left ventricular return. Running dry of the left ventricle is

consequently inescapable during complete pulmonary bypass if there are no additional, yet unexplored vascular connections that ensure left ventricular return. This fact has not been discussed before.

With my chosen default compartment sizes in the simulation, the left ventricle can empty the pulmonary vessels within three heartbeats (Fig. 23 D). Afterwards, it is cut off from blood return and remains 'empty', most likely containing a small and immobile residual blood volume. An 'empty ventricle syndrome' can occur in humans as a consequence of anaphylaxis and quickly results in cardiac arrest if left untreated (e.g. Simons, 2010), and the same effect must be expected in crocodiles during complete pulmonary bypass, too. Shelton and Jones (1991) report that cardiac output decreased substantially as a consequence of ceasing left ventricular return when they mechanically occluded the pulmonary arteries of *Alligator mississippiensis* 'very briefly'. I hypothesize that crocodiles cannot sustain complete pulmonary bypass steadily for a longer time, e.g. during prolonged diving. I assume that pulmonary bypass in crocodiles is either incomplete or limited to a few heartbeats. The inhomogeneity in the results of experimental studies trying to measure complete pulmonary bypass over a longer period might be caused by this fact.

4.3.7 Numerical example: Application of the simulation results to a crocodile of mass 10 kg

Carmena-Suero et al. (1979) reported that total blood volume/100 g body mass is between 3.6 ml (females) and 4.0 ml (males) in juvenile *Crocodylus rhombifer* aged approximately 3.5 years and that these animals have a body mass of around 10 kg. A fictive 10 kg juvenile crocodile with compartment sizes as used for the simulation and a total blood volume of 380 ml would, according to the simulation and under the assumption that it does not bypass the lungs consequently have a total cardiac stroke volume of slightly more than 12.5 ml/heartbeat. To obtain volumes pumped in a minute, I here assume a mean heart rate of 40 bpm. Under these conditions, cardiac output would be 500 ml/min without pulmonary bypass in the exemplary crocodile.

This number is close to the cardiac output of around 52 ml min^{-1} kg^{-1} (520 ml/min for a 10 kg animal) measured by Shelton and Jones (1991) for *Alligator mississippiensis*. Assuming a *Foramen Panizzae* and aortic anastomosis flow coefficient of 30%, cardiac stroke volume would be distributed as follows: around 6 ml blood/heartbeat would be pumped into the lung (240 ml/min), around 2 ml blood/heartbeat into the anterior body (80 ml/min), and around 3.5 ml blood/heartbeat into the posterior body (140 ml/min). The digestive tract would receive less than 1 ml/heartbeat (40 ml/min) under these conditions. Without pulmonary bypass, net blood flow through the *Foramen Panizzae* from the right into the left aorta would be around 0.3 ml/heartbeat (12 ml/min) and net blood flow through the aortic anastomosis would be approximately 1 ml/heartbeat (40 ml/min), which means it is more than 3 times higher than *Foramen Panizzae* flow. To extrapolate these values to human conditions: If an adult human being has 5 l total blood volume, than more than half a liter of blood would pass his aortic anastomosis per minute (if he had one).

Complete pulmonary bypass presumably cannot be sustained for more than a few heartbeats. Therefore, a left aortic flow coefficient of 80% to calculate an example of incomplete and thus sustainable pulmonary bypass is assumed, combined with an intermediate *Foramen Panizzae* and aortic anastomosis flow coefficient of 30% as above. Under these conditions, total cardiac stroke volume is reduced to around 9.5 ml/heartbeat (380 ml/min) after equilibration due to ceasing left ventricular return and output. This smaller output is distributed as follows: Blood supply of the lungs and the anterior and posterior body are both reduced to around 25%: The lungs receive around 1.3 ml/heartbeat (52 ml/min) instead of 6 ml/heartbeat without pulmonary bypass. The anterior body receives around 0.6 ml/heartbeat (24 ml/min) instead of 2 ml/heartbeat. Supply to the posterior body is less restricted (about halved), it receives about 2.1 ml/heartbeat (84 ml/min) instead of 4.5 ml/heartbeat. The digestive tract receives 5.5 ml/heartbeat (220 ml/min) instead of 1 ml/heartbeat (40 ml/ min). The increment in blood supply of the digestive tract is the most notable change in blood supply of any of the body compartments. Net blood flow through the *Foramen*

Panizzae and the aortic anastomosis has reversed and is now from the left into the right aorta. It is around 0.3 ml/heartbeat (12 ml/min), the same volume as without pulmonary bypass. Net blood flow through the aortic anastomosis is 50% higher than in the example without pulmonary bypass: approximately 1.5 ml/heartbeat (60 ml/min).

4.3.8 Physiological function of bypass

As summarized in section 1.2, several hypotheses about the functional significance of pulmonary bypass in ectotherm sauropsids have been developed and partly examined in the past, most of them focusing on its impact on the lungs and digestive tract.

The simulation model simulation tracks changes in several physiologically relevant parameters resulting from modifying flow coefficients of the left aorta, the *Foramen Panizzae* and the aortic anastomosis in crocodiles. The results indicate that, apart from its impact on the lungs and digestive tract, pulmonary bypass reduces blood supply of the anterior and posterior body regions. Up to now this impact has largely been neglected for the interpretation of the physiological function of pulmonary bypass. Although the simulation cannot model changes in blood gas levels resulting from blood volume redistribution, I will attempt to relate blood volume redistribution and changes in oxygen and carbon dioxide content in order to allow some physiological conclusions.

Because pulmonary bypass reduces blood flow to the lungs, it has been discussed as a mechanism that contributes to long diving durations in crocodiles and turtles (e.g. Kardong, 1995). It has been hypothesized that redirecting oxygen-poor, carbon-dioxide-rich blood into the body instead of the lungs increases oxygen delivery to the tissues as a result of the Bohr Effect (oxygen dissociation from hemoglobin is increased by lower blood pH). The model shows that pulmonary bypass in crocodiles results in reduced blood supply of the anterior and posterior body regions while blood supply of the digestive tract increases. According to the model, oxygen supply to the

anterior and posterior body regions is reduced because of 1) ceasing oxygen content of the blood caused by apnoea, and 2) reduced blood supply because of pulmonary bypass. This will result in physiologically problematic situations: The reduced blood supply of the anterior body region may harmfully effect the brain, and it is functionally unclear why increased blood supply of the digestive system during diving should be of advantage. A recent study by Jensen et al. (2014a) showed that turtles protect their cells from anoxia-induced damage by upregulation of nitrite and other NO metabolites in the tissues. Thus, they increase their anoxia tolerance during diving. A similar mechanism in crocodiles might lead to an increased anoxia-tolerance in the anterior and posterior body regions, reducing the negative effects of pulmonary bypass during diving for these body areas, nevertheless increased perfusion of the digestive tract does not seem to be advantageous.

Farmer et al. (2008) showed that pulmonary bypass occurs during digestion in crocodiles. Crocodiles ingest large, unchewed prey items that contain bones and fur. This diet requires large amounts of gastric acid for digestion, leading to postprandial alkalinisation of the blood. This is also true in other ectotherm sauropsids that consume large prey items. Farmer et al. (2008) suggested that pulmonary bypass occurs during digestion, because supply of the digestive tract with carbon-dioxide-rich blood facilitates gastric acid production by providing protons to HCl formation and buffers the alkaline tide via the hydrogen carbonate buffer system. During pulmonary bypass the digestive tract receives larger blood volumes than before (coming from the right ventricle via the left aorta instead of from the left ventricle via the *Foramen Panizzae*) that are oxygen-poor and carbon dioxide-rich without the need for hypoventilation. However, this hypothesis has only recently been challenged by a study by Malte et al. (2016). There modelling approach predicts that pulmonary bypass during digestion will compromise oxygen uptake and that hypoventilation has a much smaller negative impact on oxygen supply.

Crocodilian vascular topography is unique in that parts of the digestive tract, i.e. the small intestine and the rectum, are supplied with blood from vessels emerging from

the right aorta in addition to the 'standard supply' via the left aorta (Campen and Starck, 2012; Hafferl, 1933; Hochstetter, 1898; see also Fig. 8, 9 and 10, 'posterior body'). This makes hypotheses on the meaning of pulmonary bypass for digestive performance even more complex: Without pulmonary bypass, the small intestine and the rectum receive oxygen-rich right aortic blood via both aortae (directly via the right aorta plus indirectly via the left aorta through the *Foramen Panizzae* and the aortic anastomosis). Concurrently, all other organs of the digestive tract, e.g. the stomach, large intestine and liver, also receive oxygen-rich right aortic blood, but exclusively via the left aorta (see previous paragraph). At the onset of (incomplete) pulmonary bypass, mean blood gas composition of the blood that supplies the small intestine and the rectum begins to differ from mean blood composition of the blood supplying the rest of the digestive tract: The right aortic, oxygen-rich blood supply of the small intestine and rectum decreases in volume, but continues to provide blood coming directly from the lungs, with a higher oxygen level than left aortic blood (which has already passed the body tissues). Concurrently, supply of the small intestine and rectum with oxygen-poor blood from the left aorta increases. Meanwhile, the rest of the digestive tract receives only oxygen-poor blood without admixtures. Therefore, the small intestine and rectum receive blood with a higher mean oxygen content and lower mean carbon dioxide content than other parts of the digestive tract during all degrees of pulmonary bypass. With this vascular arrangement, it is possible to supply the stomach and large intestine with oxygen-poor, carbon-dioxide-rich blood and at the same time supply the small intestine and rectum, as well as the anterior and posterior body with blood with higher oxygen and lower carbon dioxide content, because all blood coming from the lungs passes the small intestine first, before it reaches the digestive tract after it circulated through the right ventricle for a second time (compare Fig. 10). The supply of parts of the digestive tract by the right aorta has not been taken into account in the modeling approach of Malte et al. (2016).

As summarized by Campen and Starck (2012), there are many infrequently feeding species amongst the Chelonia, Squamata, and Crocodylia that show the same

principle pattern of gastrointestinal plasticity to adjust to fluctuating functional demands. The physiological advantage of pulmonary bypass for digestion might therefore be the same in crocodiles and snakes. Scattered data both on constrictor snakes and crocodilians suggest a functional integration of the digestive system's functional plasticity and digestive function with the cardiovascular system. Both systems appear to be integrated on various levels: conductive (increased blood volume), mechanical (hydraulic pump), and acid–base balancing (bicarbonate buffer and alkaline tide). Central cardiac shunting and circuitry of the major arteries suggest that morphological features might have evolved specifically to serve these functions.

Leite et al. (2013; 2014) conducted unilateral left vagotomy on *Crotalus durissus* to examine the long-term consequences of an abolition of the control of pulmonary arterial resistance on oxygen uptake, specific dynamic action, growth, fasting, and thermoregulation. The snakes that underwent surgery did show no differences concerning oxygen uptake resting or after feeding compared to the control group, grew equally fast, lost weight equally fast during fasting, and there was no metabolic reaction to reduced temperatures. Supported by the results of Eme et al. (2009; 2010), the functional relevance of pulmonary bypass for the control of metabolic rates or digestion in 'reptils' have been doubted and it has been suggested that they represent rather an ancestral trait without negative effects that has not been selected against (Burggren et al., 2013).

However, if the ability for pulmonary bypass exists and if the animal can benefit from it, it is probably used whenever it is useful for the animals. Pulmonary bypass shifts blood volumes from the peripheral anterior and posterior body regions, including the skin and superficial locomotor muscles, to the more central digestive tract. It might therefore play a role for heating in ectotherm sauropsids: Heated blood from the skin and muscles is shifted away to the more central body regions during basking, accelerating warming of the whole crocodile body and enabling heat storage. Pulmonary bypass has, for example, been found to accompany heating in the lizard *Iguana iguana* (Baker and White, 1970). Aside from heating support and heat storage

by blood volume redistribution, pulmonary bypass might reduce heat loss via the lungs (Baker and White, 1970). Nevertheless, the possible function of pulmonary bypass for warming has, to my knowledge, only been considered for non-crocodilian sauropsids so far. The available studies are summarized by Hicks and Krosniunas (1998).

4.3.9 The effects of blood flow through the *Foramen Panizzae* and the aortic anastomosis of crocodiles on blood and oxygen supply to the digestive tract and the anterior and posterior body regions

The simulation results show that pulmonary bypass influences the extent and direction of blood flow through the *Foramen Panizzae* and the aortic anastomosis. Fill level differences between corresponding aorta sections can serve as approximation for pressure differences in the simulation, as I chose the same compartment sizes for the corresponding compartments (proximal right and left aorta for flow through the *Foramen Panizzae* and distal right and left aorta for flow through the aortic anastomosis). Based on the comparison of the fill level during each time step, net blood flow through the *Foramen Panizzae* and the aortic anastomosis is predicted to be from the right into the left aorta without pulmonary bypass, which is in accordance with observations by Greenfield and Morrow (1961) and Axelsson and Fritsche (1991). Flow direction reverses at the onset of pulmonary bypass. This reversion of flow direction is experimentally supported and entitled ‘reversed *Foramen* flow’ and ‘reversed anastomosis flow’ (Axelsson et al., 1996; Axelsson et al., 1997).

When the lungs are not bypassed, the left aorta and consequently also the digestive tract would not receive blood, if there is no *Foramen Panizzae* and aortic anastomosis. The simulation model supports the idea that the digestive tract receives oxygen-rich, carbon-dioxide-poor blood from the left ventricle via the right aorta through the *Foramen Panizzae* and the aortic anastomosis under these conditions. Both the *Foramen* Panizzae and the aortic anastomosis therefore guarantee blood supply of the digestive tract when the left aorta is not directly supplied.

The reduced blood supply of the anterior body regions during pulmonary bypass can, to a certain degree, be buffered by a large *Foramen Panizzae* (Fig. 24 B), supplying the right aorta with left aortic (oxygen-poor, carbon-dioxide-rich) blood. The advantage of this admixture depends on the rest oxygen stored in this blood and the admixed portion of left aortic blood.

A large anastomosis could serve as an indirect mechanism to improve right aortic blood supply of the anterior body during incomplete pulmonary bypass. This is not intuitive at first glance, because the aortic anastomosis is positioned behind the branching-off of the vessels supplying the anterior body. The mechanism is indirect and based on changed pressures in the aortae that are caused by flow through the aortic anastomosis: Blood flow through the aortic anastomosis from the left into the right aorta increases blood fill level (pressure) in the distal right aorta. Consequently, the distal right aorta's capacity is reduced (pressure increases), leading to a larger fraction of oxygen-rich blood from the proximal right aorta being ejected into the anterior body compartment. Unlike for the anterior body, there is no possibility to buffer the reduced supply of the posterior body with right aortic blood during pulmonary bypass. A large aortic anastomosis could effectively buffer the reduced blood flow to the posterior body quantitatively (see Fig. 24 C), but it supplies the posterior body with oxygen-poor, carbon-dioxide-rich blood. This provokes the consideration whether sufficiently high blood supply of the posterior body might be important for other reasons than oxygen supply. One plausible reason could be to keep up renal blood pressure and blood flow to maintain kidney functions.

4.4 Comprehensive conclusion and perspective

Both the various 3D-morphological studies and the simulation experiment in this thesis provide some new insights to modify current functional hypothesis of the heart conditions in snakes and crocodiles, and provoke ideas for further research:

1) Pulmonary (and systemic) bypass have been measured in a variety of ectotherm sauropsids. However, bypass could not be clearly assigned to a certain physiological condition. Pulmonary and systemic bypass might not occur for time spans in the range of hours or days as assumed until now, but might be regulated on a beat by beat basis reflecting the current physiological demands on oxygen delivery and carbon dioxide disposal. The precise timing of bypass during digestion has not been fully explored. If shunting provides a beat-by-beat regulation of the acid–base balance one needs to apply fine-tuned measurements with the appropriate timely resolution. All published studies are, to a different degree, long-term studies. Thus, each study may report accurate results, but reflect animals in different physiological states (which have not been recorded) thereby precluding direct comparisons among them. This could also explain the inhomogeneity of past results (Campen and Starck, 2012).
2) I cannot support the textbook paradigm that pulmonary bypass in crocodiles increases diving performance. The simulation model shows that pulmonary bypass leads to reduced blood supply of the anterior and posterior body regions. During diving, oxygen supply to the anterior and posterior body regions is therefore reduced by two factors: a) Ceasing oxygen content of the blood caused by apnoea and pulmonary bypass, and b) reduced blood supply of the anterior and posterior body regions because of pulmonary bypass. I assume that the Bohr Effect cannot compensate for this so that the disadvantages of pulmonary bypass exceed the advantages of the Bohr Effect for oxygen supply. The digestive tract receives more blood during pulmonary bypass. I cannot explain why this should be of advantage during diving.

3) Morphological and anatomical examinations are not sufficient to unveil the possible degree or direction of bypass in ectotherm sauropsids. Especially the concept of pressure-tight separations cannot be tested using these methods. Future studies on the topic must include ventricular dynamics, pressure and interventricular turbulences, and vascular resistance and dilatability, because their interaction is significant for blood volume distribution.
4) Pulmonary bypass in crocodiles increases blood supply of the digestive tract with oxygen-poor, carbon-dioxide-rich blood. This supports the digestive performance hypothesis. Supplying the digestive tract, especially the stomach, with carbon-dioxide-rich blood influences the hydrogen carbonate buffer system, dampens the post-prandial alkaline tide and facilitates stomach acid secretion. Pulmonary bypass reduces the mean oxygen levels of the blood dramatically during increased post-prandial metabolic rates. Therefore, the advantage of pulmonary bypass for digestion has recently been doubted. The special vascular topography of crocodiles allows for the supply of the stomach and large intestine with carbon-dioxide-poor blood while the small intestine and rectum receive blood with a higher oxygen content. This has not been considered in any study on functional relevance of pulmonary bypass in crocodiles for digestion yet.
5) Pulmonary bypass in crocodiles reduces blood supply of the anterior and posterior body regions including the skin and superficial muscle layers. It might therefore improve heating and heat storage in crocodiles by shifting heated blood volumes into the central body regions and reducing heat loss over the lungs. The benefits of pulmonary bypass for heating and heat storage have not been considered or measured in crocodiles yet.
6) Balancing of cardiac dynamics and blood volume distribution in crocodiles only takes a few heartbeats after changes in the flow coefficient of the left aorta, the *Foramen Panizzae* or the aortic anastomosis in the simulation model.

7) The duration of complete pulmonary bypass in crocodiles must be limited to a few heartbeats. After a few heartbeats, the pulmonary circulation is empty and left ventricular return stops. This is assumed to disturb myocardial function severely and might lead to cardiac arrest. I therefore hypothesize that pulmonary bypass is incomplete or its duration must be limited. Future studies should take this fact into account.
8) The physiological function of pressure separation in non-crocodilian reptiles remains unclear.
9) Up to now, experimental studies are dominated by highly invasive studies, including open heart surgery or perfused heart models, and do not represent the condition of an undisturbed heart. Anaesthesia has strong effects on the heart and respiratory system and is therefore another disturbing factor. I encourage the use of non-invasive methods as Doppler-ultrasonography and respirometry. Simulation models can be an alternative, but their results have to be validated by physiological measurements.
10) The aim of future studies should include the provision of the important yet missing quantitative data, like ventricle/ ventricle cava volume, complete blood volume, bypass volume under different physiological conditions, timely fine-tuning of bypass and associated changes in blood acid-base balance or blood pH.
11) As a consequence of 10), a possible next step could be the computational simulation of blood streams within a moving ectotherm sauropsid ventricle. Such simulations are already performed for human hearts and could be adapted for ‘reptile’ hearts based on 3D reconstructions of the heart.

Bibliography

Aescht, E., Büchl-Zimmermann, S., Burmester, A., Dänhardt-Pfeiffer, S., Desel, C., Hamers, C., Jach, G., Kässens, M., Makovitzky, J., Mulisch, M., et al. (2010). *Romeis Mikroskopische Technik*. (ed. Mulisch, M.) and Welsch, U.) Heidelberg: Spektrum Akademischer Verlag.

Akani, G. C., Luiselli, L., Eniang, E. A., Amuzie, C. C. and Ebere, N. (2008). Aspects of the ecology of the spotted blindsnake, *Typhlops punctatus punctatus* in Port-Harcourt, Nigeria. *Afr. J. Ecol.* **46**, 533–539.

Altimiras, J., Franklin, C. E. C. and Axelsson, M. (1998). Relationships between blood pressure and heart rate in the saltwater crocodile *Crocodylus porosus*. *J. Exp. Biol.* **201**, 2235–2242.

Altmann, G. G. (1972). Influence of starvation and refeeding on mucosal size and epithelial renewal in the rat small intestine. *Am. J. Anat.* **133**, 391–400.

Andersen, J. B., Rourke, B. C., Caiozzo, V. J., Bennett, A. F., Hicks, J. W., Beeli, G., Esslen, M. and Jäncke, L. (2005). Postprandial cardiac hypertrophy in pythons. *Nature* **434**, 37–8.

Andrade, D. V. (2004). Ventilatory compensation of the alkaline tide during digestion in the snake *Boa constrictor*. *J. Exp. Biol.* **207**, 1379–1385.

Axelsson, M. and Franklin, C. E. (1997). From anatomy to angioscopy: 164 years of crocodilian cardiovascular research, recent advances, and speculations. *Comp. Biochem. Physiol. Part A Physiol.* **118**, 51–62.

Axelsson, M. and Franklin, C. E. (2001). The calibre of the *Foramen of Panizza* in *Crocodylus porosus* is variable and under adrenergic control. *J. Comp. Physiol. B Biochem. Syst. Environ. Physiol.* **171**, 341–346.

Axelsson, M. and Fritsche, R. (1991). Gut blood flow in the estuarine crocodile, *Crocodylus porosus*. *Acta Physiol Scand.* **142**, 509–16.

Axelsson, M., Franklin, C. E., Lofman, C. O., Nilsson, S. and Grigg, G. C. (1996). Dynamic anatomical study of cardiac shunting in crocodiles using high- resolution angioscopy. *J. Exp. Biol.* **199**, 359–365.

Axelsson, M., Franklin, C., Fritsche, R., Grigg, G. and Nilsson, S. (1997). The sub-pulmonary conus and the arterial anastomosis as important sites of cardiovascular regulation in the crocodile *Crocodylus porosus*. *J. Exp. Biol.* **200**, 807–814.

Axelsson, M., Olsson, C., Gibbins, I., Holmgren, S. and Franklin, C. E. (2001). Nitric oxide, a potent vasodilator of the aortic anastomosis in the estuarine crocodile, *Crocodylus porosus*. *Gen. Comp. Endocrinol.* **122**, 198–204.

Baker, L. A. and White, F. N. (1970). Redistribution of cardiac output in response to heating in *Iguana iguana*. *Comp. Biochem. Physiol.* **35**, 253–262.

Beddard, F. E. and Mitchell, P. C. (1895). On the structure of the heart of the alligator. *Proc. Zool. Soc. L.* **1895**, 343–349.

Bennett, A. A. F. (1994). Exercise performance of reptiles. *Adv. Vet. Sci. Comp. Med.* **38**, 113.

Bennett, A. F. A. and Licht, P. (1972). Anaerobic metabolism during activity in lizards. *J. Comp. Physiol.* **8**, 277–288.

Bennett, A., Dawson, W. and Bartholomew, G. (1975). Effects of activity and temperature on aerobic and anaerobic metabolism in the Galapagos marine iguana. *J. Comp. Physiol.* **100**, 317–329.

Berger, P. and Heisler, N. (1977). Estimation of shunting, systemic and pulmonary output of the heart, and regional blood flow distribution in unanaesthetized lizards (*Varanus exanthematicus*) by injection of radioactively labelled microspheres. *J. Exp. Biol.* **71**, 111–121.

Boza, J. J., Moennoz, D., Vuichoud, J., Jarret, A. R., Gaudard-de-Weck, D., Fritsche, R., Donnet, A., Schiffrin, E. J., Perruisseau, G. and Ballevre, O. (1999). Food Deprivation and Refeeding Influence Growth, Nutrient Retention and Functional Recovery of Rats. *J. Nutr.* **129**, 1340–1346.

Brücke, E. W. von (1852). *Beiträge zur vergleichenden Anatomie und Physiologie des Gefäss-Systemes*.

Burggren, W. W. (1982). Pulmonary blood plasma filtration in reptiles: a “wet” vertebrate lung? *Science* **215**, 77–8.

Burggren, W. (1987). Form and function in reptilian circulations. *Am. Zool.* **19**, 5–19.

Burggren, W. and Johansen, K. (1982). Ventricular haemodynamics in the monitor lizard *Varanus exanthematicus*: pulmonary and systemic pressure separation. *J. Exp. Biol.* 343–354.

Burggren, W. W., Christoffels, V. M., Crossley, D. A., Enok, S., Farrell, A. P., Hedrick, M. S., Hicks, J. W., Jensen, B., Moorman, A. F. M., Mueller, C. A., et al. (2013). Comparative cardiovascular physiology: future trends, opportunities and challenges. *Acta Physiol.* **2010**, 257–276.

Buschmann, R. J. and Manke, D. J. (1981a). Morphometric analysis of the membranes and organelles of small intestinal enterocytes. I. Fasted hamster. *J. Ultrastruct. Res.* **76**, 1–14.

Buschmann, R. J. and Manke, D. J. (1981b). Morphometric analysis of the membranes and organelles of small intestinal enterocytes. II. Lipid-fed hamster. *J. Ultrastruct. Res.* **76**, 15–26.

Busk, M. and Overgaard, J. (2000). Effects of feeding on arterial blood gases in the American alligator Alligator mississippiensis. *J. Exp. Biol.* **3124**, 3117–3124.

Campbell, J. A. and Lamar, W. W. (2004). *The Venomous Reptiles of the Western Hemisphere*. Ithaca: Comstock Publishing Associates.

Campen, R. (2009). Funktionsweise des Pythonherzens während unterschiedlicher physiologischer Zustände (Diploma Thesis).

Campen, R. and Starck, J. M. (2012). Cardiovascular circuits and digestive function of intermittent-feeding sauropsids. In *Comparative physiology of fasting, starvation, and food limitation* (ed. McCue, M.), pp. 133–154. Heidelberg New York: Springer Verlag.

Carmena-Suero, A., Siret, J. R. J., Callejas, J. and Carmena, D. (1979). Blood volume and hematological values of crocodile (*Crocodylus rhombifer Cuvier*). *Comp. Biochem. Physiol. Part A Physiol.* **64**, 597–600.

Carr, A., Ross, P. and Carr, S. (1974). Internesting Behavior of the Green Turtle, *Chelonia mydas*, at a Mid-Ocean Island Breeding Ground. *Copeia* **3**, 703–706.

Coulson, R. A., Hernandez, T. and Dessauer, H. C. (1950). Alkaline Tide of the Alligator. *Exp. Biol. Med.* **74**, 866–869.

Cramp, R. L. and Franklin, C. E. (2005). Arousal and re-feeding rapidly restores digestive tract morphology following aestivation in green-striped burrowing frogs. *Comp. Biochem. Physiol. A. Mol. Integr. Physiol.* **142**, 451–60.

Cramp, R. L., Franklin, C. E. and Meyer, E. a (2005). The impact of prolonged fasting during aestivation on the structure of the small intestine in the green-striped burrowing frog, Cyclorana alboguttata. *Acta Zool.* **24**, 13–24.

Cramp, R. L., Kayes, S. M., Meyer, E. A. and Franklin, C. E. (2009). Ups and downs of intestinal function with prolonged fasting during aestivation in the burrowing frog, *Cyclorana alboguttata*. *J. Exp. Biol.* **212**, 3656–63.

Davies, F., Francis, E. T. B. and King, T. S. (1951). Electrocardiogram of the Crocodilian Heart. *Nature* **167**, 146.

Denk, W. and Horstmann, H. (2004). Serial Block-Face Scanning Electron Microscopy to Reconstruct Three-Dimensional Tissue Nanostructure. *PLOS Biol.* **2**, e329.

Douglas, C. G. and Haldane, J. S. (1922). The regulation of the general circulation rate in man. *J. Physiol.* **56**, 69–100.

Dunel-Erb, S., Chevalier, C. and Laurent, P. (2001). Restoration of the jejunal mucosa in rats refed after prolonged fasting. *Comp. Biochem. Physiol. Part A* **129**, 933–947.

Durán, a C., López, D., Guerrero, A., Mendoza, A., Arqué, J. M. and Sans-Coma, V. (2004). Formation of cartilaginous foci in the central fibrous body of the heart in Syrian hamsters (*Mesocricetus auratus*). *J. Anat.* **205**, 219–227.

Elad, D. and Einav, S. (2004). Physical and flow properties of blood. In *Standard handbook of biomedical engineering and design* (ed. Kutz, M.), pp. 1–25. New York: McGraw-Hill.

Eme, J., Gwalthney, J., Blank, J. M., Owerkowicz, T., Barron, G. and Hicks, J. W. (2009). Surgical removal of right-to-left cardiac shunt in the American alligator (*Alligator mississippiensis*) causes ventricular enlargement but does not alter apnoea or

metabolism during diving. *J. Exp. Biol.* **212**, 3553–63.

Eme, J., Gwalthney, J., Owerkowicz, T., Blank, J. M. and Hicks, J. W. (2010). Turning crocodilian hearts into bird hearts: growth rates are similar for alligators with and without right-to-left cardiac shunt. *J. Exp. Biol.* **213**, 2673–80.

Farmer, C. G. (2011). On the evolution of arterial vascular patterns of tetrapods. *J. Morphol.* **272**, 1325–41.

Farmer, C. and Hicks, J. (2002). The intracardiac shunt as a source of myocardial oxygen in a turtle, *Trachemys scripta*. *Integr. Comp. Biol.* **42**, 208–215.

Farmer, C. G., Uriona, T. J., Olsen, D. B., Steenblik, M. and Sanders, K. (2008). The right-to-left shunt of crocodilians serves digestion. *Physiol. Biochem. Zool.* **81**, 125–37.

Farrell, A. and Gamperl, A. (1998). Comparative aspects of heart morphology. In *Biology of the Reptilia, vol. 19* (ed. Gans, C.) and Gaunt, A.), p. Ithaka: Society for the Study of Amphibians and Reptiles.

Filogonio, R., Wang, T., Taylor, E. W., Abe, A. S. and Leite, C. A. C. (2016). Vagal tone regulates cardiac shunts during activity and at low temperatures in the South American rattlesnake, *Crotalus durissus*. *J. Comp. Physiol. B* **186**, 1059–1066.

Filogonio, R., Alcantara Costa Leite, C. and Wang, T. (2017). Vascular distensibilities have minor effects on intracardiac shunt patterns in reptiles. *Zoology* **122**, 46–51.

Franklin, C. E. and Axelsson, M. (2000). Physiology: An actively controlled heart valve. *Nature* **406**, 847–848.

Franklin, C. E., Söderström, V., Nilsson, G. E. and Renshaw, G. M. C. (1999). Hypoxia stimulates cerebral blood flow and blood pressure in the estuarine crocodile (*Crocodylus porosus*). *Neurosci. Lett.* **267**, 1–4.

Galli, G. L. J., Skovgaard, N., Abe, A. S., Taylor, E. W. and Wang, T. (2005). The role of nitric oxide in the regulation of the systemic and pulmonary vasculature of the rattlesnake, *Crotalus durissus terrificus*. *J. Comp. Physiol. B.* **175**, 201–8.

Galli, G. L. J., Skovgaard, N., Abe, A. S., Taylor, E. W. and Wang, T. (2007). The adrenergic regulation of the cardiovascular system in the South American rattlesnake, *Crotalus durissus*. *Comp. Biochem. Physiol. A. Mol. Integr. Physiol.* **148**, 510–20.

Gardner, M. N., Sterba-Boatwright, B. and Jones, D. R. (2011). Ligation of the left aorta in alligators affects acid–base balance: A role for the R→L shunt. *Respir. Physiol. Neurobiol.* **178**, 315–322.

Gatten, R. (1984). Aerobic and anaerobic metabolism of freely-diving loggerhead musk turtles (*Sternotherus minor*). *Herpetologica* **40**, 1–7.

Gegenbauer, C. (1901). *Vergleichende Anatomie der Wirbelthiere mit Berücksichtigung der Wirbellosen, Band 2*. Leipzig: Verlag von Wilhelm Engelmann.

Gelman, S. (2008). Venous Function and Central Venous Pressure: A Physiologic Story.

Anesthesiology **108**, 735–748.

Gleeson, T., Nicol, C. and Johnston, I. (1984). Capillarization, mitochondrial densities, oxygen diffusion distances and innervation of red and white muscle of the lizard *Dipsosaurus dorsalis*. *Cell Tissue Res.* 253–258.

Greenfield, L. and Morrow, A. (1961). The cardiovascular hemodynamics of Crocodilia. *J. Surg. Res.* **1**, 97–103.

Grigg, G. and Johansen, K. (1987). Cardiovascular dynamics in *Crocodylus porosus* breathing air and during voluntary aerobic dives. *J. Comp. Physiol. B* **157**, 381–392.

Hafferl (1933). *Handbuch der vergleichenden Anatomie der Wirbeltiere, Bd. VI.* Berlin: Urban und Schwarzenberg.

Hansen, K., Pedersen, P. B. M., Pedersen, M. and Wang, T. (2013). Magnetic Resonance Imaging Volumetry for Noninvasive Measures of Phenotypic Flexibility during Digestion in Burmese Pythons. *Physiol. Biochem. Zool.* **86**, 149–158.

Hartzler, L. and Munns, S. (2006). Metabolic and blood gas dependence on digestive state in the Savannah monitor lizard *Varanus exanthematicus*: an assessment of the alkaline tide. *J. Exp. Biol.* **209**, 1052–1057.

Hartzler, L., Munns, S., Bennett, A. and Hicks, J. (2006). Recovery from an activity-induced metabolic acidosis in the American alligator, *Alligator mississippiensis*. *Comp. Biochem. Physiol. - A Mol. Integr. Physiol.* **143**, 368–74.

Hicks, J. W. and Bennett, A. F. (2004). Eat and run: prioritization of oxygen delivery during elevated metabolic states. *Respir. Physiol. Neurobiol.* **144**, 215–24.

Hicks, J. and Krosniunas, E. (1998). Physiological states and intracardiac shunting in non-crocodilian reptiles. In *EBO - Experimental biology online Annual*, pp. 35–57. Berlin Heidelberg: Springer.

Hicks, J. and Malvin, G. (1992). Mechanism of intracardiac shunting in the turtle *Pseudemys scripta*. *Am. J. Physiol.* **262**, 986–992.

Hicks, J. W. and Wang, T. (1996). Functional role of cardiac shunts in reptiles. *J. Exp. Zool.* **216**, 204–216.

Hicks, J. W. and Wang, T. (1999). Hypoxic hypometabolism in the anesthetized turtle, *Trachemys scripta*. *Am J Physiol Regul. Integr. Comp Physiol* **277**, 18–23.

Hicks, J. W. and White, F. N. (1992). Pulmonary gas exchange during intermittent ventilation in the American alligator. *Respir. Physiol.* **88**, 23–36.

Hicks, J., Ishimatsu, A. and Molloi, S. (1996). The mechanism of cardiac shunting in reptiles: a new synthesis. *J. Exp. Biol.* **199**, 1435–1446.

Hicks, J., Wang, T. and Bennett, A. (2000). Patterns of cardiovascular and ventilatory response to elevated metabolic states in the lizard *Varanus exanthematicus*. *J. Exp. Biol.* **2445**, 2437–2445.

Hillman, S. S., Hedrick, M. S., Drewes, R. C. and Withers, P. C. (2010). Lymph flux rates from various lymph sacs in the cane toad *Rhinella marina*: an experimental

evaluation of the roles of compliance, skeletal muscles and the lungs in the movement of lymph. *J. Exp. Biol.* **213**, 3161–6.

Hillman, S. S., Hedrick, M. S. and Kohl, Z. F. (2014). Net cardiac shunts in anuran amphibians: physiology or physics? *J. Exp. Biol.* **217**, 2844–2847.

Hochstetter, F. (1898). Über die Arterien des Darmkanals der Saurier. *Morph Jahrb* **26**, 215–273.

Hoffman, L., Fisher, P. and Sales, J. (2000). Carcass and meat characteristics of the Nile crocodile (*Crocodylus niloticus*). *J. Sci. Food Agric* **80**, 390–396.

Hofmann, A. F. (2011). Overview of Bile Secretion. *Compr. Physiol.* 549–566.

Hopkinson, J. P., Pancoast, J. and Society, A. P. (1837). On the visceral anatomy of the python (Cuvier), described by Daudin as the *Boa reticulata*. *Trans. Am. Philos. Soc.* **5**, 121–134.

Iwakiri, R., Gotoh, Y. and Noda, T. (2001). Programmed cell death in rat intestine: effect of feeding and fasting. *Scand J Gastroentero* **36**, 39–47.

Jensen, B., Nielsen, J. M., Axelsson, M., Pedersen, M., Löfman, C. and Wang, T. (2010a). How the python heart separates pulmonary and systemic blood pressures and blood flows. *J. Exp. Biol.* **213**, 1611–7.

Jensen, B., Nyengaard, J. R., Pedersen, M. and Wang, T. (2010b). Anatomy of the python heart. *Anat. Sci. Int.* **85**, 194–203.

Jensen, B., Larsen, C. K., Nielsen, J. M., Simonsen, L. S. and Wang, T. (2011). Change of cardiac function, but not form, in postprandial pythons. *Comp. Biochem. Physiol. Part A Mol. Integr. Physiol.* **160**, 35–42.

Jensen, B., Wang, T., Christoffels, V. M. and Moorman, A. F. M. (2013). Evolution and development of the building plan of the vertebrate heart. *Biochim. Biophys. Acta - Mol. Cell Res.* **1833**,.

Jensen, F. B., Hansen, M. N., Montesanti, G. and Wang, T. (2014a). Nitric oxide metabolites during anoxia and reoxygenation in the anoxia-tolerant vertebrate *Trachemys scripta*. *J. Exp. Biol.* **217**, 423 LP-431.

Jensen, B., Moorman, A. F. M. and Wang, T. (2014b). Structure and function of the hearts of lizards and snakes. *Biol. Rev. Camb. Philos. Soc.* **89**, 302–336.

Johansen, K. and Hol, R. (1960). A Cineradiographic Study of the Snake Heart. *Circ. Res.* **8**, 253–259.

Jones, D. and Shelton, G. (1993). The physiology of the alligator heart: left aortic flow patterns and right-to-left shunts. *J. Exp. Biol.* **176**, 247–269.

Jones, D., Round, J. and De Haan, A. (2004). *Skeletal muscle - from molecules to movement*. Philadelphia: Churchill Livingstone.

Joyce, W., Gesser, H. and Wang, T. (2014). Purinoceptors exert negative inotropic effects on the heart in all major groups of reptiles. *Comp. Biochem. Physiol. - A Mol. Integr. Physiol.* **171**, 16–22.

Joyce, W., Axelsson, M. and Wang, T. (2016). Autoregulation of cardiac output is overcome by adrenergic stimulation in the anaconda heart. *J. Exp. Biol.*

Kagstrom, J., Olsson, C., Axelsson, M. and Franklin, C. E. (1998). Peptidergic control of gastrointestinal blood flow in the estuarine crocodile, *Crocodylus porosus*. *Am J Physiol Regul. Integr. Comp Physiol* **274**, R1740-1750.

Karasov, W. H. and Diamond, J. M. (1983). A simple method for measuring intestinal solute uptake in vitro. *J. Comp. Physiol. B* **152**, 105–116.

Karasov, W., Pinshow, B., Starck, J. and Afik, D. (2004). Anatomical and histological changes in the alimentary tract of migrating blackcaps (*Sylvia atricapilla*): a comparison among fed, fasted, food-restricted, and refed birds. *Physiol Biochem Zool* **77**, 149–160.

Kardong, K. (1995). *Vertebrates: Comparative anatomy, function, evolution*. Wm. C. Brown Publishers, Dubuque.

Karila, P., Axelsson, M., Franklin, C. E., Fritsche, R., Gibbins, I. L., Grigg, G. C., Nilsson, S., Holmgren, S. and Franklin, E. (1995). Neuropeptide immunoreactivity and co-existence in cardiovascular nerves and autonomic ganglia of the estuarine crocodile, *Crocodylus porosus*, and cardiovascular effects of neuropeptides. *Regul. Pept.* **58**, 25–39.

Kashyap, H. (1950). The structure of the heart of Typhlops (Reptilia: Ophidia). *J Zool Soc India* **2**, 42–48.

Klabunde, R. E. (2005). *Cardiovascular physiology concepts*. 1st ed. Philadelphia: Lippincott Williams & Wilkins.

Köhler, G. (2005). *Kornnattern: Lebensweise, Pflege, Zucht, Erkrankungen*. Offenbach: Herpeton.

Lee, M. S. Y., Hugall, A. F., Lawson, R. and Scanlon, J. D. (2007). Phylogeny of snakes (Serpentes): Combining morphological and molecular data in likelihood, Bayesian and parsimony analyses. *Syst. Biodivers.* **5**, 371–389.

Leite, C. A. C., Taylor, E. W., Wang, T., Abe, A. S. and de Andrade, D. O. V. (2013). Ablation of the ability to control the right-to-left cardiac shunt does not affect oxygen uptake, specific dynamic action or growth in the rattlesnake Crotalus durissus. *J. Exp. Biol.* **216**,.

Leite, C. A. C., Wang, T., Taylor, E. W., Abe, A. S., Leite, G. S. P. C. and de Andrade, D. O. V (2014). Loss of the ability to control right-to-left shunt does not influence the metabolic responses to temperature change or long-term fasting in the South American rattlesnake *Crotalus durissus*. *Physiol. Biochem. Zool.* **87**, 568–575.

Lignot, J. and Secor, S. (2002). Postprandial morphological changes of the intestinal villi and enteropytes in the Burmese pythons. *Integr. Comp. Biol.* **42**,.

Lignot, J. H., Helmstetter, C. and Secor, S. M. (2005). Postprandial morphological response of the intestinal epithelium of the Burmese python (*Python molurus*). *Comp. Biochem. Physiol. - A Mol. Integr. Physiol.* **141**, 280–291.

Lindinger, M. (2005). Applying physicochemical principles to skeletal muscle acid-base status. *Am J Physiol Regul Integr Comp Physiol* **289**, R891-4-910.

López, D. and Durán, A. (2003). Formation of cartilage in the heart of the Spanish terrapin, *Mauremys leprosa* (Reptilia, Chelonia). *J. morph* **258**, 97–105.

Mahendra, B. C. and Viviridis, F. L. A. (1942). Contributions to the Bionomics, Anatomy, Reproduction and Development of the Indian House-Gecko, *Hemidactylus Flaviviridis* Rüppel. *Proc. Indian Acad. Sci. - Sect. B* **15**, 231–252.

Malte, C. L., Malte, H., Reinholdt, L. R., Findsen, A., Hicks, J. W. and Wang, T. (2016). Right-to-left shunt has modest effects on CO2 delivery to the gut during digestion, but compromises oxygen delivery. *J. Exp. Biol.*

Mathur, P. N. (1944). The anatomy of the reptilian heart. *Proc. Indian Acad. Sci. - Sect. B* **20**, 1–29.

McCauley, W. J. (1956). The gross anatomy of the lymphatic system of *Alligator mississippiensis*. *Am. J. Anat.* **99**, 189–209.

McCue, M. (2006). Specific dynamic action: a century of investigation. *Comp. Biochem. Physiol. Part A* **144**, 381–94.

McCue, M., Bennett, A. and Hicks, J. (2005). The effect of meal composition on specific dynamic action in Burmese pythons (*Python molurus*). *Physiol. Biochem. Zool.* **78**, 182–192.

Millen, J. E., Murdaugh, H. V., Bauer, C. B. and Robin, E. D. (1964). Circulatory Adaptation to Diving in the Freshwater Turtle. *Science (80-.).* **145**, 591–593.

Mooseker, M. S. (1982). Nucleated polymerization of actin from the membrane-associated ends of microvillar filaments in the intestinal brush border. *J. Cell Biol.* **95**, 223–233.

Mortimer, J. A. (1981). The Feeding Ecology of the West Caribbean Green Turtle (*Chelonia mydas*) in Nicaragua. *Biotropica* **13**, 49–58.

Munns, S. L., Hartzler, L. K., Bennett, A. F. and Hicks, J. W. (2005). Terrestrial locomotion does not constrain venous return in the American alligator, *Alligator mississippiensis*. *J. Exp. Biol.* **208**, 3331–9.

Niv, Y. and Fraser, G. G. M. (2002). The alkaline tide phenomenon. *J. Clin. Gastroenterol.* **35**, 5–8.

Panizza, B. (1833). Sulla struttura del cuore e sulla circolazione del sangue del *Crocodilus lucius*. *Biblioth. Ital.* **70**, 87–91.

Penzlin, H. (1991). *Lehrbuch der Tierphysiologie*. 5th ed. Jena: Gustav Fischer Verlag.

Pflanzer, R. G. and Wertenberger, E. (1970). Circulatory response to experimental diving of three species of crocodilians. *Physiologist* **13**, 283.

Platzack, B. and Hicks, J. W. (2001). Reductions in systemic oxygen delivery induce a hypometabolic state in the turtle *Trachemys scripta*. *Am J Physiol Regul. Integr. Comp Physiol* **281**, R1295-1301.

Poelmann, R. E., Gittenberger-De Groot, A. C., Vicente-Steijn, R., Wisse, L. J., Bartelings, M. M., Everts, S., Hoppenbrouwers, T., Kruithof, B. P. T., Jensen, B., De Bruin, P. W., et al. (2014). Evolution and development of ventricular septation in the amniote heart. *PLoS One* **9**, e106569.

Poelmann, R. E., Gittenberger-de Groot, A. C., Biermans, M. W. M., Dolfing, A. I., Jagessar, A., van Hattum, S., Hoogenboom, A., Wisse, L. J., Vicente-Steijn, R., de Bakker, M. A. G., et al. (2017). Outflow tract septation and the aortic arch system in reptiles: lessons for understanding the mammalian heart. *Evodevo* **8**, 9.

Pritchard, J. B. (2002). Comparative models and biological stress. *Am. J. Physiol. Regul. Integr. Comp. Physiol.* **283**, R807-9.

Raab, S., Leiser, R., Kemmer, H. and Claus, R. (1998). Effects of energy and purines in the diet on proliferation, differentiation, and apoptosis in the small intestine of the pig. *Metabolism* **47**, 1105–1111.

Rathke, H. (1866). *Untersuchungen über die Entwickelung und den Körperbau der Krokodile*. (ed. von Wittich, W. H.) F. Vieweg.

Rhoads, D. (2008). *The Complete Suboc - A Comprehensive Guide to the Natural History, Care, and Breeding of the Trans-Pecos Ratsnake*. 1st ed. Lansing: ECO Herpetological Publishing/Serpent's Tale NHBD.

Riquelme, C., Magida, J. and Harrison, B. (2011). Fatty acids identified in the Burmese python promote beneficial cardiac growth. *Science (80-.).* **334**, 528–531.

Robergs, R. (2004). Biochemistry of exercise-induced metabolic acidosis. *Am J Physiol Regul Integr Comp Physiol* **287**, R502-16.

Ross, C. A. (2002). *Krokodile und Alligatoren*. München: Verlagsgruppe Randomhouse.

Ruben, J. (1976). Aerobic and anaerobic metabolism during activity in snakes. *J. Comp. Physiol.* **157**, 147–157.

Sabatier, A. (1873). Etudes sur le coeur et la circulation centrale dans la série des vertébratés.

Schmidt, R. and Thews, G. (1980). *Physiologie des Menschen*. 20th ed. Berlin, Heidelberg: Springer.

Secor, S. M. (2001). Regulation of digestive performance: a proposed adaptive response. *Comp. Biochem. Physiol. Part A* **128**, 565–77.

Secor, S. (2003). Gastric function and its contribution to the postprandial metabolic response of the Burmese python *Python molurus*. *J. Exp. Biol.* **206**, 1621–1630.

Secor, S. (2005). Evolutionary and cellular mechanisms regulating intestinal performance of amphibians and reptiles. *Integr. Comp. Biol.* **294**, 282–294.

Secor, S. (2008). Digestive physiology of the Burmese python: broad regulation of integrated performance. *J. Exp. Biol.* **211**, 3767–74.

Secor, S. M., Stein, E. D. and Diamond, J. (1994). Rapid upregulation of snake intestine in response to feeding: a new model of intestinal adaptation. *Am J Physiol*

Gastrointest Liver Physiol **266**, G695-705.

Secor, S., Hicks, J. and Bennett, A. (2000). Ventilatory and cardiovascular responses of a python (*Python molurus*) to exercise and digestion. *J. Exp. Biol.* **2454**, 2447–2454.

Secor, S. M., Lane, J. S., Whang, E. E., Ashley, S. W. and Diamond, J. (2002). Luminal nutrient signals for intestinal adaptation in pythons. *Am. J. Physiol.* **283**, 1298–1309.

Secor, S. M., Taylor, J. R. and Grosell, M. (2012). Selected regulation of gastrointestinal acid-base secretion and tissue metabolism for the diamondback water snake and Burmese python. *J. Exp. Biol.* **215**, 185–196.

Shelton, G. and Burggren, W. (1976). Cardiovascular dynamics of the Chelonia during apnoea and lung ventilation. *J. Exp. Biol.* **64**, 323–343.

Shelton, G. and Jones, D. (1991). The physiology of the alligator heart: the cardiac cycle. *J. Exp. Biol.* **564**, 539–564.

Simons, F. E. R. (2010). Anaphylaxis. *J. Allergy Clin. Immunol.* **125**, 161–81.

Skovgaard, N., Abe, A. S., Andrade, D. V and Wang, T. (2005). Hypoxic pulmonary vasoconstriction in reptiles: a comparative study of four species with different lung structures and pulmonary blood pressures. *Am. J. Physiol. Regul. Integr. Comp. Physiol.* **289**, R1280-8.

Skovgaard, N., Abe, A. S., Taylor, E. W. and Wang, T. (2017). Cardiovascular effects of histamine in three widely diverse species of reptiles. *J. Comp. Physiol. B* 1–10. https://doi.org/10.1007/s00360-017-1108-3

Slay, C. E., Enok, S., Hicks, J. W. and Wang, T. (2014). Reduction of blood oxygen levels enhances postprandial cardiac hypertrophy in Burmese python (*Python bivittatus*). *J. Exp. Biol.* **217**, 1784 LP-1789.

Smits, A. W. and Lillywhite, H. B. (1985). Maintenance of blood volume in snakes: transcapillary shifts of extravascular fluids during acute hemorrhage. *J. Comp. Physiol. B.* **155**, 305–10.

Starck, J. M. (1996). Intestinal Growth in Altricial European Starling (*Sturnus vulgaris*) and Precocial Japanese Quail (*Coturnix coturnix japonica*). *Cells Tissues Organs* **156**, 289–306.

Starck, J. M. (2005). Structural flexibility of the digestive system of tetrapods: patterns and processes at the cellular and tissue level. In *Physiological and ecological adaptation to feeding in vertebrates* (ed. Starck, J.) and Wang, T.), pp. 175–200. Enfield: Sci. Publ. Inc.

Starck, J. (2009). Functional morphology and patterns of blood flow in the heart of *Python regius*. *J. Morphol.* **270**, 673–87.

Starck, J. and Beese, K. (2001). Structural flexibility of the intestine of Burmese python in response to feeding. *J. Exp. Biol.* **335**, 325–335.

Starck, J. M. and Beese, K. (2002). Structural flexibility of the small intestine and liver

of garter snakes in response to feeding and fasting. *J. Exp. Biol.* **205**, 1377–1388.

Starck, J. and Moser, P. (2004). Pythons metabolize prey to fuel the response to feeding. *Proc Biol Sci* **271**, 903–8.

Starck, J. and Wimmer, C. (2005). Patterns of blood flow during the postprandial response in ball pythons, *Python regius*. *J. Exp. Biol.* **208**, 881–9.

Starck, J., Cruz-Neto, A. and Abe, A. (2007). Physiological and morphological responses to feeding in broad-nosed caiman (*Caiman latirostris*). *J. Exp. Biol.* **210**, 2033–45.

Stecyk, J. A. W. (2004). Adrenergic regulation of systemic peripheral resistance and blood flow distribution in the turtle *Trachemys scripta* during anoxic submergence at 5 C and 21 C. *J. Exp. Biol.* **207**, 269–283.

Steggerda, F. R. and Essex, H. E. (1957). Circulation and Blood Pressure in the Great Vessels and Heart of the Turtle (*Chelydra serpentina*). *Am. J. Physiol.* **190**, 320–326.

Syme, D., Gamperl, K. and Jones, D. (2002). Delayed depolarization of the cog-wheel valve and pulmonary-to-systemic shunting in alligators. *J. Exp. Biol.* **1851**, 1843–1851.

Taylor, E. W., Andrade, D. V, Abe, A. S., Leite, C. A. C. and Wang, T. (2009). The unequal influences of the left and right vagi on the control of the heart and pulmonary artery in the rattlesnake, *Crotalus durissus*. *J. Exp. Biol.* **212**, 145–51.

Tucker, V. A. (1966). Oxygen transport by the circulatory system of the green iguana (*Iguana Iguana*) at different body temperatures. *J. Exp. Biol.* **44**, 77–92.

Tucker, A. D. and Read, M. A. (2001). Frequency of foraging by gravid green turtles (*Chelonia mydas*) at Raine Island, Great Barrier Reef. *J. Herpetol.* **35**, 500–503.

Valentinuzzi, M. E., Hoff, H. E. and Geddes, L. A. (1969). Observations on the electrical activity of the snake heart. *J. Electrocardiol.* **2**, 39–50.

Waas, S., Werner, R. and Starck, J. (2010). Fuel switching and energy partitioning during the postprandial metabolic response in the ball python (*Python regius*). *J. Exp. Biol.* **213**, 1266–71.

Wallach, V. and Ineich, I. (1996). Redescription of a rare Malagasy blind snake, *Typhlops grandidieri Mocquard*, with placement in a new genus (Serpentes: Typhlopidae). *J. Herpetol.*

Walls, J. G. (1998). *The Living Pythons: A Complete Guide to the Pythons of the World*. Neptune: TFH Publications.

Wang, T. and Hicks, J. W. (1996a). Cardiorespiratory synchrony in turtles. *J. Exp. Biol.* **1800**, 1791–1800.

Wang, T. and Hicks, J. (1996b). The interaction of pulmonary ventilation and the right-left shunt on arterial oxygen levels. *J. Exp. Biol.* **2129**, 2121–2129.

Wang, T. and Hicks, J. (2002). An integrative model to predict maximum O2 uptake in animals with central vascular shunts. *Zoology* **105**, 45–53.

Wang, T., Taylor, E. W., Andrade, D. and Abe, A. S. (2001a). Autonomic control of heart rate during forced activity and digestion in the snake *Boa constrictor*. *J. Exp. Biol.* **204**, 3553–3560.

Wang, T., Busk, M. and Overgaard, J. (2001b). The respiratory consequences of feeding in amphibians and reptiles. *Comp. Biochem. Physiol. Part A Mol. Integr. Physiol.* **128**, 533–547.

Wang, T., Altimiras, J. and Axelsson, M. (2002). Intracardiac flow separation in an in situ perfused heart from Burmese python *Python molurus*. *J. Exp. Biol.* **2723**, 2715–2723.

Wang, T., Altimiras, J., Klein, W. and Axelsson, M. (2003). Ventricular haemodynamics in *Python molurus*: separation of pulmonary and systemic pressures. *J. Exp. Biol.* **206**, 4241–4245.

Webb, G. J. W. (1979). Comparative cardiac anatomy of the reptilia. III. The heart of crocodilians and an hypothesis on the completion of the interventricular septum of crocodilians and birds. *J. Morphol.* **161**, 221–240.

Webb, G., Heatwole, H. and Bavay, J. De (1971). Comparative cardiac anatomy of the Reptilia. I. The chambers and septa of the varanid ventricle. *J. Morphol.* **134**, 335–350.

Webb, G., Heatwole, H. and Bavay, J. de (1974). Comparative cardiac anatomy of the reptilia. II. A critique of the literature on the Squamata and Rhynchocephalia. *J. Morphol.* **142**, 1–20.

Wells, R., Beard, L. and Grigg, G. (1991). Blood viscosity and hematocrit in the estuarine crocodile, *Crocodylus porosus*. *Comp Biochem Physiol* **99**, 41–44.

White, F. N. (1956). Circulation in the reptilian heart (*Caiman sclerops*). *Anat. Rec.* **125**, 417–431.

White, F. (1959). Circulation in the reptilian heart (Squamata). *Anat. Rec.* **135**, 129–134.

White, F. (1968). Functional anatomy of the heart of reptiles. *Am. Zool.* **219**, 211–219.

White, F. (1969). Redistribution of cardiac output in the diving alligator. *Copeia* **1969**, 567–570.

White, F. N. (1985). Role of intracardiac shunts in pulmonary gas exchange in chelonian reptiles. In *Cardiovascular shunts: Phylogenetic, ontogenetic and clinical aspects* (ed. Johansen, K.) and Burggren, W.), pp. 296–309. Copenhagen: Munksgaard.

White, F. and Ross, G. (1966). Circulatory changes during experimental diving in the turtle. *Am J Physiol* **211**, 15–18.

White, F. N., Hicks, J. W. and Ishimatsu, A. (1989). Relationship between respiratory state and intracardiac shunts in turtles. *Am J Physiol Regul. Integr. Comp Physiol* **256**, R240-247.

Willis, R. (2009). Transthyretin gene (TTR) intron 1 elucidates crocodylian phylogenetic

relationships. *Mol. Phylogenet. Evol.* **53**, 1049–1054.

Young, B. (1994). Cartilago cordis in serpents. *Anat. Rec.* **247**, 243–247.

Zaar, M., Overgaard, J., Gesser, H. and Wang, T. (2007). Contractile properties of the functionally divided python heart: two sides of the same matter. *Comp. Biochem. Physiol. Part A Mol. Integr. Physiol.* **146**, 163–173.

Zhao-Xian, W., Sun, N. and Mao, W. (1991). The breathing pattern and heart rates of *Alligator sinensis*. *Comp Biochem Physiol* **98**, 77–87.

List of Tables and Figures

Figures

Tables

Simulation Algorithm

Simulation Algorithm

Parameters and variables

If n is the number of compartments, the model is parameterized by specifying the minimum and maximum fill levels, v_i^{min} and v_i^{max} for $i = 1, 2, \ldots, n$, and permeabilities $p_{i,j}$ for $i, j = 1, 2, \ldots, n$. Additionally, we need to specify the initial fill levels $V_{i,0}$. In each simulation run, we keep track of how the fill levels of the various compartments $V_{i,t}$ ($i = 1, 2, \ldots, n$) change over time. In each time step t, we also store the total input to each compartment, $I_{i,t}$, and the total output from each compartment, $O_{i,t}$. One hundred time steps correspond to the length of one heart beat. During diastole (time steps 1 to 70 of a heart cycle), the permeability of the Foramen Panizzae, i.e. between right and left proximal aorta, is zero in both directions.

Algorithm

Given the fill levels of the compartments 1 to n in time step $t-1$, we determine the fill levels in time step t through a series of computations:

First, the capacities and excess volumes are computed for each compartment. As illustrated by Fig. 2 in the main text, the capacity of compartment i at time t is defined as

$$\kappa_i := v_i^{max} - V_{i,t-1} \tag{1}$$

and the corresponding excess volume (multiplied by a factor p_i) is

$$\epsilon_i := \left(V_{i,t-1} - v_i^{min}\right) \cdot p_i, \tag{2}$$

where p_i is chosen such that over the time span of one heart beat the excess volume would be reduced by a factor 1000. In other words, p_i is the solution of $(1 - p_i)^{t_{transfer}} = 0.001$, where $t_{transfer}$ is the number of time steps per heart beat during which the respective compartment can transfer blood (30 for the ventricles, 70 for the veins, and 100 for all other compartments). Note that to simplify the notation, we dropped the time index from κ_i and ϵ_i. We will do the same for the other "helper" variables (all denoted by Greek letters) that we will need in the following steps to finally obtain the fill levels at time step t. During diastole (time steps 1 to 70 of one heart cycle), no blood can leave the heart and the excess volumes of both ventricles are set to zero. During systole

(time steps 71 to 100) no blood can enter the heart and the excess volumes of the pulmonary and systemic veins are set to zero.

Second, we compute how the excess volumes are distributed among the possible acceptor compartments. For this, we weight the permeabilities by the capacities of the respective acceptor compartments:

$$\delta_{i,j} := p_{i,j} \cdot \kappa_j \tag{3}$$

and normalize

$$\delta'_{i,j} := \frac{\delta_{i,j}}{\sum_{k=1}^{n} \delta_{i,k}}. \tag{4}$$

If the denominator is zero, $\delta'_{i,j}$ is set to zero. We then compute preliminary transfer volumes from compartment i to j:

$$\tau_{i,j} := \delta'_{i,j} \cdot \epsilon_i. \tag{5}$$

The total volume that would then flow into compartment i from all other compartments is

$$\iota_i := \sum_{k=1}^{n} \tau_{k,i}. \tag{6}$$

To ensure that the total input into a compartment does not exceed its capacity, we multiply all transfer volumes by a factor

$$\phi_i := \min\left(\frac{\kappa_i}{\iota_i}, 1\right), \tag{7}$$

such that

$$\tau'_{i,j} := \tau_{i,j} \cdot \phi_i. \tag{8}$$

Finally, we can sum up everything to obtain the total input into compartment i

$$I_{i,t} := \sum_{k=1}^{n} \tau'_{ki} \tag{9}$$

and its total output

$$O_{i,t} := \sum_{k=1}^{n} \tau'_{ik}. \tag{10}$$

Thus the new fill level of compartment i is

$$V_{i,t} := V_{i,t-1} + I_{i,t} - O_{i,t}. \tag{11}$$

Danksagung

Zu einer so lang andauernden Arbeit haben natürlich über die Jahre viele Personen beigetragen. Es gab reichlich Probleme während des Verlaufs, die manchmal fast zur Aufgabe der Arbeit geführt hätten. Die Tatsache, dass die Arbeit nun tatsächlich fertig ist, zeigt, dass es Menschen gab, die mich fachlich und emotional so unterstützten, dass ich trotzdem weitermachen konnte und wollte. Diesen allen danke ich von ganzem Herzen für ihren Beistand.

Ich danke Prof. Dr. Gerhard Haszprunar für die Übernahme der Erstkorrektur der Arbeit und für die immer konstruktive und ermutigende Betreuung in den späteren Jahren. Prof. Dr. J. Matthias Starck danke ich für die Möglichkeit, die Arbeit zunächst in seiner Arbeitsgruppe durchzuführen sowie für die Inspiration zum bearbeiteten Thema. Prof. Dr. Dirk Metzler und Dr. Maike Wittmann gilt mein Dank für ihren Beitrag zum Modellierungsteil der Arbeit und dafür, dass sie mich zeitweise in ihren Büros beherbergten. Zudem danke ich Dr. Philipp Rautenberg von GNode für die Umschreibung des Modellierungscodes in die Programmiersprache Python und die Hilfe beim Verwalten einer gigantischen Datenbank. Dr. Markus Settles aus der Radiologie am Klinikum rechts der Isar danke ich für seine Unterstützung bei den Magnetresonanzscans und Dr. Bernhard Ruthensteiner für die Möglichkeit, mit ihm die µCT-Scans durchzuführen. Ihm und PD Dr. Martin Hess, der mich als erstes, noch während des Studiums, für das BioImaging begeistert hat, gilt mein großer Dank für die Unterstützung in Sachen 3D Imaging.

Prof. Dr. Benedikt Grothe, Prof. Dr. Gisela Grupe, Dr. Andreas Herz und PD Dr. Bettina Bölter gilt mein Dank dafür, dass Sie sich bereit erklärt haben, mein TAC-Kommitee zu bilden und die Arbeit zu evaluieren. Prof. Dr. Grothe, danke für die Möglichkeit für Gespräche in den Krisenzeiten der Arbeit. Dieser Beistand hat mir sehr geholfen.

Ich danke den technischen Assistentinnen Julia Faltermeier und Heidi Gensler für die Weitergabe ihres Wissens im Bereich Histologie.

Meinen Kolleginnen Dr. Nadine Gerth, Dipl. Biol. Kathrin Jakob, Dr. Marina Vohberger, Dipl. Biol. Nadja Hoke und Dr. Carolin Ruoss möchte ich von ganzem Herzen für ihre Freundschaft danken. Unsere mittäglichen Hundegassirunden, abendlichen Lauftreffs, wochenendlichen Bergwanderungen, wissenschaftlichen Kaffeepausen, gelegentlichen Feierabendbierchen und jede Menge Blödsinn haben zu meiner körperlichen und geistigen Gesundheit sehr beigetragen und fehlen mir noch immer sehr. Es war eine tolle Zeit mit euch! Das gilt natürlich auch für alle anderen Freunde aus dem Biozentrum, von denen mir zum Glück heute noch einige gelegentlich über den Weg laufen: Dr. Andreas Zunhammer, Dr. Jens Nagel, Dr. Hilmar Strickfaden, Dr. Andreas Rott, und viele weitere.

Meinem Chef, Dr. Klaus Hellmann von der Klifovet AG, danke ich dafür, dass er mich mit dem bloßen Versprechen einer Dissertation eingestellt hat und auch nach fast drei Jahren noch nicht die Geduld oder den Glauben an die Promotion verloren hat. Danke, dass Du mich so unterstützt hast sowie für die Möglichkeit, jetzt als Projektleitung wieder wissenschaftlich zu arbeiten.

Ich danke meinen Eltern Birgit und Bernd Campen sowie meiner Großmutter Margarete Campen für ihre Unterstützung in den vielen Jahren, die durch diese Doktorarbeit geprägt waren.

Matthias Brunner, als wir uns 2011 kennengelernt haben, war ich schon mitten in dieser Doktorarbeit. Als Du 2015 dann so wirklich in mein Leben getreten bist, gab es sie immer noch. Danke, dass Du immer für mich da bist. Was lange währt, wird endlich gut. Ich liebe Dich.

Per aspidas ad astra.

Eidesstattliche Erklärung

Ich versichere hiermit an Eides statt, dass die vorgelegte Dissertation von mir selbständig und ohne unerlaubte Hilfe angefertigt ist.

München, den 21.09.2017 Ulrike Campen

(Unterschrift)

Erklärung

Hiermit erkläre ich, *

☒ dass die Dissertation nicht ganz oder in wesentlichen Teilen einer anderen Prüfungskommission vorgelegt worden ist.

☒ dass ich mich anderweitig einer Doktorprüfung ohne Erfolg **nicht** unterzogen habe.

☐ ~~dass ich mich mit Erfolg der Doktorprüfung im Hauptfach ..... und in den Nebenfächern ..... bei der Fakultät für ..... der .....~~

(Hochschule/Universität)

~~unterzogen habe.~~

☐ ~~dass ich ohne Erfolg versucht habe, eine Dissertation einzureichen oder mich der Doktorprüfung zu unterziehen.~~

München, den 21.09.2017 Ulrike Campen

(Unterschrift)

*) Nichtzutreffendes streichen